

# A Multi-Objective Collaborative Optimization Framework to Understand Trade-offs Between Naval Lifetime Costs Considering Production, Operation, and Maintenance

by

Dylan W. Temple

A dissertation submitted in partial fulfillment  
of the requirements for the degree of  
Doctor of Philosophy  
(Naval Architecture and Marine Engineering)  
in the University of Michigan  
2015

Doctoral Committee:

Assistant Professor Matthew Collette, Chair  
Associate Professor Joaquim R.R.A Martins  
Assistant Professor David J. Singer  
Professor Nickolas Vlahopoulos

©Dylan W. Temple

---

2015

## ACKNOWLEDGMENTS

First, I want to thank my advisor and mentor, Dr. Matthew Collette, for his guidance and support throughout my Ph.D. Through his mentorship I have grown as an engineer, a researcher, and a person. My time at the University of Michigan has allowed me to explore new avenues of ship design, visit countries across the globe, and continuously challenge myself academically. None of this would have been possible if I had not been fortunate enough to do my Ph.D. under Dr. Collete, and I will never cease to be thankful for this. I would also like to thank the rest of my thesis committee: Dr. David Singer, Dr. Nickolas Vlahopoulos, and Dr. Joaquim R.R.A. Martins. Their words of encouragement, as well as their challenging questions and criticisms have made this thesis the best that it could have been.

I would like to acknowledge the Science, Mathematics, & Research for Transformation Scholarship for giving me the opportunity to pursue a Ph.D. in a research topic that I was passionate about. The funding that they provided allowed me to choose a research path that was pertinent to my interests as well as my future career. I would like to thank John Hoyt for encouraging me to apply for the scholarship and aiding me in receiving it. Beyond that, I would like to thank Mr. Hoyt for his years of guidance on both my career and my skills as an engineer. I do not believe I would have taken the path I did if he had not been there to encourage me.

I would like to express my sincere gratitude to my parents, Dr. Elise Temple and Nox Connelly, for everything they have done for me. Without their support throughout my life I would never have been able to achieve the things that I have. They have always been there for me through the highs and lows of my career, and I

cannot thank them enough for that.

Lastly, though most importantly, I would like to thank my wife, Lauren Sheram. There is no doubt in my mind that it is because of her encouragement, support, and love, that this dissertation exists. She has pushed me to be the best I can be as both a person and an engineer. It is because of her unwavering belief in me through my time as a Ph.D. student that I was able to finish the work presented in this thesis. I will forever be grateful for her love and support in my life.

# TABLE OF CONTENTS

ACKNOWLEDGMENTS . . . . .	ii
LIST OF FIGURES . . . . .	vi
LIST OF TABLES . . . . .	ix
ABSTRACT . . . . .	x
<b>Chapter</b>	
<b>1 Introduction . . . . .</b>	<b>1</b>
1.1 Research Overview . . . . .	1
1.2 Research Contributions . . . . .	4
<b>2 Background . . . . .</b>	<b>9</b>
2.1 Overview . . . . .	9
2.2 Design Optimization . . . . .	9
2.2.1 Multi-Objective Optimization . . . . .	11
2.2.2 Multi-Disciplinary Optimization . . . . .	19
2.3 Hydrodynamic Optimization . . . . .	24
2.3.1 Resistance Calculation . . . . .	27
2.3.2 Lifetime Resistance . . . . .	30
2.4 Production Cost . . . . .	32
2.4.1 Fuzzy Logic . . . . .	35
2.4.2 Fuzzy Complexity Metric . . . . .	39
2.5 Maintenance Cost . . . . .	44
2.5.1 Corrosion Damage . . . . .	45
2.5.2 Fatigue Damage . . . . .	46
2.5.3 Maintenance Schedules . . . . .	48
2.6 Summary . . . . .	50
<b>3 Structural Trade-Offs . . . . .</b>	<b>51</b>
3.1 Maintenance Cost Estimation . . . . .	51
3.2 Trade-Offs Between Maintenance and Production . . . . .	59
3.2.1 Trade Spaces . . . . .	61
3.2.2 Effects of Service Life Extension . . . . .	65
3.3 Contributions . . . . .	67

<b>4</b>	<b>Hydrodynamic Trade-Offs</b>	<b>69</b>
4.1	Trade-Offs Between Resistance and Complexity	69
4.1.1	Transformation Functions	72
4.1.2	Problem Formulation	74
4.1.3	Trade-Spaces	78
4.2	Multi-Disciplinary Optimization of Propeller-Hull Systems	82
4.2.1	Vessel Performance	84
4.2.2	Problem Formulation	89
4.2.3	Propeller-Hull Results	93
4.3	Contributions	96
<b>5</b>	<b>Enhanced MOCO</b>	<b>99</b>
5.1	Enhanced MOCO Framework (eMOCO)	99
5.1.1	Goal Programming at the Discipline Level	101
5.1.2	Locally Elitist Genetic Algorithm (LEGA)	105
5.2	Test Problems	108
5.2.1	Multi-Objective Test Problems	108
5.2.2	Multi-Disciplinary Test Problem	113
5.3	Naval Design Case Study	117
5.3.1	Objective Function Calculation	118
5.3.2	Optimization	118
5.3.3	Results	122
5.4	Contributions	125
<b>6</b>	<b>Three Dimensional Trade Spaces</b>	<b>127</b>
6.1	Resistance-Maintenance-Production	127
6.1.1	Pareto Fronts	132
6.1.2	Design Comparisons	136
6.2	Maintenance Scheduling	147
6.2.1	Schedule Optimization	147
6.2.2	Effects of Service Extension	151
6.3	Effect of Schedule on Trade-Spaces	154
6.4	Contributions	157
<b>7</b>	<b>Conclusions</b>	<b>160</b>
7.1	Conclusions and Contributions	160
7.2	Recommendations for Future Work	165
	<b>Bibliography</b>	<b>168</b>

## LIST OF FIGURES

2.1	An example of a Pareto-front for two functions, $f_1$ and $f_2$ . . . . .	12
2.2	The process followed by a genetic algorithm to evolve a population towards their optimum. . . . .	13
2.3	A 2-dimensional example of the cuboid whose perimeter is used for the crowding distance metric. . . . .	18
2.4	XDSM for collaborative optimization architecture . . . . .	22
2.5	Example probabilistic mission profile. . . . .	31
2.6	Example of a fuzzy set and traditional set . . . . .	36
2.7	Example output fuzzy set for size . . . . .	37
2.8	An example of backset for a panel. In this example the backset is defined as $\frac{h}{L}$ . . . . .	40
2.9	The geometry that is used to calculate the backset at a given station. . .	40
2.10	The fuzzy membership set for the degree of curvature ( $b_1$ values). . . . .	43
2.11	The fuzzy membership set for the relative direction of curvatures ( $b_2$ values). . . . .	43
2.12	The fuzzy membership set for the relative cost output values. . . . .	43
3.1	The structural discretization scheme used in the proposed maintenance costing framework. . . . .	53
3.2	Probability distribution for extending the service life from 0 to 15 years. . . . .	57
3.3	Flow chart showing the calculations performed within the maintenance cost analysis. . . . .	58
3.4	Original midship section for nominal naval combatant. . . . .	62
3.5	Pareto front found using the problem formulation in equation 3.10. . . . .	62
3.6	Maintenance costs for two different ship structures. . . . .	64
4.1	Mission profiles for the two vessels . . . . .	71
4.2	A potential function for $T_l(x)$ . Note that the ends of the domain always map to zero. . . . .	73
4.3	A potential function for $T_v(z)$ . Note that the ends of the domain always map to zero. . . . .	74
4.4	The points used to formulate the constraints for the sectional area curve. . . . .	75
4.5	The points used to formulate the constraints for the waterplane area curve. . . . .	76
4.6	The two hull forms used in the optimization routine. . . . .	78
4.7	Pareto fronts for each vessel type found when solving equation 4.6. . . . .	79
4.8	Hullforms represented by nearest to utopian point in Figure 4.7. . . . .	81

4.9	Sectional area curves for ‘nearest to utopian’ vessels. . . . .	82
4.10	An example of a propeller-hull matching exercise showing the required thrust at the endurance speed of $V = 20$ kts, the open water thrust coefficient, and efficiency curves. . . . .	86
4.11	Specific fuel consumption as a function of percentage of load for the L51/60DF engine. . . . .	88
4.12	Data and process flow diagram for the hull-propeller design optimization process. . . . .	92
4.13	Convergence history of the gradient of the Lagrangian plotted against major iteration count. . . . .	93
4.14	Original container ship hullform. . . . .	94
5.1	The production cost for a structure as a function of the stiffener spacing in a single functional location. . . . .	100
5.2	The maintenance cost for a structure as a function of the stiffener spacing in a single functional location. . . . .	101
5.3	CONSTR Problem - solved with eMOCO and NSGA-II. . . . .	112
5.4	TNK Problem - solved with eMOCO and NSGA-II. . . . .	112
5.5	Basic data flow for the two-discipline example. . . . .	113
5.6	An example of a true Pareto front and threshold front. . . . .	115
5.7	The results for th MDO test problem for both the traditional and enhanced MOCO. . . . .	116
5.8	Bodyplan for nominal naval combatant . . . . .	121
5.9	Internal structure for nominal combatant. . . . .	122
5.10	Pareto front for nominal naval combatant . . . . .	123
5.11	The hull forms and structures for the vessels at the extreme ends of the Pareto front. . . . .	124
6.1	Three dimensional Pareto front for resistance, maintenance, and production. . . . .	133
6.2	Contour plots for the Pareto-front shown in Figure 6.1. . . . .	135
6.3	Bodyplans, structure, and yearly maintenance for vessels in ‘knee’ regions of various Pareto zones. . . . .	137
6.4	Bulbous bows for vessels in the ‘knee’ region. . . . .	139
6.5	Different regions of the sectional area curves for vessels A through D. . . . .	140
6.6	Different regions of the waterplane area curves for vessels A through D. . . . .	140
6.7	Yearly maintenance costs for vessels $A$ , $B$ , $C$ , and $D$ (In millions of USD). . . . .	144
6.8	Design details for vessels $R$ and $M$ . . . . .	146
6.9	The maintenance cycles found for the problem formulation in equation 6.7 for $n = 3, 4, 5$ . . . . .	149
6.10	Yearly costs for different values of $n$ and the original schedule. . . . .	150
6.11	The maintenance cycles found using no possible service life extension (ship B). . . . .	151
6.12	The maintenance cycles found using a 45 year service life (ship C). . . . .	152
6.13	Contour plot for scheduled optimization formulation. . . . .	154
6.14	Structure and Bodyplan for vessel $S$ from Figure 6.13. . . . .	156



6.15 Yearly maintenance costs for vessel  $S$ . . . . . 157

## LIST OF TABLES

2.1	Relative cost of plate based on backset values . . . . .	42
2.2	Functional locations used for modeling corrosion rates, their location code via Paik’s definitions, and the corresponding corrosion rates. . . . .	46
3.1	Minimum and maximum scantlings for each functional location ( $m$ ). . . . .	61
3.2	original and optimum scantlings for each functional location ( $m$ ). . . . .	64
3.3	Maintenance Costs for both vessels if 30 year life is realized (normalized by initial design). . . . .	66
3.4	Maintenance Costs for both vessels if 45 year life is realized (normalized by initial design). . . . .	66
4.1	Principle dimensions for initial hull forms. . . . .	78
4.2	NSGA-II parameters used in the optimization. . . . .	79
4.3	Comparison of results for different optimization methods. . . . .	95
5.1	Average generations to converge for the traditional ( $tMOCO$ ) and enhanced ( $eMOCO$ ) MOCO over 100 samples. . . . .	117
6.1	Run Parameters for System-Level Optimizer. . . . .	132
6.2	Scantlings for vessels $A$ , $B$ , $C$ , and $D$ ( $t_P$ , $t_w$ , $t_f$ ). Units are all $m$ . . . . .	142
6.3	Scantlings for vessels $A$ , $B$ , $C$ , and $D$ ( $h_w$ and $b_f$ ). Units are all $m$ . . . . .	142
6.4	Aspects of maintenance cost for different schedules ( $USD \times 10^3$ ). . . . .	149
6.5	Total maintenance cost for optimum maintenance schedules when using a deterministically 40 year service life. ( <b>Millions of USD</b> ). . . . .	153
6.6	Total maintenance cost for optimum maintenance schedules when using a deterministically 30 year service life. ( <b>Millions of USD</b> ). . . . .	153

# ABSTRACT

A Multi-Objective Collaborative Optimization Framework to Understand Trade-offs  
Between Naval Lifetime Costs Considering Production, Operation, and Maintenance

by

Dylan W. Temple

Chair: Matthew Collette

The lifetime cost of naval vessels is an increasingly important factor to ship owners and, subsequently, to ship designers. A vessel's lifetime cost is composed of various cost categories such as production, operation, and maintenance. The impact of each of these categories is important and in many instances they may be competing with each other. Design decisions regarding the hull form and structure will dictate these costs, however, in what way decisions will impact them is difficult to understand. This is especially true for naval vessels as their service life is uncertain, and changes to the operational life of a vessel can have significant unforeseen costs with respect to maintenance and operation. In order to reduce the overall lifetime cost the trade-offs between these different categories must be understood. This thesis explores a linked resistance, production, and maintenance costing model and develops a novel enhanced multi-disciplinary optimizer capable of solving the resulting problem.

Most work in cost optimization has focused on reducing a single category of cost and considering other disciplines operational constraints at best. This type of sequential or single-discipline optimization does not reveal the trade-space to the designer

and may result in non-optimal designs being developed when considering the full life-cycle cost of the vessel. Unfortunately understanding these trade-offs is difficult and traditional multi-objective optimization algorithms are unable to resolve the Pareto-fronts effectively. Presented here is a framework to aid designers in finding these trade spaces using a multi-disciplinary optimization environment.

In order to realistically represent the problem being solved a maintenance costing algorithm is developed that tracks physical damage throughout a ship's lifetime. Given that the design life of a vessel may be prolonged a probabilistic service life is implemented to account for this uncertainty. A hydrodynamic search method is also developed that facilitates efficiently searching large design spaces using a minimal number of design variables. These models allow for the development of trade-spaces that reflect the nuances of the naval design problem.

In order to utilize these models to understand the trade-offs in lifetime cost an enhanced multi-disciplinary optimization framework is developed. This algorithm uses novel techniques to facilitate solving this difficult design problem. The algorithm (eMOCO) is adopted from a multi-objective collaborative optimization framework with two enhancements. The first is the use of a decision support process, goal-programming, at the sub-system level in order to allow the discipline optimizers to reduce objective functions local to that discipline. This means that the discipline-level solutions that returned to the system-level optimizers are minimized with respect to their local variables. Secondly, a new single-objective genetic algorithm is developed specifically as a discipline-level optimizer in distributed MDO architectures. This novel GA, called the locally-elitist genetic algorithm (LEGA,) allows the discipline problem to be solved in a single execution of the discipline-level optimizer. These enhancements, tailored specifically to the naval design problem, facilitate solving for these difficult and unique trade-spaces.

This model is used to develop trade spaces between production, maintenance, and

resistance in order to understand the interaction between the different categories of cost. The results show that the trade-spaces are difficult to fully resolve and the use of a multi-disciplinary environment is necessary. They also show that by developing the trade-spaces unique understanding into the interaction between cost categories can be found that allow an engineer to design ships that have minimal lifetime cost and are robust to changes in operation or service life.

# CHAPTER 1

## Introduction

### 1.1 Research Overview

Understanding the lifetime cost of naval vessels is an inherently multi-disciplinary problem. There are different categories of lifetime cost associated with various design disciplines within naval architecture. For instance, the operational cost of a ship is tied mainly to its hydrodynamic performance via the resistance curve, whereas the maintenance cost for a ship is largely dictated by its structure. The production may be tied to its structure via raw steel cost, however, it is also influenced by the hull shape through producibility concerns. However, none of these cost categories is driven by a single discipline alone. Inevitably, each will affect the other, and these trade-offs are vital to understand in order to reduce the overall ownership costs of the ship. In current literature a large amount of work has been presented on optimizing these categories individually, however, the trade-offs between them have not been explored. Resolving these trade-spaces is difficult to impossible to do with current multi-objective optimization algorithms given the unique nature of the design space and the multi-disciplinary aspect of the problem.

In order to develop these trade-spaces it is intuitive to use multi-objective optimization routines. At a general level a designer would want to solve the following

problem in order to understand the interaction between different categories of cost:

$$\begin{aligned} & \text{minimize: } \textit{lifetime cost} (\textit{Hull}, \textit{structure}, \textit{logistics}, \dots) \\ & \text{subject to: } \textit{operational requirements} \\ & \quad \vdots \\ & \quad \textit{safety standards} \\ & \quad \vdots \\ & \quad \textit{production requirements} \\ & \quad \vdots \\ & \quad \textit{logistical requirements} \end{aligned} \tag{1.1}$$

In equation 1.1 the designer is primarily focused on reducing the cost of the vessel with respect to various naval architecture disciplines. Within this problem it is important to ensure the ship meets the vessel requirements set out for it, as can be seen in the constraints. If the maintenance cost was reduced to the point where the hydrodynamic performance was not sufficient enough to carry out its mission, the vessel design would not be adequate. Similarly, if the structural integrity was reduced for the sake of resistance to the point where the vessel was unsafe, it would clearly be a poor design choice. However, if the basic system requirements are met it may be possible to reduce the lifetime cost of the vessel by simultaneously considering these different cost categories and reducing them in a multi-disciplinary environment.

In order to be able to understand these trade-offs it is important to be able to effectively analyze and search the respective disciplines. The lifetime maintenance cost for naval vessels is difficult to analyze given that it involves projecting costs over a significant number of years. This is made even more difficult by the fact that many naval ships have their service lives extended beyond the original design life. Most estimations of maintenance cost in current literature are weight and coefficient-

based, however; in order to properly understand this trade-space it is important to use physics-based analyses to ensure the accuracy of the resulting Pareto-front. Similarly, it is important for the framework to be able to account for the inherent uncertainty in the service life of the vessel, given that a large amount of maintenance related costs can be incurred during service life extensions. In developing a maintenance costing algorithm that can account for these aspects, it becomes possible to explore the trade-offs between ship maintenance costs and other categories of lifetime cost.

It is also important to be able to effectively search the hydrodynamic sub-space, considering a large swath of the design space, while keeping a small number of design variables. It is possible for shape optimization to quickly grow in the number of design variables in order to have direct control over the ship. However, this can lead to problems becoming intractable due to the length of the design vector. Therefore, it is important to develop optimization tools that allow for large transformations to a hull form while allowing the designer to retain direct control over the shape of the hull.

However, even with analysis and optimization tools that can aid in the development of the trade-spaces, they are still difficult to resolve. As one can imagine, there are complex interactions between the various design disciplines shown in equation 1.1. Traditional optimization routines struggle to resolve Pareto-fronts between these differing design spaces, and may miss key areas of the trade-space. This means that in order to effectively solve this problem a new optimization framework is necessary. An optimization framework that can solve this problem must be able to handle the large differences between these design spaces, and the inherent difficulty in the trade-spaces. Using such an algorithm, it is possible to develop trade-spaces between different categories of lifetime cost and gain a greater understanding of the trade-offs.

Therefore this research examines if it possible to develop a framework that can effectively analyze these different disciplines in a way that takes into account the



nuances of the naval design problem. The framework this thesis aims to develop uses analyses that can account for the maintenance, operation, and production costs of a naval vessel while considering specifics such as the uncertainty in a vessel's operational life. It aims to use this proposed framework to develop trade-spaces between these cost categories and explore what benefits naval architects can gain from the ability to visualize this complex trade-space.

## 1.2 Research Contributions

The overall contribution of this thesis is the development of an optimization framework that is capable of effectively developing trade-spaces between three different categories of lifetime cost: production, operation and maintenance. This framework involves contributions in the cost analysis for lifetime maintenance, the hydrodynamic transformation method, and the overall optimizer that solves this difficult problem. While researchers in the past have developed methods to minimize individual aspects of lifetime cost, this type of multi-disciplinary optimization in order to understand the trade-offs has not been previously published. This is due to the inherent difficulties in this problem such as the drastically different nature of the sub-spaces and the flatness and weak minima present in the global trade-space. In order to solve this problem the following contributions to the field of naval design are presented in this thesis:

1. In chapter 3, a maintenance costing algorithm is developed that takes a unique approach to estimating this category of lifetime cost. Instead of taking the common weight or coefficient based approach this framework analyzes the specific structural damage throughout a ship's structure in every year of operation. The damage accounts for corrosion, fatigue, and some interaction between the two. Depending on the extent of the damage specific structural components are re-

placed, and the cost to do so is calculated. One novel feature of this algorithm is its ability to account for the facilities where the repairs are taken and the cost differences if the maintenance is planned or unplanned. This means there is an associated maintenance schedule that dictates the planned repairs for the vessel, and this can be changed or even optimized. A second is the inclusion of a probabilistic service life to account for some of the inherent uncertainty in the operational life of a naval vessel. This unique feature allows the optimizer to minimize maintenance costs for a naval ship, while ensuring these costs are robust to changes in the ship's life. This framework can be used to more effectively understand the trade-offs between the maintenance cost and other cost categories for a naval vessel.

2. Chapter 4 presents a novel transformation and constraint method for use in hydrodynamic optimization problems. The transformation method uses two perpendicular transformation functions that slide stations and waterplanes along the longitudinal and vertical axis of the ship. The optimizer alters control points that dictate the shape of this transformation function. This allows the optimizer to vary the shape of the hull greatly while only controlling a small number of design variables. However, using this method the designer has little control over the shape of the vessel, therefore, a constraint method is introduced to work with this design vector. The sectional area curve and waterplane area curve are both parametrized by the bulbous bow, the parallel midbody, and the sheer strake of the vessel. The constraints of the optimization problem then control the amount that the area curves can be altered from the initial design. The designer can easily change the degree to which these constraints are enforced, allowing them to have direct control over the shape of the vessel using constraints that are simple to implement and intuitive to understand. This transformation and constraint method allows for effective searching of a hydro-

dynamic sub-space and, thus, facilitates solving the multi-disciplinary lifetime cost problem.

3. Chapters 3 and 4 present analysis and optimization methods within individual sub-spaces of the overall problem. However, in both chapters preliminary results are shown that reveal the difficulty traditional optimizers have in solving this problem. Even in the problems examining only a single sub-space the Pareto-fronts have sharp knees or difficult to resolve regions that are important for a designer to understand. This leads to the development of an enhanced multi-disciplinary optimization (eMOCO) framework presented in chapter 5. The framework is based on a traditional multi-objective collaborative optimization (MOCO) algorithm, however, it utilizes two novel enhancements that allow it to solve the naval lifetime cost problem. In order to account for the stark differences in the hydrodynamic and structural sub-spaces a distributed approach to MDO is taken, so that completely different optimizers can be used at the discipline level that are tailored to the specific space. To take advantage of this a decision support process (DSP), goal-programming, is implemented at the discipline level. Goal-programming ensures that the usual interdisciplinary feasibility function present in a MOCO is minimized first. However, the optimizer can then minimize any number of local-objective functions (objective functions in the problem that are only affected by variables from a single discipline). This allows the discipline optimizer to pass design points to the system level optimizer that are locally minimized for each of the discipline objectives. The nature of goal-programming also allows the engineer using the algorithm to use their intuition to affect the outcome of the optimization. This can be done by altering the hierarchy of different discipline objectives in the sub-system problem to reflect the importance the designer believes they warrant.

The eMOCO also utilizes a unique discipline level optimizer that has been

developed as part of this thesis. This discipline level optimizer is called the locally-elitist genetic algorithm (LEGA) and it allows the discipline problem to be solved in a single execution of a genetic algorithm. For sub-system problems that utilize population-based optimizers this represents a significant improvement in computational efficiency for distributed MDO architectures when the system-level optimizer is also population-based. These two novel enhancements work together to create an optimization framework that is uniquely capable of solving the lifetime cost problem in the naval design space.

4. Using the eMOCO developed in chapter 5, three dimensional fronts between lifetime resistance, maintenance cost, and production cost are developed. These results are novel, as this trade-space has not yet been explored in this manner. The results show that the three dimensional front has steep sides with a small knee, making it well suited for the multi-objective approach taken. They also show that by developing these trade-spaces an important nature regarding the shape of the design space can be gained. The ‘knee’ region of this front shows that by using a multi-disciplinary approach to this optimization vessels can be designed that are balanced between the different categories of lifetime cost, and robust with respect to lifetime cost due to changes later in their life.
5. The effects of considering the maintenance schedule as a design variable were then explored. A proof of concept, showing that by doing this the overall maintenance cost could be reduced, was done using a single-objective optimization where the only design variable was the schedule. This shows that varying the maintenance schedule allows for further reduction to the maintenance cost. However, the schedules found differ significantly from fixed-interval maintenance schedule indicating that formal optimization for each design may be necessary to achieve the best performance. The three-dimensional problem was then solved

again, now allowing for the schedule to be among the structural design variable. These results revealed that by doing this, the nature of the trade-spaces can be altered to give the designer more flexibility in their choices without causing unexpected increased in lifetime cost.

## CHAPTER 2

# Background

### 2.1 Overview

This chapter will cover the current literature in the topics this thesis uses. The work presented here relies heavily on work done in the field of engineering optimization; specifically multi-objective and multi-disciplinary optimization. Brief overviews of hydrodynamic analysis and optimization, as well as structural optimization are covered. An overview of hydrodynamic analysis techniques, such as the calculation of a ship's total resistance and expected lifetime resistance metrics will be explained. Structural analysis focusing on maintenance, production, and producibility will also be discussed. The work presented in the subsequent chapters will build off these concepts to present the unique contributions of this thesis.

### 2.2 Design Optimization

Design optimization is the concept of formulating mathematical representations of engineering problems in order to minimize or maximize various performance ob-

jectives. In general terms an optimization problem is written as follows:

$$\begin{aligned} & \text{minimize: } f(\mathbf{x}) \\ & \text{with respect to: } \mathbf{x} = (x_1, x_2, \dots, x_n) \\ & \text{subject to: } g_i(\mathbf{x}) = 0, \quad i = 1, 2, \dots, k \\ & \quad \quad \quad \hat{g}_j(\mathbf{x}) \geq, \quad j = 1, 2, \dots, \hat{k} \end{aligned} \tag{2.1}$$

In equation 2.1 an objective function,  $f(\mathbf{x})$  is being minimized with respect to a vector of design variables,  $\mathbf{x} = (x_1, x_2, \dots, x_n)$ . The problem can be subjected to a number of equality,  $\mathbf{g}(\mathbf{x})$ , and inequality,  $\hat{\mathbf{g}}(\mathbf{x})$  constraints. Constraints are functions of one or more of the design variables that must be satisfied at an optimum point.

Solving these problems can become difficult, especially when the function in question is a general engineering analysis. There have been many proposed methods to finding solutions to these problems that take different approaches. One of the most common family of approaches are ‘gradient-based’ methods. As the name suggests these approaches utilize the gradient of  $f(\mathbf{x})$  in order to find a direction in variable space to search in. For functions that are  $C_1$  continuous and possesses well-defined minima these methods are extremely effective.

When the objective function or constraints are discontinuous, possess weaker minima, or contain many local minima it can be difficult for gradient-based algorithms to converge. In these cases a family of approaches known as ‘gradient-free’ can be used. These methods are mainly heuristic algorithms that rely on a variety of ways to reduce an objective function that do not require any information on its derivatives. While these methods are robust in their ability to minimize difficult functions they often take significantly longer to converge due to a larger number of required function evaluations.

Both of these approaches have merits and are tools that must be applied in the

proper circumstance to be most effective. In the case of problems such as those found in naval design there are engineering analyses that are best suited for both types of optimization. Therefore, this work focuses on developing a novel method to integrate both into a single framework that can perform effective design optimization in the naval engineering environment.

### 2.2.1 Multi-Objective Optimization

In the above discussion on optimization a single objective function is being minimized. However, in many cases in engineering there are multiple competing objectives that a designer is interested in. In order to understand the trade-offs between the different aspects of lifetime cost for naval vessels designers need to visualize the trade-space they are working in. Due to the desire to develop trade-spaces for various competing factors of lifetime cost multi-objective optimization routines are an obvious choice to use within any framework developed to solve this problem. Multi-objective algorithms are effective at developing fronts that highlight this type of trade-off and will be a key part of the proposed optimization method. A generalized multi-objective optimization is shown in equation 2.2.

$$\begin{aligned}
 &\text{minimize: } \mathbf{f}(\mathbf{x}) = (f_1(\mathbf{x}), f_2(\mathbf{x}), \dots, f_m(\mathbf{x})) \\
 &\text{with respect to: } \mathbf{x} = (x_1, x_2, \dots, x_n) \\
 &\text{subject to: } g_i(\mathbf{x}) = 0, \quad k = 1, 2, \dots, k \\
 &\quad \hat{g}_j(\mathbf{x}) \geq 0, \quad k = 1, 2, \dots, \hat{k}
 \end{aligned} \tag{2.2}$$

In equation 2.2 the objective vector,  $\mathbf{f}(\mathbf{x})$ , is being minimized with respect to the design vector,  $\mathbf{x}$ , while satisfying equality constraints,  $g_i(\mathbf{x})$ , and inequality constraints,  $\hat{g}_j(\mathbf{x})$ . If each entry of  $\mathbf{f}(\mathbf{x})$  follows the same trends with respect to  $\mathbf{x}$  then a single design that minimizes the objective vector can be found. However, in most



practical engineering applications of multi-objective optimization this will not be the case, and the objectives will compete with each other. A simple example of this could be the cost of a structure and its strength. In most cases low-cost structures will be weaker, whereas constructing the strongest possible solution will be expensive. When this is the case it is not possible to arrive at a single design, instead a Pareto-Optimal front - or a set of design points which cannot be said to be better than each other without more information given by the designer or customer is defined. An example of a Pareto-Front from [Deb \(2008\)](#) can be seen in Figure 2.1.

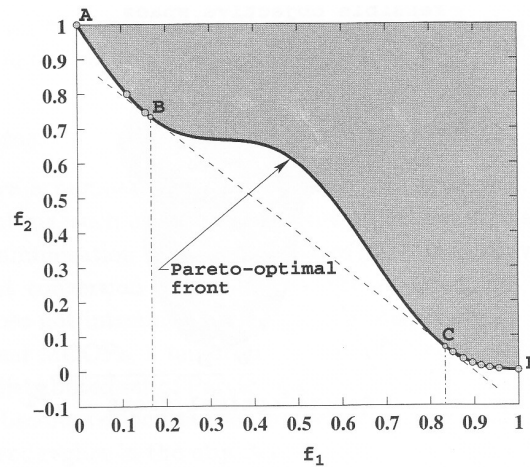


Figure 2.1: An example of a Pareto-front for two functions,  $f_1$  and  $f_2$ .

Similarly to the single objective problems discussed previously both gradient-based and gradient-free algorithms can be used to solve multi-objective problems. A common variation of the gradient-free algorithms are population based approaches. These approaches utilize a group, or population, of candidate solutions and use various heuristic methods to move the population towards the Pareto front. Their population-based nature means they are also able to search large areas of a design space in a single execution, increasing the probability of determining an optimal Pareto front. However, as they analyze entire populations of solutions they require higher numbers of calls to the objective functions than gradient-based algorithms, which increases computation time significantly. Most of the algorithms also utilize various pseudo-

random parameters to drive the evolution of the population over time, which means that as the dimension of the design vector grows, convergence becomes increasingly difficult for the routine.

Multi-objective genetic algorithms (MOGAs) are a family of gradient-free optimizers that attempt to mimic the natural processes involved in evolution to improve the objective function of a problem. This is done by by evolving a set of solutions towards an optimum point or Pareto-optimal front. A flow chart adapted from [Deb \(2008\)](#) explaining the basic idea behind genetic algorithms can be seen in Figure 2.2. The algorithm is driven by three ‘evolutionary operators’: selection, crossover,

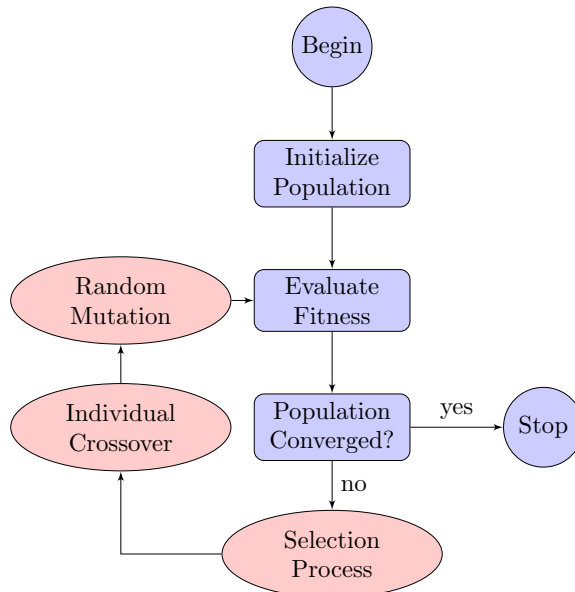


Figure 2.2: The process followed by a genetic algorithm to evolve a population towards their optimum.

and mutation (executed during the flow chart steps represented by ellipses). These operators attempt to simulate the evolutionary process in nature and advance the population of individuals towards an optimal solution within the design space with each successive generation.

The population is made up of randomly generated individuals within the design space represented by a design vector, or chromosome. Each individual is made up

of genes,  $\{x_1, x_2, \dots, x_n\}$  that define the chromosome and represents a single possible solution to the proposed problem. During the selection phase an operator is applied to the population of individuals to select various chromosomes that will continue on to the next generation. Specific pairs of these solutions are then chosen for the crossover phase in which the genes are mixed together to create a new chromosome or child individual. In the mutation phase randomly selected individuals have their genes perturbed to create new mutated individuals. Once the evolutionary operators have been applied the population must be sorted, or ranked, in some fashion. In a single-objective problem this is straight forward, however, with more than one objective function it becomes more complicated. One commonly used strategy is to give each point a rank based on domination. Domination is a method to rank two individual solutions against one another in a multi-objective problem. Given two solutions,  $x_1$  and  $x_2$ , it is defined that  $x_1$  dominates  $x_2$  if two conditions are satisfied:

1.  $x_1$  is strictly more fit than  $x_2$  for at least one objective in the multi-objective problem
2.  $x_1$  is no worse than  $x_2$  in all other objectives in the problem

In the above definition ‘more fit’ means the objective is better than the other individual. This can mean less or more depending on if the objective is being maximized or minimized. Through these evolutionary techniques the solutions are driven towards the Pareto front during each generation.

The selection of evolutionary operators that are robust and powerful is an aspect of using the MOGA that people have spent a considerable amount of time researching. The choices available depend on whether the algorithm is ‘real-coded’ or ‘binary-coded’. Some of the first implementations of the genetic algorithm were binary coded algorithms. This means that each gene within the design vector is encoded from a floating-point decimal value to a binary one during the application of evolutionary

operators and then, possibly, decoded back to its real value during the objective function evaluation. The benefit of binary coding is that it allows for intuitive and simple to implement evolutionary operators. The most common method of binary crossover is single-point crossover. This is done by randomly selecting a crossover point for two binary-coded variable values and swapping binary values around it, creating two child solutions. For example given two binary-coded values:

$$x_1 = b_1|b_2|b_3|b_4|b_5$$

$$x_2 = c_1|c_2|c_3|c_4|c_5$$

And a crossover point of 2 the resulting children would be:

$$y_1 = b_1|b_2|c_3|c_4|c_5$$

$$y_2 = c_1|c_2|b_3|b_4|b_5$$

This can be extended to multiple-point crossover by selecting any number of crossover points and performing the same operation.

Mutation is similarly straight forward when using binary coding. The most common method is to select a random binary integer from within a variable and swap it from 0 to 1 or vice versa depending on its value. While these methods are easy to implement some of the information about the problem can be lost. In some problems it is more intuitive to use real-coded design variables, as they represent some engineering problems in a more complete sense. Unfortunately, developing effective evolutionary operators can also be more difficult.

One commonly applied real-coded MOGA is the non-dominated sorting genetic algorithm II or NSGA-II. This was developed in [Deb et al. \(2002\)](#) and has been shown to be effective at developing Pareto fronts. It uses a sorting method based on individual feasibility, domination status and a crowding distance metric. Within

the algorithm specific evolutionary operators are also used to promote the effective development of a Pareto-front. For crossover the NSGA-II uses an operator called simulated binary crossover (SBX) [Deb et al. \(2002\)](#). As the name suggests it attempts to simulate the search power of single-point binary crossover. The method will create two offspring from two parents using equations 2.3 and 2.4.

$$x_i^{(1,t+1)} = 0.5 \left[ (1 + \beta_{q_i}) x_i^{(1,t)} + (1 - \beta_{q_i}) x_i^{(2,t)} \right] \quad (2.3)$$

$$x_i^{(2,t+1)} = 0.5 \left[ (1 - \beta_{q_i}) x_i^{(1,t)} + (1 + \beta_{q_i}) x_i^{(2,t)} \right] \quad (2.4)$$

In these equations  $x_i^{(1,t)}$  and  $x_i^{(2,t)}$  are the two parent solutions and  $x_i^{(1,t+1)}$  and  $x_i^{(2,t+1)}$  are their offspring.  $\beta_{q_i}$  is a parameter governing the distribution of the children with respect to their parents. It is calculated using equation 2.5.

$$\beta_{q_i} = \begin{cases} (2u_i)^{\frac{1}{\eta_c+1}} & \text{if } u_i \leq 0.5; \\ \left[ \frac{1}{2(1-u_i)} \right]^{\frac{1}{\eta_c+1}} & \text{, otherwise} \end{cases} \quad (2.5)$$

In equation 2.5  $\eta_c$  is the crossover distribution index and is chosen by the user of the algorithm and  $u_i$  is a random number in the interval  $[0, 1)$ . This is part of the stochastic nature of the algorithm, as the crossover operator will produce different offspring each time given identical parent solutions. Using these equations each pair of parent solutions can create two offspring that represent a blend of both of their chromosomes.

The second evolutionary operator the NSGA-II uses is a mutation function. The purpose of mutation is to make small perturbations in a chromosome to try and find superior regions of the design space. The NSGA-II uses the following mutation operator:

$$y_i^{(1,t+1)} = x_i^{(1,t+1)} + \left( x_i^{(U)} - x_i^{(L)} \right) \bar{\delta}_i \quad (2.6)$$

In this equation  $y_i^{(1,t+1)}$  is the new individual obtained via the mutation of individual  $x_i^{(1,t+1)}$ . The variables  $x_i^{(U)}$  and  $x_i^{(L)}$  are the upper and lower bounds of the individual being mutated and  $\bar{\delta}_i$  is a distribution of the mutated individual represented by equation 2.7.

$$\bar{\delta}_i = \begin{cases} (2r_i)^{\frac{1}{\eta_m+1}} - 1 & \text{if } r_i < 0.5 \\ 1 - [2(1 - r_i)]^{\frac{1}{\eta_m+1}} & \text{, otherwise} \end{cases} \quad (2.7)$$

The  $\bar{\delta}_i$  equation is similar to 2.5. In the equation  $r_i$  is a random variable that is an element of  $[0, 1)$  and  $\eta_m$  is known as the mutation distribution index and is chosen by the user.

The crossover and mutation operators are the primary mechanisms through which the NSGA-II is able to develop Pareto optimal fronts. One common issue associated with MOGAs is clustering. This means that, while an algorithm is able to develop Pareto-fronts, it will find solutions in clusters with large empty spaces between them. To combat this tendency the NSGA-II uses a crowding distance metric. This metric measures the Euclidean distance between a solution and the nearest neighbors on its domination front. In order to do this a cuboid is formed between the two nearest neighbors as seen in Figure 2.3 adapted from [Deb \(2008\)](#).

The crowding distance metric is then calculated using equation 2.8.

$$d_{I_j^m} = d_{I_j^m} + \frac{f_m^{(I_{j+1}^m)} - f_m^{(I_{j-1}^m)}}{f_m^{max} - f_m^{min}} \quad (2.8)$$

In equation 2.8  $d_{I_j^m}$  is the crowding distance for the individual,  $f_m^{(I_{j+1}^m)}$  and  $f_m^{(I_{j-1}^m)}$  are the objective function values of the nearest neighbors in the front, and  $f_m^{max}$  and  $f_m^{min}$  are the endpoints of the front containing individual  $i$ . The endpoints of the front are defined to have a crowding distance of  $\infty$ . This ensures that the extreme points of each domination front are not lost in subsequent generations.

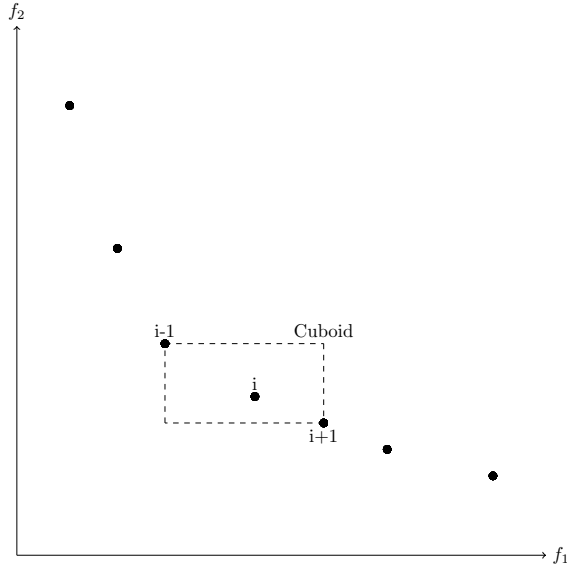


Figure 2.3: A 2-dimensional example of the cuboid whose perimeter is used for the crowding distance metric.

The final algorithm of note in the NSGA-II is its selection mechanism. The NSGA-II uses an elitist selection method, meaning that if two parents produce offspring solutions with fitness worse than their own the parents will move into the next generation while the offspring will not. This algorithm uses the following four steps to move from one generation to the next:

1. Combine parents and children into a single population of size  $2n$  (where  $n$  is the size of the original population).
2. Sort entire population according to domination status.
3. Within each domination front in the new generation sort individuals according to their crowding distance metric.
4. Use the best  $n$  individuals for the successive generation.

This process ensures that the fittest of the population move forward and that there is an even spread of solutions along the Pareto-front. Given the effectiveness of the NSGA-II in multi-objective optimization it is relied upon heavily in the work

presented in this thesis. Modified versions of it are used at both the system and sub-system level in order to facilitate the development of the trade-spaces that are being sought.

## 2.2.2 Multi-Disciplinary Optimization

The design of any large-scale engineering system is an inherently interdisciplinary problem. Naval ship design incorporates hydrodynamic, structural, electrical, combat system, firefighting, and various other systems that all interact with one another within the final product. Multi-disciplinary design optimization (MDO) focuses on simultaneously optimizing various systems, attempting to capture the inherent coupling between them to develop a solution that is optimal on a global system level. MDO has been utilized in many fields of engineering design research to optimize coupled disciplines simultaneously. Some examples of applications in different fields can be found in [Hannapel \(2012\)](#); [Hart and Vlahopoulos \(2009\)](#); [He et al. \(2011\)](#); [Li et al. \(2010\)](#); [Seto \(2010\)](#); [Windhorst et al. \(2006\)](#); ?.

Despite the obvious advantages to a multi-disciplinary approach when designing complex engineering systems, actually solving these problems can be difficult. There have been many different proposed methods, or architectures, to solve MDO problems, each of which has different strengths and weaknesses.

### 2.2.2.1 Monolithic and Distributed MDO Architectures

Monolithic architectures consider the coupled problem to be a single optimization to solve and use different multi-disciplinary analysis (MDA) tools to solve the coupled analysis within the optimization routine. Since many designers already have MDA tools that are used throughout the design of an engineering system these architectures can be less time consuming to execute. They also show strong capability for converging to a discipline and problem feasible solution when compared to other ar-



architectures (Tedford and Martins (2009)). Given that during each objective function analysis MDA tools are implemented to find coupled solutions they are particularly useful when the coupling between two disciplines is both difficult to capture and vital to the problem.

Distributed architectures, on the other hand, decompose the problem into sub-problems based on the different disciplines being analyzed. An overview of many of the methods that have been proposed can be found in ?. These architectures have the advantage that the different subspaces within the global optimization problem can be analyzed independently, allowing the various sub-problems to exploit specifics of each subspace to find globally optimal designs. Since they are decomposed at a discipline-level they also lend themselves to parallelization when being solved. However, the discretization of the problem into multiple sub-problems means that multiple optimization procedures must be executed within the system level optimizer's loop. If population-based optimizers are being utilized at both the sub-system and system level this can lead to large computational times given the need to run full population-based algorithms for each candidate solution in the system-level population.

The optimization and cost-estimation framework developed in this thesis will utilize these distributed architectures. This is because the life-time cost design space has subspaces that are inherently different in their nature. The hydrodynamic subspace, for example, is a  $C_1$  continuous subspace that is well behaved, making it a candidate for solving with gradient-based methods. However, the structural cost sub-space, which can include things such as logistical data in the form of maintenance schedules, is inherently discrete and flat, making it a problem suited for gradient-free algorithms. By using a distributed architecture the system-level problem can be decomposed into different sub-spaces and the inherent differences between the spaces can be exploited to converge on an optimum solution.

### 2.2.2.2 Collaborative Optimization

Collaborative Optimization (CO) is a distributed MDO architecture that has been applied extensively in engineering design literature. This architecture uses copies of shared design variables and coupling variables within each sub-problem of the system-level definition. The system-level problem then focuses on minimizing the objective function, while each sub-problem ensures that system-level constraints are satisfied as well as interdisciplinary compatibility (that each individual discipline agrees on the final solution when the algorithm terminates). This high level of decomposition makes the architecture a good choice when a problem has a small amount of shared information. The system-level problem can be written as (?):

$$\begin{aligned}
 & \text{minimize: } f(\mathbf{x}) \\
 & \text{with respect to: } \mathbf{x} = (x_0, \hat{x}_1, \dots, \hat{x}_N, \hat{y}) \\
 & \text{subject to: } J_i^* = \|\hat{x}_{0i} - x_0\|_2^2 + \|\hat{x}_i - x_i\|_2^2 + \|\hat{y}_i - y_i\|_2^2 = 0 \text{ for } i = 1, \dots, N \\
 & \qquad \qquad \qquad g_0(\mathbf{x}) \geq 0 \qquad \qquad \qquad (2.9)
 \end{aligned}$$

In equation 2.9 the problem is minimizing a single objective function,  $f(\mathbf{x})$ . However, the design vector  $\mathbf{x}$  now consists of shared design variables,  $x_0$ , that are used in more than one discipline analysis, discipline design variables,  $x_i$  for  $i = 1, \dots, N$ , that are only used in a single discipline analysis, and coupling variables,  $y$ , that represent information passed between the various disciplines in the analysis. The  $\hat{(\ )}$  notation represents a copy of a variable that is used by the system level. The first constraint,  $J_i^*$ , is an interdisciplinary compatibility function that ensures the copies, or targets, are equal to the variables found for each of the  $N$  disciplines. The second constraint ensures feasibility with respect to the constraints that involve shared variables and, therefore, cannot be enforced within the sub-problems.

The sub-problems can be defined as (?):

$$\begin{aligned}
& \text{minimize: } J_i(\hat{x}_0, x_i, y_i) \\
& \text{with respect to: } \hat{x}_{0_i}, x_i \\
& \text{subject to: } g_i(\hat{x}_{0_i}, x_i, y_i) \geq 0
\end{aligned} \tag{2.10}$$

In equation 2.10 the problem is minimizing the  $i^{\text{th}}$  interdisciplinary compatibility function,  $J_i$  while enforcing the sub-space specific constraints of the problem,  $g_i$ .

In order to visualize the MDO architecture a technique called Extended Design Structure Matrix (XDSM) from [Lambe and Martins \(2012\)](#) is used. This method also includes a set of notation to describe an architecture to facilitate the understanding of the problem. The XDSM for CO is shown in Figure 2.4 ?.

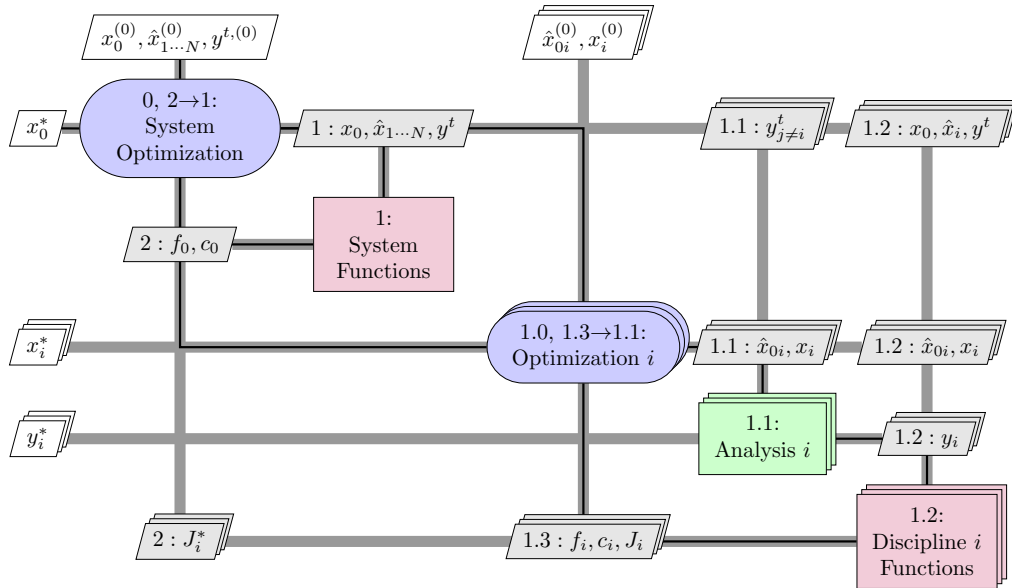


Figure 2.4: XDSM for collaborative optimization architecture

In figure 2.4 the gray lines represent the flow of data between the different aspects of the architecture and the black lines represent the flow of the process (the order in which the different pieces are executed). The colored nodes show the execution of various analysis/optimization routines, and the gray boxes show the variables that

are produced from each analysis and where they are used subsequently. For a detailed description of XDSM see [Lambe and Martins \(2012\)](#).

The description of CO above shows a single-objective formulation. However, by replacing the system-level objective with an objective function vector, as shown previously in equation 2.2, the architecture can be applied to multi-objective problems. This opens up the ability for various means of analyzing the multiple objectives, as well as methods to allow certain discipline-specific objectives to be analyzed during the sub-problem in some fashion.

There has been research into developing multiple-objective collaborative optimization (MOCO) frameworks within the MDO community. Some of this work simply uses weighted combination of the objectives within a single-objective CO framework to optimize within a multi-objective framework such as, [Long et al. \(2008\)](#); [Tapeta and Renaud \(1997\)](#). Other work has utilized decision-based metrics such as goal-programming or physical-programming to handle the multi-objective environment [Lewis et al. \(1994\)](#); [McAllister et al. \(2004\)](#). There has also been work into solving for decomposed multi-objective problems by solving for sub-problem specific Pareto fronts and combining these into system-level grand-Pareto fronts that are handled by a system-level optimizer [Aute and Azarm \(2006\)](#); [Depince et al. \(2005\)](#); [Gunawan et al. \(2003\)](#); [Ruiyi et al. \(2011\)](#). An advantage of using a distributed architecture such as CO is that different types of optimizers can be used in the discipline analysis. This allows the routine to take advantage of the nature of each individual sub-space and use algorithms that will be most robust at solving it.

One of the drawbacks of using a distributed architecture is that the scale of the problem can quickly become intractable. This is especially true when a population based algorithm, such as a GA, is used at both the system and sub-system level. If a MOGA is used to analyze the system level problem then each discipline will receive a full population of individuals to analyze. In the case of a gradient-based discipline

optimizer it is straight forward to use each candidate solution in the system-level population as the starting point for the discipline optimizer. However, when a sub-system is being solved by single objective GA current literature has always taken the approach of performing a small design of experiments around each point in the system level population and using this as an initial population for the discipline optimizer. This results in an entire genetic algorithm execution being performed for every point in the system population, which can become incredibly computationally expensive for all but the most simple of mathematical problems.

In order to address this issue a new type of single-objective algorithm, termed a ‘locally-elitist genetic algorithm’ (LEGA) is developed specifically for use as a discipline-level optimizer in distributed MDO architectures and explained in detail in chapter 5. The LEGA uses novel selection and crossover techniques to allow for the entire system-level population to be analyzed using a single execution of the genetic algorithm. It takes advantages of similarities in different regions of a single engineering design space to minimize the inter-disciplinary feasibility of the problem and find discipline-feasible points.

## 2.3 Hydrodynamic Optimization

Hydrodynamic design has a rich body of work in using optimization. Especially as CFD has become more powerful and widespread it is useful to utilize optimization to analyze complex flow patterns to improve a vessel’s performance. This has led to a large amount of work done on developing methods to effectively search a hydrodynamic design space to make solving these problems computationally tractable. A nonlinear transformation method was developed in [Zalek et al. \(2008\)](#), and a linear one in [Kuhn et al. \(2007\)](#), both to be used in hull form optimization routines. The authors of [Han et al. \(2012, 2013\)](#) used a parametric model based on fairness

optimized B-Spline curves to optimize a container ship and LPG tanker for total resistance. These parametric modeling techniques - in which hull form parameters are used to generate curves representing the vessels hull form that can be optimized and transformed - have been used and explored in [Harries et al. \(2001\)](#); [Sariz \(2006\)](#) and shown to be effective tools for reducing the drag of various hull forms. Similar parametric modeling techniques were used in [Brenner and Sener \(2011\)](#) to minimize the environmental impact of a hull form based on EEDI compliance. Narli also used a B-Spline approximation technique to fair a ship's lines using an optimization routine [Narli and Sariz \(1998\)](#). The work in [Geremia et al. \(2012\)](#) couples a high speed flow solver with multivariate optimization to optimize the fore section of a vessel described parametrically. In [Mahmood and De-bo \(2011\)](#) a genetic algorithm was used to effectively improve the hydrodynamic performance of a trimaran by transforming the vessel's shape.

Many of these methods focus on using a single objective optimization algorithm to arrive at a single, resistance optimum, hull design. While this can be useful, the work here focuses on using design optimization as a method of informing the designer to complex economic trade-offs in the design space they are working. The trends over a large portion of the space are important to understand and visualize in order to determine designs that will have minimized total owner ship costs with respect to multiple cost elements. In order to achieve this a robust and flexible transformation method is developed that can effectively search a large swath of the design space with minimal design variables. It utilizes two independent transformation vectors defined by simple B-spline curves along the vertical and longitudinal axes of the hull. The shape of the vessel is constrained by a parametric representation of the ship's sectional and water plane area curves. By using constraints that can be tightened or relaxed and a transformation method that is controlled by a small number of design variables the designer can develop trade-spaces in hydrodynamic disciplines efficiently.

Effort has also been made to develop methods of analysis to optimize or rank hull forms effectively and accurately. The authors of [Percival et al. \(2001\)](#) used a simplified CFD to find rough estimates of total resistance and were able to rank hullforms in the same manner as when experimental model test data was used, showing that capturing trends can lead to understanding a design space despite accuracy. However, in order to arrive at hydrodynamic designs through optimization alone researchers have worked to find ways to utilize higher fidelity calculations within optimization routines. This can be difficult because optimization routines need to make multiple calls to their objective function over the course of an execution, therefore, if an analysis is very computationally expensive the optimization process can become infeasibly long to complete. An approach used in [Kim et al. \(2012\)](#) is to use variable fidelity optimization, in which a low-fidelity solution is called for the majority of the objective function analysis, and a high-fidelity model is occasionally used to check the accuracy of the low-fidelity solution throughout the design space. Using high-fidelity CFD solutions directly has also been used, as in [Brizzolara et al. \(2011\)](#). Solutions such as this are especially important when attempting to make finely-focused changes to local regions of a ship's hull. In this type of circumstance it is important to have a detailed understanding of the flow around the area in order to ensure the solution is meaningful. However, when searching large areas of a design space in order to understand trends within it, it is not cost-effective to utilize such high-fidelity computations. To this end the work presented here utilizes thin-ship theory; a reasonably accurate method of finding hydrodynamic solutions that is significantly easier computationally than a non-linear CFD solution.

### 2.3.1 Resistance Calculation

The total resistance experienced by the vessel,  $R_T$  at a given speed,  $V$ , can be calculated using equation 2.11.

$$R_T = R_W + R_F + R_A + R_{Ca} \quad (2.11)$$

$R_W$  is the wave resistance,  $R_F$  is the frictional resistance,  $R_A$  is the air resistance, and  $R_{Ca}$  is a correlation allowance. The wave resistance,  $R_W$ , is the most difficult portion to solve for and it is where thin-ship theory is utilized in this work. In this implementation the resistance of a vessel at a given speed,  $U$ , can be estimated by integrating over the wave heading angles generated by the hull's wake as shown in equation 2.12:

$$R_w = \pi \rho U^2 \int_{-\frac{\pi}{2}}^{\frac{\pi}{2}} |A(\theta)| \cos^3(\theta) d\theta \quad (2.12)$$

In equation 2.12,  $\rho$  is the fluid density and  $|A(\theta)|$  is the complex wave amplitude function. The  $|A(\theta)|$  term can be calculated using Michell's integral, which is shown in equation 2.13.

$$|A(\theta)| = \frac{2}{\pi} \nu \sec^3(\theta) \iint_{cp} \frac{\partial \eta}{\partial x} e^{\nu \sec^2(\theta)(z+ix \cos(\theta))} dz dx \quad (2.13)$$

This is an integral over the vessel's centerplane and is a function of the slope of the hull in the longitudinal direction,  $\frac{\partial \eta}{\partial x}$ , and  $\nu$ ; as defined in equation 2.14.

$$\nu = \frac{g}{U^2} \quad (2.14)$$

This represents the maximum wave number for a theoretical deep water wave generated by the ship's wake. Thin ship theory using Michell's integral has been shown to yield estimates of wave resistance quickly with reasonable accuracy in [Maki et al.](#)



(2008); Tuck (1989); Tuck and Lazauskas (2008). This approach to calculating wave resistance aids in the optimization process as it is computationally inexpensive. One of the commonly cited issues with this theory is that, due to the secant term in the exponent, the integral is oscillatory, which can lead to inaccuracies. However, this issue is mainly present at the extreme ends of resistance curves, i.e. the lowest and highest speeds of a vessel's operational profile. This makes it a good approach when combined with the probabilistic profile method described below, since the resistance at higher speeds will be multiplied by a much lower probability, making it a smaller contribution to the overall resistance metric. This whitewashes some of the noise created by the oscillations in Michell's integral and makes it a strong choice for use in the design optimization framework presented here. Michell's integral also neglects some hydrodynamic effects that contribute to the ship's resistance such as flow separation, wave breaking resistance, and spray resistance. However, given that the purpose of this work is to better understand trends in the design space, as oppose to calculate exact performance numbers, Michell's integral yields a good balance of accuracy and computational speed that benefits this work.

Many of these parametric approaches to design optimization focus on making local changes to a mostly-realized hull form in order to improve the resistance at design speeds. This could, for example, mean altering the bulbous bow or curvature of the stern to increase performance by a small percentage. However, the framework that is being proposed here needs to make large global changes to an initial hull form in order to do large sweeps of the design space and give the designer a full picture of the trade-space. Because of that transformation functions are used that have direct control over the offsets of the hull themselves, and can produce shapes that vary significantly from the initial design. These functions are covered in detail in chapter 4.

Once the wave resistance has been determined the remaining components of the total resistance can be calculated. To calculate frictional resistance equation 2.15 can

be used:

$$R_F = \frac{1}{2} C_F \rho V^2 S_W \quad (2.15)$$

In equation 2.15  $S_W$  is the wetted surface area for the vessel and  $C_F$  is the coefficient of friction. This can be calculated using different friction lines proposed based on flat plate experiments. One such line is the ITTC-57 friction line as seen in equation 2.19.

$$C_{F,ITTC-57} = \frac{0.075}{(\log_{10}(R_n - 2))^2} \quad (2.16)$$

Where  $R_n$  is the Reynolds number, a non-dimensionalization of the vessel's forward speed by the kinematic viscosity of the fluid it is moving through,  $\nu$ :

$$R_n = \frac{VL}{\nu} \quad (2.17)$$

A second, more complicated friction line, is Grigson's friction line. This estimation attempts to account for differences in the frictional resistance as the boundary layer on the vessel's hull transitions from laminar to turbulent. This algorithm can be found in [Grigson \(1999\)](#). The coefficient of friction based on this theory is shown in equation 2.18.

$$C_F = (C_{F,ITTC-57}) G_1 \quad (2.18)$$

Grigson's formula is presented in terms of a coefficient,  $G_1$ , that is multiplied to the coefficient of friction for the vessel found from the ITTC-57 friction line. The ITTC-57 friction line is seen in equation 2.19 and  $G_1$  can be seen in equation 2.20.

$$C_{F,ITTC-57} = \frac{0.075}{(\log_{10}(R_n - 2))^2} \quad (2.19)$$

$$G_1 = \begin{cases} 0.09335 + 0.147x^2 - 0.071x^3 & \text{if } 1.5 \times 10^6 \leq R_n < 2 \times 10^7 \\ 1.0096 + 0.0456x - 0.013944x^2 + 0.0019444x^3 & \text{if } 2 \times 10^7 \leq R_n < 6 \times 10^9 \end{cases} \quad (2.20)$$

In these equations  $x$  is a variable based on  $R_n$  as seen in equation 2.21.

$$x = \begin{cases} \log_{10}(R_n) - 6.3 & \text{if } 1.5 \times 10^6 \leq R_n < 2 \times 10^7 \\ \log_{10}(R_n) - 7.3 & \text{if } 2 \times 10^7 \leq R_n < 6 \times 10^9 \end{cases} \quad (2.21)$$

Either of these friction lines can be used to calculate  $C_F$  in equation 2.15. The air resistance for the exposed portion of the vessel is calculated using equation 2.22 from [Manen et. al \(1988\)](#).

$$R_A = K\rho_{air} (0.3S_D) V^2 \quad (2.22)$$

In this equation  $K$  is a form factor, set to 0.6 in most cases. The density of air is  $\rho_{air}$  and  $S_D$  is the exposed, or dry, surface area. The correlation factor,  $R_{Ca}$ , is estimated using equation 2.23.

$$\frac{1}{2}C_{Ca}\rho V^2 S_W \quad (2.23)$$

Where  $C_{Ca}$  is a correlation coefficient, usually set to 0.0004. These four resistance factors sum together to determine the total resistance at a given speed.

### 2.3.2 Lifetime Resistance

One of the issues with many hydrodynamic optimization approaches is that they will consider only a few, or possibly even a single, design speed when minimizing resistance. This approach can lead to off-design performance that is significantly worse than expected and, because ships will operate at many speeds throughout an operational envelope, this can lead to worse life time performance. One approach to addressing this is to use probabilistic mission profiles to express the likelihood

a vessel will operate at various points throughout a given envelope. The expected resistance the ship will experience can then be considered as the expected value of the probability function and the resistance characteristics of the vessel. For instance, if a vessel had a probabilistic mission profile,  $p(v)$ , resembling the one in Figure 2.5, then the expected resistance for the vessel,  $R_{TE}$ , could be calculated using equation 2.24.

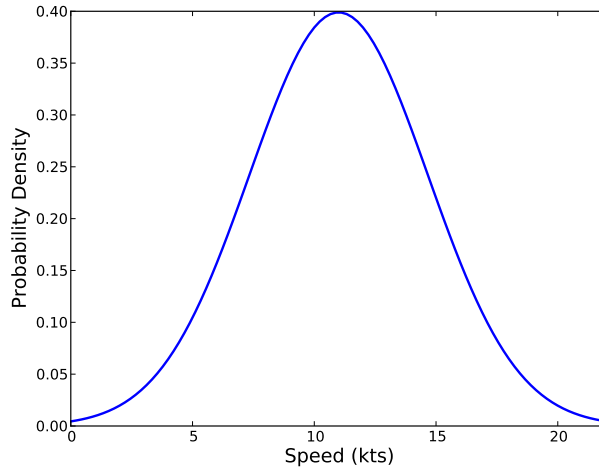


Figure 2.5: Example probabilistic mission profile.

$$R_{TE} = \int_V p(V)R_T(V)dV \quad (2.24)$$

The use of such operational profiles, especially for naval vessels, has been recommended in [Anderson et al. \(2013\)](#), where the authors used operational data from multiple DDG-class warships to construct detailed operational profiles. The results showed that the profiles were varied enough from a single design speed that it was important to account for it in design.

This approach has been used to analyze various aspects of hydrodynamic design. Kramer used a probabilistic mission profile to analyze the efficiency of water-jets on surface effect ships in [Kramer et al. \(2010\)](#). This work used a joint probabilistic density function of the ship’s speed and the sea state to define the mission profile of

the vessel. The diameter of the water-jet was optimized to maximize the efficiency of the jet over this operational envelope. Using this probabilistic method they were able to find water-jets that yielded 3-10% increases in overall efficiency compared to those designed using a single-speed design approach. Motely et. al used a similar probabilistic density function as [Kramer et al. \(2010\)](#) in [Motley and Young \(2011\)](#) to examine the use of composite based propellers for Naval combatants. The paper was investigating the use of composite materials in the construction of propellers to allow for adaptable shapes in changing flow conditions. In order to analyze and design the propellers the joint probabilistic density function was used. The designs were compared against similar propeller designs made using traditional Nickel Aluminum Bronze alloy. This shows that by utilizing a probabilistic mission profile a more complete picture of the vessel's operational envelope can be analyzed, resulting in increased lifetime hydrodynamic performance.

## 2.4 Production Cost

Designing for production has, recently, become more important to ship owners trying to reduce lifecycle costs. In [O'Rourke \(2005\)](#) the author explains that the production cost for a new naval vessel is a large amount of the acquisition project and it is important to put effort into reducing it. In [Bankes and Spicknall \(1991\)](#); [Gratsos et al. \(2009\)](#); [Rigo \(2001\)](#) the authors further discuss the importance of reducing production costs. The producibility of a vessel can often be at odds with its hydrodynamic performance and it is important to understand these trade-offs. In the vein of striving to design and manage a ship with a lifecycle cost perspective these cost elements are critical to analyze. The authors in [Inozu et al. \(2006\)](#) cite the rising emphasis on life cycle cost as a factor for shipyards to pursue efficiency improving strategies to drive-down the cost to produce vessels. A method to estimate

the production cost for a vessel during the concept design stage was proposed in [Bole \(2007\)](#). In [Krol \(1991\)](#) used a bi-level optimization scheme to minimize the cost to produce a vessel's midship section. The author's of [Mermiris et al. \(2005\)](#) formulated an optimization problem that combined both cost and structural integrity in order to reduce the initial cost of a vessel's structure while maintaining the strength of the vessel. In [Yang and Hwang \(2002\)](#) multi-objective optimization was used to optimize corrugated bulkheads for both production cost and weight, showing the potential of these algorithms in structural design. The authors of [Fafandjel et al. \(2010\)](#) used an optimization routine to find the most profitable production cost structure for a shipyard. Most work on production cost are based on the raw cost of steel and labor. This can lead to designs that ignore the producibility of the vessel, which can have a large impact on its overall production cost.

One method that focuses on steel cost and labor is from [Rahman and Caldwell \(1995\)](#), and is adapted for the presented framework. The metric calculates the cost to produce a stiffened panel based on various components of construction. The cost to produce a structural component,  $C_P$ , can be calculated using equation 2.25.

$$C_P = \sum_{i=1}^n \sum_{j=1}^9 C_{j_i} \quad (2.25)$$

In equation 2.25  $C_{j_i}$  is the cost of the  $j_{th}$  construction component for the  $i_{th}$  panel in the structure. The nine different components of construction that are used are as follows:

$C_1$  = cost of materials for hull plates

$C_2$  = cost of materials for longitudinal stiffeners

$C_3$  = cost of materials for longitudinal framers

$C_4$  = cost of welding for longitudinal stiffeners

$C_5$  = cost of welding for transverse frames

$C_6$  = cost of intersections between longitudinal stiffeners and transverse frames

$C_7$  = cost of preparation of brackets and joints

$C_8$  = cost of electricity and electrodes

$C_9$  = fabrication cost of longitudinal stiffeners and transverse frames

The equations for the calculation of each of these components can be found in [Rahman and Caldwell \(1995\)](#).

Apart from the raw cost of steel and labor, research has been done on the ‘producibility’ or complexity of a ship’s structure. Equation 2.25 does not account for the difficulty to produce a structural component which, as shown in [Rigterink et al. \(2013\)](#), can have a significant impact on the delivery cost of the vessel. There has been some research into the quantification of hull complexity. In [Bunch \(1993\)](#) a catalogue of ideas to improve the producibility of naval vessels was produced. In more recent work [Caprace and Rigo \(2012\)](#) created a complexity metric taking into account a multitude of areas including shape, assembly and material. In [Rigterink et al. \(2013\)](#) it was shown that there is a trade-off between traditional production costing metrics and producibility, the authors concluded that it is important to take producibility into consideration during design optimization in addition to conventional cost measures. The work presented here utilizes a fuzzy metric in order to assess build complexity

based on ideas proposed in [Parsons et al. \(1998\)](#). The work developed a fuzzy metric based on the backset of a plate of hull steel to determine a relative cost value for curving the steel plate based on curvature definitions in [Lamb \(1994\)](#). Each plate of the steel in the hull form is analyzed and an average of the relative cost values over the entirety of the hull is taken to generate a final crisp cost value for the entire ship.

In [Parsons et al. \(1998\)](#) the fuzzy metric was applied to a tanker ship with varying levels of parallel mid-body and the algorithm was found to produce good estimates of the producibility while accounting for the vagueness of measuring a concept such as build complexity. A similar metric was used by [Caprace et al. \(2009\)](#) to assess the producibility of straightening stiffened panels used in ship production. They were able to use the same approach as [Parsons et al. \(1998\)](#) to develop a metric for measuring producibility from a different viewpoint than [Parsons et al. \(1998\)](#).

### 2.4.1 Fuzzy Logic

The work in [Parsons et al. \(1998\)](#) uses a fuzzy logic metric to assess hull complexity. Fuzzy logic is a method of handling situations such as the relative cost presented above. It uses fuzzy membership sets instead of conventional membership sets to determine the truth value of an item within the set. Fuzzy logic, introduced in [Zadeh \(1965\)](#), is a way to handle logical assessments of inherently imprecise phenomena. A brief introduction has been presented in [Li and Parson \(1996\)](#) and is used in part here. The primary difference between fuzzy logic and traditional logic is that an element may belong to multiple sets to varying degrees, rather than the traditional binary choice of belonging or not belonging. A given fuzzy set will have a corresponding membership function that defines the degrees to which an element may belong to it. A common example, male height, is shown in Figure 2.6. This figures, taken from [Li and Parson \(1996\)](#), shows both fuzzy sets and traditional sets for short and tall men.



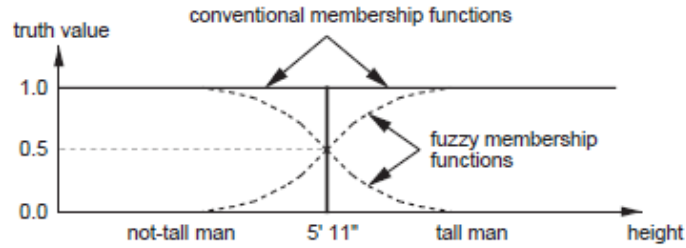


Figure 2.6: Example of a fuzzy set and traditional set

In Figure 2.6 the ‘cut-off’ point for a tall man is 5’11”. When using the traditional logic set a man who is any bit below this cut-off is designated as ‘not-tall’ and any man above the point is ‘tall’. The fuzzy logic set, however, takes into account ambiguity about the definition of ‘tall’. As can be seen by the fuzzy membership functions a man below a certain height belongs 100% to the ‘not-tall’ set and similarly so with the ‘tall-set’. However, in the region surrounding the 5’11” cut-off point an element would belong, to some degree, to both sets. At the cut-off point itself a man would belong equally to both the ‘not-tall’ and ‘tall’ set.

In order to use fuzzy logic to analyze hull producibility a fuzzy system is utilized. Fuzzy systems use fuzzy logic to take a group of crisp (single value) variables to a crisp output variable through the introduction of various fuzzy sets. A fuzzy system consists of four different operations:

1. Fuzzification
2. Linguistic rule activation
3. Fuzzy inference
4. Defuzzification

In step 1 each variable is assigned a corresponding fuzzy set and is given a truth value from that sets membership function. Based on the number of variables a fuzzy rule matrix is created that corresponds to the output variable of the fuzzy system. For

example: one could easily imagine a similar fuzzy membership function to Figure 2.6, yet for a man’s weight. Two sets would exist for ‘light man’ and ‘heavy man’ with some cut-off point where each set had a 50% truth value.

In this example an output variable could then be a man’s size. In this case three outputs would be possible: small, medium, and large. In step 2 linguistic fuzzy are rules are generated to represent the mapping of the input fuzzy sets to the output fuzzy set. These rules take the form of *IF* statements and the size example would have the following four rules:

1. IF a man is ‘tall’ AND ‘heavy’ THEN he is ‘large’
2. IF a man is ‘tall’ AND ‘light’ THEN he is ‘medium’
3. IF a man is ‘short’ AND ‘heavy’ THEN he is ‘medium’
4. IF a man is ‘short’ AND ‘light’ THEN he is ‘small’

Since a single element can be a part of multiple sets any number of these rules can be activated to different degrees. For example a man who falls 50% in ‘tall’ and ‘50% in ‘short’, but 100% in ‘heavy’ would activate rules 3 and 4. This leads to step 3 in which an output fuzzy set is needed. An example of this can be seen in Figure 2.7.

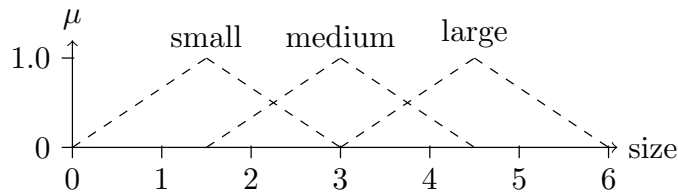


Figure 2.7: Example output fuzzy set for size

In Figure 2.7 the variable ‘size’ has been given a numeric value in the set [1, 7]. Three fuzzy membership sets for ‘small’, ‘medium’, and ‘large’ have been generated based on these values. In order to return a crisp output the activated rules must be combined with these fuzzy sets through fuzzy inference. Inference dictates what

truth value an element has in each of the output membership functions based on the rules that are activated. A common inference rule is Correlation-Minimum Inference and is described in equation 2.26.

$$\mu_z = \min [\mu_x, \mu_y] \quad (2.26)$$

Equation 2.26 says that the for an arbitrary linguistic rule: IF x AND y THEN z an element belongs to ‘z’ with a truth value corresponding to the smaller truth value of ‘a’ or ‘b’. In the ‘size’ example used above both rules 3 and 4 have been activated. Therefore the truth values in the ‘medium’ and ‘large’ sets would be as follows:

$$\mu_{large} = \min [\mu_{tall}, \mu_{heavy}] = \min [0.5, 1.0] = 0.5 \quad (2.27)$$

$$\mu_{medium} = \min [\mu_{short}, \mu_{heavy}] = \min [0.5, 1.0] = 0.5 \quad (2.28)$$

The output function is then ‘clipped’ at the corresponding truth value. In this case, this operation would generate a trapezoid from the clipped triangular membership function.

Once the truth values for each output membership function have been determined step 4 is used to map them to a single crisp output value,  $Z$ . A common method of doing this is Centroid Defuzzification as shown in equation 2.29.

$$Z = \frac{\sum_{s=1}^{\hat{S}} A_s x_s}{\sum_{s=1}^{\hat{S}} A_s} \quad (2.29)$$

Equation 2.29 is a summation of the area,  $A_s$ , of each of the  $\hat{S}$  clipped output membership functions multiplied by their centroid,  $x_s$ . This is then normalized by the sum of their areas. In the example problem each of the activated output functions is clipped at  $0.5\mu$ , thus they each have an area of  $(\frac{3.5}{2}) 0.5 = 0.5625$ . This means that

the final size value can be found by the following:

$$\frac{(0.5625)(3) + (0.5625)(4.5)}{0.5625 + 0.5625} = 3.75 \quad (2.30)$$

This shows that the final size value for the example man is 3.75. This makes sense since this is the exact point where, according to the fuzzy size set, he is 50% in ‘medium’ and 50% in large.

## 2.4.2 Fuzzy Complexity Metric

Fuzzy logic works well when applied to concepts that have inherent ambiguity such as the size example above. Size is inherently ambiguous because what one person may think of as a ‘large’ man could differ from what another thinks. This makes it easily applicable to ship producibility metrics as well. The idea of a ‘complex’ hull is not entirely quantifiable by traditional logic metrics. The exact complexity of a hull form would be assessed, rightly so, by different people or shipyards depending on their experience, capabilities, and judgments. Due to this fact a fuzzy complexity metric is used, largely based on the one proposed in [Parsons et al. \(1998\)](#), to analyze the complexity of a hull form as it relates to production. According to [Parsons et al. \(1998\)](#) it is more expensive to form and roll the steel for plates of a hull the more curvature the plate has. A flat plate is, obviously, trivial to roll out while a plate that must be highly curved in multiple directions is more difficult to produce and, therefore, more expensive. The fuzzy metric that is used aims to capture this type of hull complexity. In order to assess a plate’s curvature the backset of the plate is used. The backset of a plate is the ratio of the tallest height of the plate above the plane defined by its furthest edges to the length between those edges. A picture showing this can be seen in Figure 2.8.

The height value can be calculated using equation 2.31 and is found at

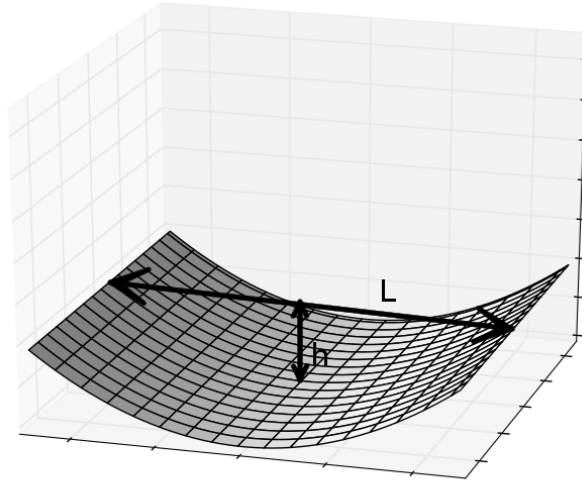


Figure 2.8: An example of backset for a panel. In this example the backset is defined as  $\frac{h}{L}$ .

each point defined in the table of offsets.

$$h = |d \cos(\phi)| \tag{2.31}$$

Where  $d$  is the distance between the edge of the hull and a flat plane connecting the previous and successive offsets and  $\phi$  is the angle between the connecting plane and a plane parallel to the ship's centerplane that passes through the previous offset. This geometry can be seen in Figure 2.9.

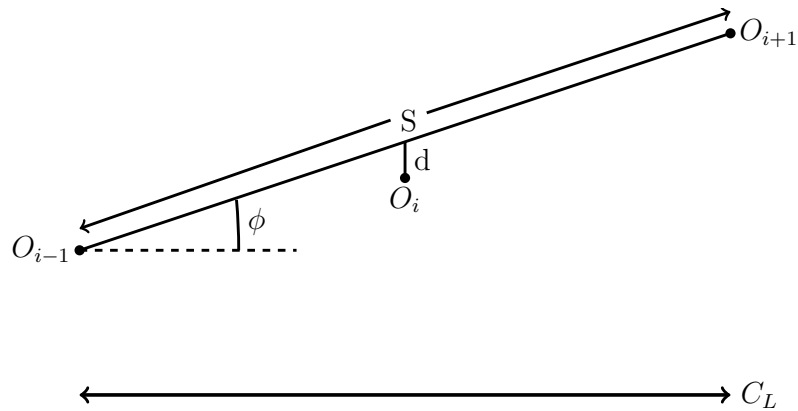


Figure 2.9: The geometry that is used to calculate the backset at a given station.

In Figure 2.9 the values  $O_i$ ,  $O_{i+1}$ , and  $O_{i-1}$  are the offsets at station  $i$ ,  $i + 1$ , and  $i - 1$ . It can be seen that the value of  $\phi$  can be found by using equation 2.32 and  $d$  can be found using equation 2.33.

$$\phi = \cos^{-1} \left( \frac{2(S_S)}{S} \right) \quad (2.32)$$

$$d = O_i - [(station\ spacing) \tan(\phi)] - O_{i-1} \quad (2.33)$$

For this work the length of each plate was defined as  $2(S_S)$  where  $S_S$  is the spacing between stations in the table of offsets. The values of  $h$  are found in both the longitudinal,  $h_l$ , and vertical directions,  $h_v$ , and are then used to form  $b_1$ , the primary backset value, and  $b_2^*$ , an intermediate secondary backset value, as seen in equations 2.34 and 2.35.

$$b_1 = \max \left\{ \frac{h_l}{L}, \frac{h_v}{L} \right\} \quad (2.34)$$

$$b_2^* = \min \left\{ \frac{h_l}{L}, \frac{h_v}{L} \right\} \quad (2.35)$$

In order to effectively assess the curvature of the plate the direction of the curvature in each principle direction must also be found. The cost is affected by the relative direction of one backset value with respect to the other - that is if the plate is curved one way in the longitudinal axis and the opposite way in the vertical axis the cost will be much higher to produce the plate than if the curvatures are in the same direction. In order to find the direction of curvature,  $K$ , equation 2.36 is used.

$$K = \frac{\text{sign}(\kappa_{longitudinal})}{\text{sign}(\kappa_{vertical})} \quad (2.36)$$

Where 2.36  $\kappa_{longitudinal}$  and  $\kappa_{vertical}$  are the curvatures of the plate in the longitudinal and vertical directions. The value of this equation will be either 1 or  $-1$ . The

curvature values can be calculated using equation 2.37.

$$\kappa = \frac{\frac{d^2y}{dx^2}}{\left[1 + \left(\frac{dy}{dx}\right)^2\right]^{\frac{3}{2}}} \quad (2.37)$$

In this equation  $\frac{dy}{dx}$  and  $\frac{d^2y}{dx^2}$  are the first and second derivatives of the curves. The values of  $b_2^*$ , and  $K$  can then be used to find the secondary backset value as seen in equation 2.38

$$b_2 = K \cdot b_2^* \quad (2.38)$$

The cost value of a plate, found in [Parsons et al. \(1998\)](#), depends on the magnitude of each backset value for the plate as well as the relative direction of curvature. The cost values corresponding to these variables are given by an industry expert as seen in table 6.4. These cost values are based on the expenses of curving the plate due to the different processes shipyards must employ depending on the extent of the curvature.

Plate	$b_1$	$b_2$	Cost
1	0.0 - 0.01	0.0 - 0.0025	1
2	0.01 - 0.16	0.0 - 0.0025	2
3	$\geq 0.16$	0.0 - 0.0025	3
4	0.01 - 0.08	0.0025 - 0.0	3
5	0.08 - 0.16	0.02 - 0.04	6
6	0.08 - 0.16	-0.02 - -0.04	9
7	$\geq 0.16$	$\geq 0.04$	8
8	$\geq 0.16$	$\leq -0.04$	12

Table 2.1: Relative cost of plate based on backset values

In Table 6.4 there are eight different plate types based on the curvatures of  $b_1$  and  $b_2$ . Given that the sensitive nature of information regarding specific costs for shipyards exact numbers are unavailable relative cost values (based on a base value of 1 for a near-flat plate) have been provided by an industry expert. However, this same ambiguity and use of relative values for output variables means that this information

is imprecise and makes it an excellent candidate for analysis with fuzzy logic. In order to do this fuzzy membership functions are made for the  $b_1$  and  $b_2$  values as well as a fuzzy output function for the relative cost values. These membership functions were proposed in [Parsons et al. \(1998\)](#). These fuzzy membership functions can be seen in Figures 2.10, 2.11, and 2.12.

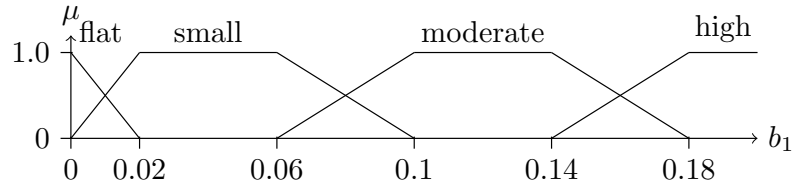


Figure 2.10: The fuzzy membership set for the degree of curvature ( $b_1$  values).

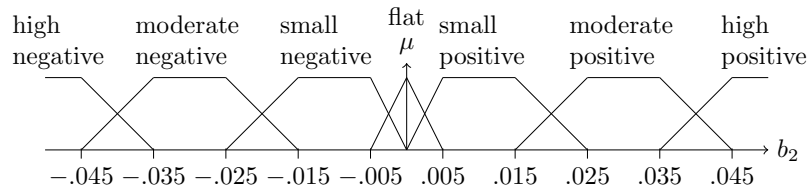


Figure 2.11: The fuzzy membership set for the relative direction of curvatures ( $b_2$  values).

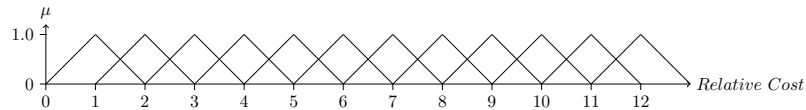


Figure 2.12: The fuzzy membership set for the relative cost output values.

Using the  $b_1$  and  $b_2$  values as described above and the fuzzy membership functions a fuzzy relative cost value,  $C_R$ , can be found. Inference and defuzzification is performed using the correlation-minimum and centroid average methods as described previously.

This calculation is done for every location defined in the table of offsets of the hull. Once the backset at every location has been determined equation 2.39 can be



used to obtain the final complexity metric,  $C_B$ .

$$C_B = \frac{\sum_{i=1}^{S_n} \sum_{j=1}^{W_n} C_R(i, j) \cdot P_A(i, j)}{SA} \quad (2.39)$$

In equation 2.39  $C_R(i, j)$  is the relative cost corresponding to the patch of hull steel at the  $i^{th}$  station and  $j^{th}$  waterline, while  $P_A(i, j)$  is the patch area of that same piece of hull steel. The values are summed across the total number of stations,  $S_n$ , and waterlines,  $W_n$  and then the double summation is divided by the total surface area of the vessel,  $SA$ .

## 2.5 Maintenance Cost

Estimating the lifetime structural maintenance cost of a vessel is a difficult problem. There are many layers of inherent uncertainty in the estimation, since it involves forecasting structural damage decades into the future for a ship that is not even fully realized yet. However, this cost will represent significant portion of the overall ownership costs for a vessel, especially if it is kept in service for years beyond its initial design point. The importance of accurately estimating maintenance cost has been discussed in [Bankes and Spicknall \(1991\)](#); [Gratsos et al. \(2009\)](#); [Rigo \(2001\)](#). In [Stambaugh and Barry \(2014\)](#) the authors outlines the current difficulty the United States Coast Guard is facing maintaining and operating their current aging fleet and the large costs associated with doing so. They posit that these costs are becoming the decisive factor that limits a vessel's service life as the economic burden becomes unsustainable. Given this state of naval design it is important to utilize the total ownership costs as a design driver, however, this overall cost include various categories such as production, operation, and maintenance.

The effect of poor maintenance policy on marine vehicles with respect to both

cost and mission capability is discussed in [Goff et al. \(2011\)](#). In [Jambulingam and Jardine \(1986\)](#) a reliability-based maintenance metric is used within a life cycle costing method to find more accurate estimates of this cost aspect. The lifetime maintenance cost of chemical tankers was used as part of the formulation of an optimization routine in [Turan et al. \(2009\)](#) using a weight-based estimation strategy. However, in order accurately predict the maintenance costs of a naval ship it is necessary to consider the physical processes of degradation that are affecting the structure. Two large sources of structural damage are corrosion and fatigue. Both of these have been the subject of much research for many years in the naval community, as well as other engineering fields.

### 2.5.1 Corrosion Damage

Corrosion damage to ship's hull represents a large portion of the structural damage it will experience over its life. This damage will contribute significantly to the cost to keep the vessel maintained and, thus, needs to be quantified in the presented work. Paik has done a number of studies on developing models for the damage ship structures experience as they age due to corrosion and the effect this damage has on their overall strength [Paik et al. \(1998, 2004, 2003a,b\)](#). These studies use statistical information from large numbers of tanker ships to develop location-based models for ship corrosion. Depending on the location within a vessel rates of decay from the corrosion damage are applied based on collected data in order to assess how fast the corrosion damage will occur throughout a vessel. In the work presented in this thesis corrosion damage is estimated based on a time-dependent model developed in [Paik et al. \(2003b\)](#) that is based on location-specific corrosion data. The model divides the vessel's structure into various functional locations and assigns corrosion rates to the plates, webs, and flanges of stiffened panels within each location. These corrosion rates are based on data taken from 230 different crude oil tankers. The functional

locations and corresponding corrosion rates used in the example presented below can be seen in table 2.2.

Table 2.2: Functional locations used for modeling corrosion rates, their location code via Paik’s definitions, and the corresponding corrosion rates.

Functional Location	Location Code	Rate ( $m/year$ )
Bottom shell plating (segregated ballast tank)	B/S-H	$0.0597 \times 10^{-3}$
Bottom shell longitudinals (web)	BSLB(W)	$0.1367 \times 10^{-3}$
Bottom shell longitudinals (flange)	BSLB(F)	$0.1127 \times 10^{-3}$
Side shell plate below draft line	B/S-V	$0.0622 \times 10^{-3}$
Side shell longitudinals in ballast tank (web)	SSLB(W)	$0.1413 \times 10^{-3}$
Side shell longitudinals in ballast tank (flange)	SSLB(F)	$0.0882 \times 10^{-3}$
Side shell plating above draft line	A/B-V	$0.06613 \times 10^{-3}$
Deck plating (segregated ballast tank)	A/B-H	$0.1084 \times 10^{-3}$
Deck longitudinals in ballast tank (web)	DLB(W)	$0.2403 \times 10^{-3}$
Deck plating	A/O-H	$0.0523 \times 10^{-3}$

Using this model a ship’s structure can be discretized into functional locations. Each panel within that location is assigned the corresponding corrosion rate and a coating life for the as-built structure. Then, during each year of operation, the thickness of each component of each panel within the different functional locations is reduced by its corrosion rate. This allows for real-time modeling of the structure’s degradation based on empirical data. This degradation can be fed back into the fatigue and strength models in order to simulate the effects of corrosion on other important structural factors.

## 2.5.2 Fatigue Damage

When estimating the lifetime cost of structural maintenance, predicting the fatigue damage the ship’s structure will experience is very important. There is a significant body of work surrounding the calculation of fatigue damage for naval vessels, a subject that is difficult to approach due to the large degree of inherent uncertainty in the processes. Due to this uncertainty a large amount of fatigue analysis uses reliability based or probabilistic calculations. Examples of these methods can be found in [Ayyub](#)

et al. (2002); Collette and Incecik (2006); Kwon et al. (2013); Souza and Ayyub (2000); Wirsching (1984). Finite element methods have also been used in Tasdemir and Nohut (2012) for the fatigue analysis of hinged-deck designs. One of the difficulties in fatigue analysis is both the prediction and detection of the initial structural flaw. The prediction of its characteristics has been addressed in Sankararaman et al. (2010) and Wang et al. (2013) provides a good overview of current sensor technology used to detect fatigue damage. A probabilistic fatigue analysis method is presented in Collette (2011) and is an adaptation of a traditional S-N approach to estimating structural fatigue. In the traditional approach the number of cycles until a fatigue crack initiates,  $N_I$ , can be seen in 2.40.

$$N_I = \frac{D_{CR}A}{K_f^m \Delta\sigma^m} \quad (2.40)$$

This equation is based off of the limit state found in Ayyub et al. (2002). In 2.40  $\Delta\sigma$  is an equivalent stress range a fatigue detail experiences,  $k_f$  is a stress uncertainty term, and  $D_{CR}$  is the Palmgren-Miner cumulative damage index. The  $A$  and  $m$  terms are experimentally determined constants. As can be seen, in a traditional formulation  $N_I$  is a deterministic variable, however, in this framework it is considered to be random. If it is assumed that  $A$ ,  $k_f$ , and  $D_{CR}$  all follow a log-normal distribution then it follows that  $N_I$  will as well. The distribution of  $N_I$  will be defined by the log-normal parameters  $\lambda_I$  and  $\zeta_I$ , which can be calculated by using 2.41 and 2.42.

$$\lambda_I = \lambda_{D_{CR}} + \lambda_A - m (\lambda_{k_f} + (\ln(\Delta\sigma))) \quad (2.41)$$

$$\zeta_I = \sqrt{\zeta_{D_{CR}}^2 + \zeta_A^2 + (m\zeta_{k_f})^2} \quad (2.42)$$

In the above equations  $\lambda_{D_{CR}}$ ,  $\lambda_A$ ,  $\lambda_{k_f}$ ,  $\zeta_{D_{CR}}$ ,  $\zeta_A$ , and  $\zeta_{k_f}$  are the parameters governing the assumed distributions of  $D_{CR}$ ,  $A$ , and  $k_f$ . Using a distribution based on  $\lambda_I$  and  $\zeta_I$  a probability density function,  $p(t)$ , and a cumulative probability function,  $P(T)$  describing the probability that a fatigue crack exists at time  $t$  can be defined.

These functions can be formed using the standard log-normal PDF and CDF as seen in equations 2.43 and 2.44.

$$p(t) = \frac{1}{\zeta_I \sqrt{2\pi t}} \exp\left(\frac{(\ln(t) - \lambda_I)^2}{2\zeta_I^2}\right) \quad (2.43)$$

$$P(T) = \int_0^\infty p(t) dt \quad (2.44)$$

If the assumption is then made that the detail is inspected at evenly spaced time-intervals,  $I$ , the probability of detecting a fatigue crack initiation in a given time interval,  $I_n$ , can be calculated using 2.45.

$$P_{crack}(I_n) = P(I_n) - P(I_{n-1}) \quad (2.45)$$

This equation can be modified to allow fatigue details to require further maintenance after an initial repair in a prior time interval by using 2.46.

$$P_{crack}(I_n) = P(I_n) - P(I_{n-1}) + \sum_{i=1}^{n-1} [P(I_i) - P(I_{i-1})][P(I_{n-i}) - P(I_{n-i-1})] \quad (2.46)$$

This method of analyzing fatigue damage is utilized in the current version of the proposed framework, along with a corrosion model based on the work done by Paik in [Paik et al. \(2003b\)](#).

### 2.5.3 Maintenance Schedules

The effect of scheduled maintenance cycles on the lifetime ownership cost of a naval vessel is significant. Firstly, it will dramatically affect the degradation of the structure as damaged structural members will be replaced over time before they fail. However, the cycles themselves represent large investments to the ship owner as the repairs and associated facilities are expensive, especially for navy ships. In most cases today

the maintenance schedule is not correlated to the engineering design of the vessel. Fixed-interval scheduling is widely utilized and is based off of fleet logistics instead of structural design. While the logistics of organizing a fleet of ships are certainly far from trivial, and vital to the mission readiness of the navy, large expenditures may be being wasted by performing maintenance cycles when the effects on the ship's operability and available service life may not be large. This makes it desirable to tailor a vessel's structure and her maintenance logistics to one another. By doing this the ship will only have scheduled repairs done to her when it will yield the most benefit for the investment. By utilizing this approach alongside an analysis of service life uncertainty a ship's structure can be designed that will have minimized structural maintenance cost and be robustly able to have its operational life extended with minimal investment put in.

In operations engineering there has been a large amount of work into machine maintenance policy for various machine layouts, repair qualities, and scheduling policies. Examples of this work can be found in [Jayabalan and Chaudhuri \(1992\)](#); [Joshi and Gupta \(1986\)](#); [Kuo and Chang \(2007\)](#); [Lee and Chen \(2000\)](#); [Lin and Huang \(2010\)](#). There is a body of work on optimizing the maintenance or inspection strategy for engineering structures. The majority of this work originates in the upkeep of bridges and other permanently monitored systems. Methods to optimize the inspection and repair strategy for bridges using a reliability-based metric to analyze fatigue damage at known stress hotspots are shown to be effective in [Chung et al. \(2006\)](#); [Junca and Sanchez-Silva \(2013\)](#); [Kim and Frangopol \(2011a\)](#); [Soliman et al. \(2013\)](#). There has been efforts to extend the methodology of this work to the naval environment. The work in [Kim and Frangopol \(2010, 2011b,c\)](#); [Kwon and Frangopol \(2012\)](#) utilizes fatigue-based reliability metrics to optimize the inspection and maintenance of single fatigue details in naval ships. The author of [Li \(2005\)](#) used a similar strategy, however, based the reliability metric off of a corrosion model. The work in [Kim et al.](#)

(2013) created a reliability metric using both fatigue and corrosion to optimize the inspection strategy for a general large engineering system such as bridges, ships and buildings.

Most of this work, however, focuses on algorithms and planning strategies developed for general engineering structures such as bridges and buildings, not specifically for naval vessels. The repair needs of naval vessels are fairly unique, as is the logistical scheduling and costs associated with repair facilities and policies. Most current work also focuses on a single, or possibly a few, structural 'hotspots' where stress is known to be concentrated. The framework utilized for this work focuses on fatigue and corrosion models specifically designed for analyzing naval vessels and monitors an entire structure to determine panel replacement and repair needs within the system.

## 2.6 Summary

Though it is clear that a large amount of work has been done to analyze and design within the spaces of resistance, maintenance, and production, very little is understood about the interaction between these three competing categories of lifetime cost. In the subsequent chapters, a framework to analyze the maintenance cost of a naval vessel is introduced along with preliminary two dimensional trade-space explorations using it. A hydrodynamic search method that is efficient at searching wide swaths of a design space is also developed. Finally an enhanced multi-disciplinary framework is developed in order to address the specific challenges of understanding the trade-offs between all three cost categories. Three dimensional Pareto-fronts are then developed to examine the nature of these trade-offs, and the potential benefit of allowing the maintenance schedule in this type of solution is explored.

## CHAPTER 3

# Structural Trade-Offs

### 3.1 Maintenance Cost Estimation

As stated earlier, the cost to maintain a ship over its lifetime is becoming an increasingly important factor to both owners and operators. In [Stambaugh and Barry \(2014\)](#) the author describes how the old adage of ‘carry cargo, not steel’ is being shown to be obsolete as governments struggle to maintain their aging military fleets. In fact, the lifetime of a ship is now being determined by the cost to continue maintaining it. This makes three things of vital importance to navy fleets moving forward:

- The maintenance cost over a ship’s lifetime is minimized as much as possible.
- It is possible to execute a service life extension program on a vessel, if unforeseen circumstances demand it.
- This service life extension can be implemented with minimal cost incurred due to extra structural maintenance.

In order to do this it is necessary to have a framework to analyze the lifetime maintenance cost of a new vessel. As has been previously stated, the current literature mainly uses two approaches to do this: either coefficient and weight based estimations or estimations based on first-principles that focus only on select structural ‘hot-spots’ in the vessel. Focusing on structural hot-spots is an excellent form of analysis to ensure



safety and prevent catastrophic failure of a vessel; which is of chief importance to a structural engineer to be sure. In the type of scenario explored in this work, however, it is assumed that the vessel is safe to operate, and the limiting factor is the cost to maintain it. This makes it desirable to have a framework that can analyze large structures using first-principles approaches to understand how the ships operation will degrade the structure and impact maintenance costs. One of the features of the proposed framework is its ability to associate a maintenance schedule with a structure. The proposed maintenance costing algorithm and the related optimization are printed in [Temple and Collette \(2015a\)](#). The schedule that a vessel is maintained on is critical to its operation, as it must be dictated years prior in accordance with the ship’s mission. It dictates when the ship can be operational, what her missions will be, and how long she will operate without maintenance. Due to the high cost of maintenance facilities for naval vessels deviation from this schedule can be incredibly costly and, therefore, it must be taken into account when analyzing the maintenance cost.

In order to do this a ship’s structure is first discretized at three different levels: functional location, stiffened panel, and fatigue details. This can be seen in Figure 3.1. The structure shown in this figure is discretized into seven functional locations, 79 stiffened plates, and 280 individual fatigue details. This shows the level of detail within the structure that the proposed framework is capable of tracking.

In order to estimate the overall maintenance cost of the vessel,  $C_{MT}$ , a yearly cost to maintain the ship is estimated,  $C_{Y_i}$ , using 3.1.

$$C_{Y_i} = \begin{cases} C_{S_i} + C_{F_i} + C_{R_i} & \text{if } i \in \{S\} \\ C_{C_i} + C_{F_i} + C_{R_i} & \text{otherwise} \end{cases} \quad (3.1)$$

In equation 3.1 the set  $\{S\}$  represents the set of all years in which planned maintenance is performed. The total yearly maintenance cost is then calculated using four

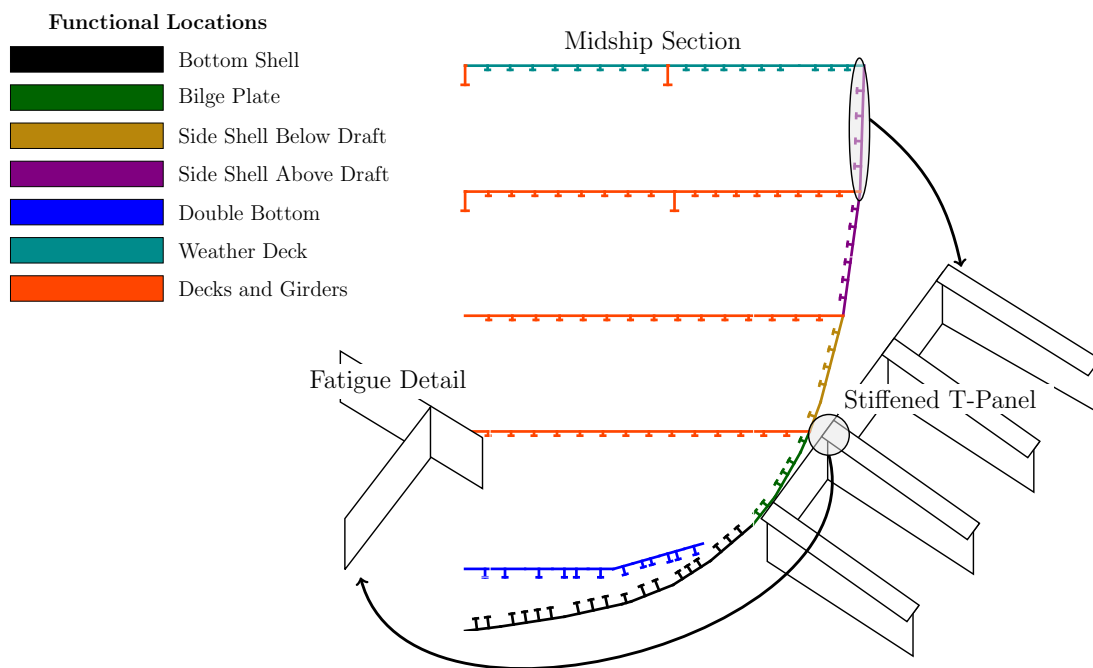


Figure 3.1: The structural discretization scheme used in the proposed maintenance costing framework.

different factors:  $C_{F_i}$ ,  $C_{C_i}$ ,  $C_{S_i}$ , and  $C_{R_i}$ . These represent costs incurred from due to fatigue damage, those due to corrosion damage, those from scheduled maintenance, and costs charged by maintenance facilities respectively. Each of these cost factors is discussed below.

The yearly costs due to fatigue damage,  $C_{F_i}$ , is calculated using equation 3.2.

$$C_{F_i} = \sum_{d=1}^m P_{crack_d}(I_n)(C_{crack}) \quad (3.2)$$

Equation 3.2 is a summation over the  $m$  fatigue details used to describe the vessel's structure of the probability a crack has occurred in that detail using equation 2.46,  $P_{crack_d}$ , times the assumed cost of repairing a fatigue crack,  $C_{crack}$ . These yearly costs, if no repairs are done to the structure, will incrementally increase over the service life of the ship if no other repairs are made as it becomes increasingly likely that a crack has been detected in each fatigue detail.

The costs due to corrosion,  $C_{C_i}$  and scheduled costs,  $C_{S_i}$ , are both calculated using the corrosion model damage model described in chapter 2. The value of  $C_{C_i}$  is based on repairs that must be done in year  $i$  of the vessel's service life in order to maintain local and global strength of structure as seen in equation 3.3.

$$C_{C_i} = \left( \sum_{j=1}^n \begin{cases} C_{p_j} & \text{if } t_{p_j}, t_{w_j}, t_{f_j} < t_{min} \\ 0 & \text{otherwise} \end{cases} \right) + C_{M_i} \quad (3.3)$$

In equation 3.3  $C_{p_j}$  is the cost to produce the  $j^{th}$  panel based on the costing components in equation 2.25. At the initialization of the framework pre-defined limits are set for the thickness of the plate,  $t_p$ , web,  $t_w$ , and flange,  $t_f$ , of each stiffened panel. If in year  $i$  any of these limits have been exceeded because of yearly corrosion for a given panel, that panel is replaced and the cost to replace it,  $C_{p_j}$  is incurred by the framework. While these costs are based on the local corrosion of panels the

term  $C_{M_i}$  is based on a global check. During each year of operation a smith-type progressive collapse analysis [Smith \(1977\)](#) is used to determine the ultimate moment in both hogging and sagging of the corroded structure. If either of these moments fail then panels in the structure are replaced until the threshold is met, and costs are incurred using equation 2.25.

The second cost factor derived from the corrosion model are the scheduled costs,  $C_{S_i}$ . These costs are based on the maintenance schedule associated with the structure at the beginning of the framework. During a year in which repairs are scheduled the framework will forecast corrosion damage out to the next scheduled maintenance cycle and replace panels that will fail within that time span. This can be seen in equation 3.4.

$$C_{S_i} = \sum_{i=1}^m C_{p_i} \quad (3.4)$$

Where  $m$  is the number of panels that will fail in the given time span and  $C_{p_i}$  is the cost to replace an individual panel. In the current model it is assumed that forecasting of structural damage is perfect and, therefore, any panel that will fail due to corrosion in that time span is replaced.

The final aspect of yearly maintenance are the facility rates,  $C_{R_i}$ . This represents the assumed costs from repair facilities and crews to carry out the maintenance described in the above sections. Another aspect of naval maintenance that separates it from other large engineering systems is the high cost and small availability of repair facilities that can accommodate them. In this work three different kinds of facility costs are considered: scheduled dry-docking, unscheduled dry-docking, and pier-side maintenance. If year  $i$  is contained in  $\{S\}$ , then the costs associated with scheduled dry-docking is incurred. If year  $i$  is not contained in  $\{S\}$  and maintenance must be performed (i.e. costs due to equation 3.3) then either the unscheduled dry-docking or pier side maintenance charge is used. The charge, in this circumstance, is chosen based on the functional location assigned to the panels that need to be replaced. For

most of the panels it is assumed that replacement must be done in dry-dock, however, for certain functional locations the panels can be replaced by pier-side maintenance crews.

One of the major difficulties with estimating the lifetime maintenance cost of naval vessels is the fact that many are being forced to remain operational for substantial time beyond their original design horizon. This uncertainty is important to capture for multiple reasons. First, it is important the vessel is able to have a service life extension, as it is possible that a government will be unable to begin a new acquisition program and it is undesirable to simply shrink the fleet. Second, it must be possible to execute a service life extension without a large cost incurred due to maintenance costs to keep the vessel operational. Capturing this uncertainty, in order to robustly design to account for it, is done in this framework using an estimate probability distribution of an extension to the vessel's service life. This is done by assuming a probability density function,  $p_e(t)$ , that represents the probability of extending the service life of the vessel to year  $t$ . In this work  $p_e(t)$  is based on a Beta distribution as seen in 3.5.

$$p_e(t) = \begin{cases} 1 & \text{if } t \leq L_D \\ \frac{x^{\alpha-1}(1-x)^{\beta-1}}{B(\alpha,\beta)} & \text{otherwise} \end{cases} \quad (3.5)$$

In 3.5  $L_D$  is the design service life of the naval ship,  $\alpha$  and  $\beta$  are the parameters of the beta distribution and  $B(\alpha, \beta)$  is the beta function, which is used in beta distributions as a normalization constant and is defined in 3.6.  $x$  is between 0 and 1 and is calculated using 3.7.

$$B(\alpha, \beta) = \int_0^1 y^{\alpha-1}(1-y)^{\beta-1} dy \quad (3.6)$$

$$x = \frac{(t - L_D)}{(L_E - L_D)} \text{ for } t = L_D, L_D + 1, L_D + 2, \dots, L_E \quad (3.7)$$

The  $\alpha$  and  $\beta$  parameters that are used in this work are 1 and 3 respectively. The design service life of the ship,  $L_D$ , is assumed to be 30 years and the maximum

extension,  $L_E$ , is assumed to be 15 years. The resulting probability distribution of extending the life of the vessel from 0 to 15 years is shown in 3.2.

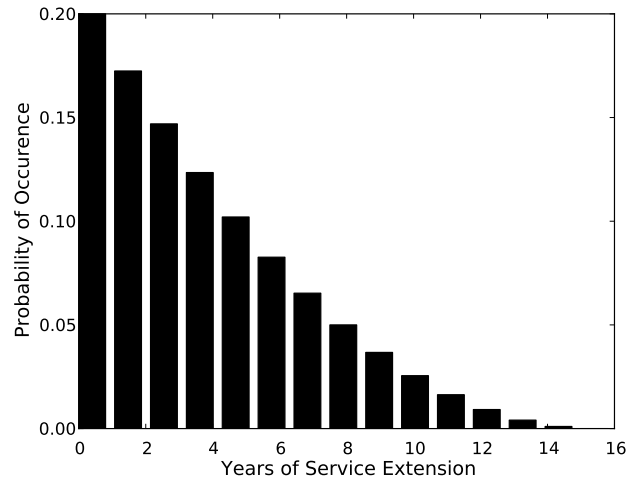


Figure 3.2: Probability distribution for extending the service life from 0 to 15 years.

The probabilistic cost of operating in year  $i$ ,  $C_{E_i}$ , then calculated using 3.8.

$$C_{E_i} = p_e(i) (C_{Y_i}) \quad (3.8)$$

This allows the total lifetime maintenance cost for the vessel's structure,  $C_T$ , to be calculated using 3.9.

$$C_T = \sum_{i=1}^{L_E} C_{E_i} \quad (3.9)$$

A flowchart showing the process used to calculate the total lifetime maintenance cost using the above equations can be seen in figure 3.3.

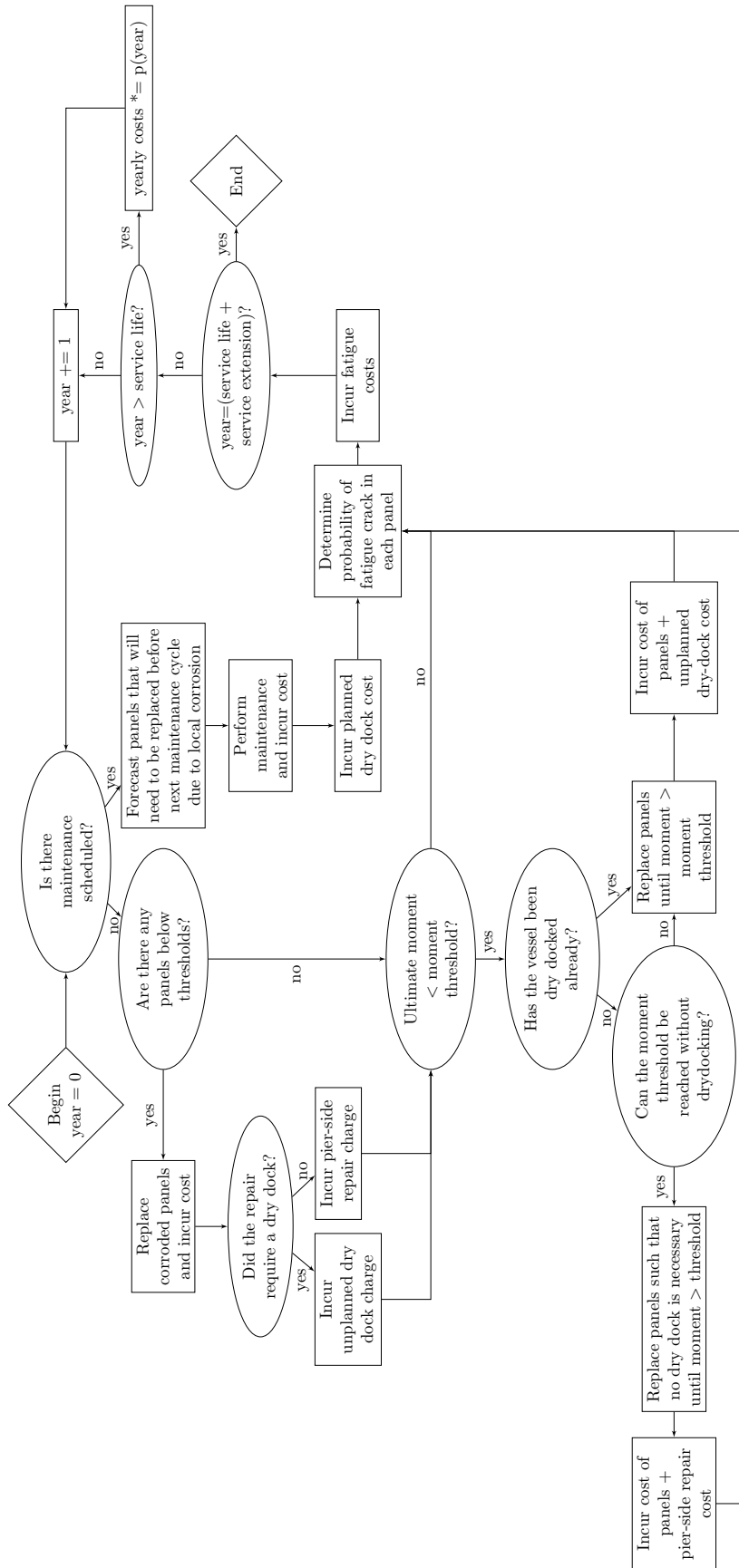


Figure 3.3: Flow chart showing the calculations performed within the maintenance cost analysis.

This maintenance costing framework is able to track dozens of panels and hundreds of fatigue details over the vessel's entire life. By using first-principle based analysis of the structural degradation along with information about the schedule and facilities of any repairs, it is able to create a picture of how much a ship structure will cost to maintain. Finally, it is able to incorporate a probabilistic service life extension in order to account for the associated costs.

## 3.2 Trade-Offs Between Maintenance and Production

Within the structural design space engineers can minimize both the cost to produce a vessel's structure and the cost to maintain it. Thus, it is important to design the internal structure of a naval vessel to strike an effective balance between these two competing aspects of costs in order to minimize the monetary impact to the ship owner over the entire lifetime of the vessel. The maintenance costing algorithm presented above is useful for understanding this type of trade-off since it is important not only to minimize maintenance costs, but also to ensure that these expenses are robust with respect to changes in the service life of the ship as it ages. The inclusion of the schedule and facility logistics in the proposed algorithm aids in accomplishing this. A MOGA is used, along with the maintenance cost framework shown above and the raw steel costing seen in equation 2.25, to develop trade-spaces between these two objectives. The trade-offs between the two, when analyzed under service life uncertainty, are then explored.

In order to use the framework described as a tool for structural design it was linked the non-dominated sorting genetic algorithm from [Deb et al. \(2002\)](#) described in chapter 2. Using the equations in the above sections the optimization problem can be formulated as seen in equation 3.10.



$$\begin{aligned}
& \text{minimize: } f(\mathbf{x}) = (C_T(\mathbf{x}), C_P(\mathbf{x})) \\
& \text{with respect to: } \mathbf{x} = (t_p, t_w, t_f, h_w, b_f, m_s)_i \text{ for } i = 1 \text{ to } n_f \\
& \text{subject to: } M_S \leq 1.10L_S \\
& \quad M_H \leq 1.10L_H \\
& \quad SM_p \leq SM_{p_I} \quad \forall p \\
& \quad \left( \frac{s_s}{t_p} \right)_p \leq \left( \frac{s_s}{t_p} \right)_{p_I} \quad \forall p \\
& \quad W_s \leq 1.10W_{orig} \\
& \quad s_{s_p} > b_{f_p} \quad \forall p \\
& \quad \min_x |c(x)_i - c(x)_j| \geq 0.085 \quad \forall i, j \tag{3.10}
\end{aligned}$$

In equation 3.10 total maintenance cost,  $C_T(\mathbf{x})$ , and the total production cost,  $C_P(\mathbf{x})$  are being minimized. The design vector,  $\mathbf{x}$ , represents the scantlings for the stiffened T-panels within the  $i^{th}$  functional location defined for the corrosion model. The scantlings modified by the genetic algorithm are the plate thickness,  $t_p$ , the web thickness,  $t_w$ , the flange thickness,  $t_f$ , the web height,  $h_w$ , and the flange breadth,  $b_f$ . The final variable within each functional locations design,  $m_s$ , is a multiplier for the stiffener spacing. The original stiffener spacing is multiplied by  $m_s$ , and then the number of stiffeners is adjusted to ensure this spacing on a given panel.

The optimizer will also ensure that a feasible design has as-built ultimate moments in sagging,  $M_S$ , and hogging,  $M_H$ , at least as great as 110% the limits set for both these moments,  $L_S$  and  $L_H$  that will be checked each year. The section modulus of each panel over all stiffeners,  $SM_P$ , is ensured to be at least as great as the section modulus of that panel in the original design,  $SM_{P_I}$  and the spacing to thickness ratio,  $\left( \frac{s_s}{t_p} \right)_p$ , is not greater than the original,  $\left( \frac{s_s}{t_p} \right)_{p_I}$ . In order to ensure that the

Pareto front does not contain ship structures significantly heavier than the original, a constraint is added to ensure that the weight of a structure,  $W_s$ , does not exceed the original,  $W_{orig}$ , by more than 10%. The last two constraints make sure that the stiffener spacing for each panel,  $s_{sp}$ , is not less than the flange breadth,  $b_{fp}$  for each panel and that two structural components (all pieces of a stiffened panel besides the plate),  $c(x)_i$  and  $c(x)_j$  are not within 8 and a half millimeters of each other. The bounds for each of the variables within each of the functional locations can be seen in table 3.1.

Table 3.1: Minimum and maximum scantlings for each functional location ( $m$ ).

Functional Location		$t_p$	$t_w$	$t_f$	$h_w$	$b_f$	$m_s$
Bottom Shell	min	0.003	0.003	0.003	0.100	0.070	50%
	max	0.012	0.010	0.015	0.300	0.150	150%
Side Shell	min	0.004	0.003	0.003	0.100	0.070	50%
	max	0.014	0.010	0.015	0.300	0.150	150%
Side Shell Below Draft	min	0.004	0.003	0.003	0.100	0.070	50%
	max	0.014	0.010	0.015	0.300	0.150	150%
Double Bottom	min	0.004	0.003	0.003	0.100	0.070	50%
	max	0.015	0.010	0.015	0.300	0.150	150%
Weather Deck	min	0.006	0.003	0.003	0.070	0.070	50%
	max	0.015	0.015	0.030	0.500	0.200	150%
Deck Plate	min	0.003	0.003	0.003	0.070	0.070	50%
	max	0.010	0.015	0.030	0.500	0.200	150%

Using this problem formulation the genetic algorithm is allowed to evolve a population of 96 individuals over 250 generations, enough to show convergence of the final Pareto front. The initial structure used is based on a nominal structure for a DTMB-5145 naval combatant found in [Ashe et al. \(2009\)](#) and can be seen in Figure 3.4.

### 3.2.1 Trade Spaces

The Pareto front found using this problem formulation can be seen in Figure 5.10. In this figure the results are normalized by the values for the original structure.

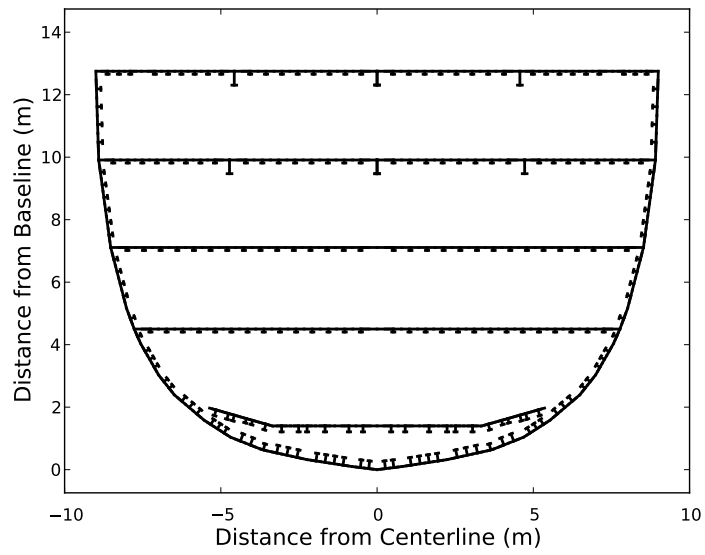


Figure 3.4: Original midship section for nominal naval combatant.

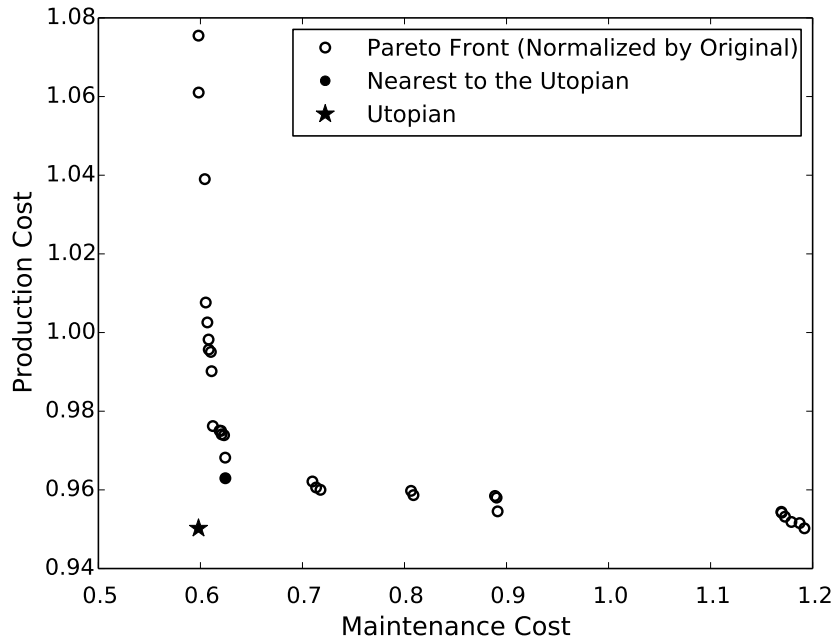


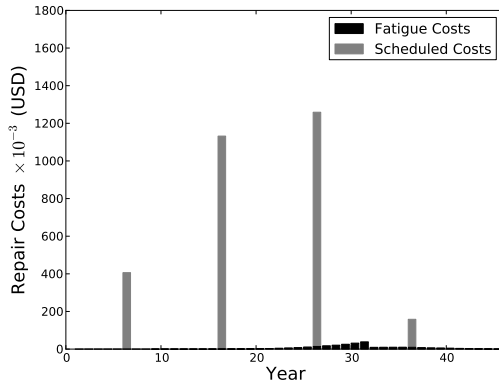
Figure 3.5: Pareto front found using the problem formulation in equation 3.10.

These results show that an optimization algorithm using the presented approach to maintenance cost estimation can develop structural designs that are superior with respect to both production and maintenance; saving the shipowner costs throughout the vessel’s life. They also show that there is a clear trade-off between these two objectives. The nature of this trade-space is valuable information for a structural engineer, as it is advantageous to design within the knee of this front. Outside of this area a small decrease in one objective will correspond to a large sacrifice in the other. The shape of the front is also important. The fact that the front has steep sides, forming close to a  $90^0$  angle, shows that single-objective optimization may result in large performance losses for one objective for the sake of minimal gains in the primary one. Since a small change in one objective leads to a large change in the other, it is vital to design within the ‘knee’ and multi-objective routines are ideal to locate this point.

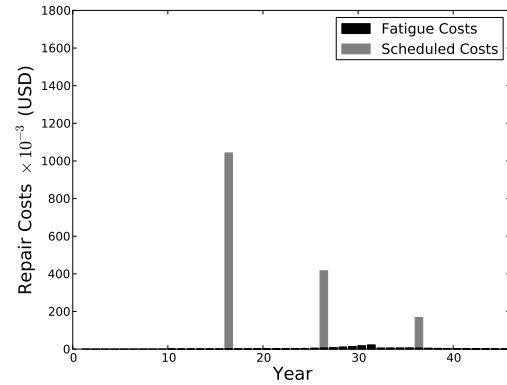
The point labeled ‘nearest to the utopian’ lies in the knee of this front. If the furthest ends of a  $k$  dimensional Pareto-front are labeled as  $(f_1^0, \dots, f_k^0)$  then the Utopian point is  $(f_1^0, \dots, f_k^0)^T$ . This point would, clearly, dominate the entire Pareto-front and, unfortunately, is not a feasible design point. However, the ‘nearest to the utopian’ is defined as the point on the Pareto-front that minimizes the Euclidean distance from the utopian point. The differences between this structure (labeled ‘opt’) and the original (labeled ‘orig’) can be seen in table 3.2. Table 3.2 shows that optimizer is increasing the overall size of stiffeners, while reducing their number in key locations. Areas of the vessel that do not need to be replaced as regularly during maintenance cycles remain largely unchanged. By utilizing this type of framework an engineer can better understand how to design structures to ensure they are within an advantageous area of the design space. In order to see how the optimizer is saving money during maintenance the yearly costs for the original design and the ‘nearest to the utopian’ structure are shown in Figure 3.6.

Table 3.2: original and optimum scantlings for each functional location ( $m$ ).

Functional Location		$t_p$	$t_w$	$t_f$	$h_w$	$b_f$	$m_s$
Bottom Shell	orig	0.0067	0.0062	0.008	0.224	0.101	100%
	opt	0.099	0.0089	0.0127	0.2097	0.0716	142.9%
Side Shell	orig	0.0072	0.0062	0.008	0.224	0.101	100%
	opt	0.0076	0.0089	0.0127	0.2097	0.0716	98.2 %
Side Shell Below Draft	orig	0.0072	0.0062	0.008	0.224	0.101	100%
	opt	0.0076	0.0089	0.0127	0.2097	0.0716	98.2%
Double Bottom	orig	0.00883	0.0062	0.008	0.224	0.101	100%
	opt	0.0086	0.0089	0.0127	0.2097	0.0716	87.6%
Weather Deck	orig	0.011	0.0043	0.0052	0.0948	0.1	100%
	opt	0.0107	0.003	0.003	0.1454	0.07	96.6%
Deck Plate	orig	0.0054	0.0043	0.0052	0.0948	0.1	100%
	opt	0.0061	0.003	0.003	0.1454	0.07	113.4%



(a) Yearly maintenance costs for original structure



(b) Yearly maintenance costs for 'utopian' structure

Figure 3.6: Maintenance costs for two different ship structures.

Figure 3.6 shows that the optimizer is reducing maintenance costs largely by minimizing structural fatigue in the latter years of the vessel’s operational life. A large amount of money is being saved by reducing the amount of repair necessary to extend the life of the vessel beyond the original service life of 30 years. This shows the ability of the this optimization framework to aid in the development of structures that are robust to changes in service life with respect to increase in lifetime cost. It also shows that by utilizing this framework during the structural design, vessels with reduced cost due to maintenance can be designed while maintaining a lower production cost as well.

### **3.2.2 Effects of Service Life Extension**

In order to examine the effects of the probabilistic service life extension used in the analysis, the optimization was executed using a deterministic 30 year design life. Similarly to the above results, the ‘nearest to the utopian’ point was found and compared to that seen in Figure 3.5. This design is cheaper to produce than the ‘utopian’ structure, as is expected since 15 years less service is being considered.

To examine how utilizing the probabilistic service life affects the total maintenance cost of the vessel two vessels are compared. Ship A was designed using the probabilistic service life assumption, whereas Ship B was designed assuming a deterministic 30 year life. In order to compare their maintenance costs, the cost to maintain the vessel given two different ‘actual’ service lives is examined. These comparisons can be seen in Tables 3.3 and 3.4. It is important to note that the ‘assumption’ represents the service life they were designed for, whereas the two tables represent the service life they actually realized. In these tables all cost values are normalized by the corresponding costs for the original structure. In these tables the vessel found using a probabilistic service life is Case A, and the deterministically optimized structure is Case B.

Tables 3.3 and 3.4 show that no panels are being replaced due to corrosion damage

Table 3.3: Maintenance Costs for both vessels if 30 year life is realized (normalized by initial design).

Ship	Service Life Assumption	$C_F$	$C_C$	$C_S$	$C_R$	$C_T$	$C_P$
A	Probabilistic	.351	1.0	0.536	1.0	0.642	0.964
B	Deterministic (30 yrs)	.226	1.0	0.534	1.0	0.631	0.963

Table 3.4: Maintenance Costs for both vessels if 45 year life is realized (normalized by initial design).

Ship	Service Life Assumption	$C_F$	$C_C$	$C_S$	$C_R$	$C_T$	$C_P$
A	Service Life Assumption	0.474	1.0	0.7355	1.0	0.691	0.964
B	Deterministic (30 yrs)	0.71	1.0	0.7053	1.0	0.747	0.963

outside of scheduled maintenance. This is expected, as unscheduled dry-docking is significantly more expensive and the optimizer is designing structures that are ensured to have their maintenance needs met during the pre-scheduled cycles. Both designs also show improvements over the original structure; showing the ability of this optimization routine to develop structures that cost less to maintain. If the original design life of 30 year is realized table 3.3 shows that Case B is slightly cheaper, as the structure found using the probabilistic method is ensuring that the structure will be operable in years that it doesn't need to be. However, the increase in cost for the structure utilizing the probabilistic service life design assumption is small, only a 2% increase in maintenance costs.

Table 3.4 shows that if the service life of the vessel gets extended out to the optimum time of 45 years, the lifetime structural maintenance cost is significantly less if the vessel is designed using the probabilistic service life extension, while still costing less to produce than the original. It also shows that the structure designed with a probabilistic life assumption actually incurs more costs during scheduled maintenance over its lifetime, however, experiences much less fatigue damage as it ages, thus making its maintenance less expensive overall. This saves considerably on lifetime maintenance and shows the ability of the probabilistic service metric to aid in the design of structures that are robust with respect to extensions to operational lifetime.

### 3.3 Contributions

This chapter has presented a framework for developing Pareto-fronts between maintenance and production costs for ship structures. The framework calculates yearly structural damage estimates based on both fatigue and corrosion in order to determine the costs to maintain the vessel in each year of operation. To account for the uncertainty in the service life of naval vessels a probabilistic service extension metric was used within the estimation of maintenance cost. The framework also allows for the inclusion of a maintenance schedule for the vessel over the course of its life, in order to model the differences in repair costs if maintenance is done during scheduled dry-dockings as opposed to emergency repairs. This type of framework is novel in the naval field and represents a way to calculate and optimize maintenance costs accounting for issues unique to the discipline.

Using this framework and a multi-objective genetic algorithm, trade-spaces have been successfully developed between maintenance and production costs for a nominal naval combatant midship structure. The Pareto-fronts show the ability of this framework to aid a designer in developing ship structures that have minimal costs with respect to both production and maintenance in order to reduce their lifetime expenses. The nature of the developed front show that it is a difficult front, and suggests that the problem is well-suited to multi-objective optimization, as single-objective routines would struggle to find the ‘knee’. The framework has also shown success in developing structures that are robust to changes in the vessel’s service life; these structures show only moderate increases if the original service life is realized whereas they are significantly less expensive if it is extended. This allows the shipowner to ensure that their lifetime costs will remain low despite uncertainty in operational life. This type of trade-off has not been examined in depth before, especially while accounting for service life uncertainty. By exploring this trade space it can be seen the importance in using multi-objective optimization to understand the



choices designers face and how those choices will impact the lifetime cost of a new vessel.

## CHAPTER 4

# Hydrodynamic Trade-Offs

### 4.1 Trade-Offs Between Resistance and Complexity

The hydrodynamic design discipline is a vital component of naval architecture and a vessel's lifetime cost. The resistance of a vessel will directly influence the cost to operate it over its life via fuel costs. However, minimizing the resistance alone can have a negative impact on other categories of cost. This can be seen in increased hull curvature that leads to a more complex structure that is more difficult to produce and maintain. This chapter will present a method to explore that trade-space that allows for an optimizer to explore large swaths of a design space with minimal design variables introduced. The method also allows for the designer to constrict or expand the design space with ease. This method will be used in an exploratory optimization to show its ability to develop trade-spaces within the hydrodynamic design space. The results show that the method is capable, however, similarly to the results in chapter 3, the Pareto-fronts are difficult to resolve with current multi-objective optimizers.

This leads to the development of a multi-disciplinary design environment to address the challenges in developing these trade-spaces. In order to show the ability of MDO to tackle naval architecture design problems an example within the hydrodynamic design space is shown. This example shows that multi-disciplinary optimization

is able to better capture the interactions between naval design decisions than sequential optimization, and an MDO framework designed to solve this problem could aid in the development of lifetime cost trade-spaces.

As shown in chapter 3 the trade-offs between different categories of lifecycle cost even within a single discipline are important to understand. In the previous chapter the trade-offs between structural maintenance and steelwork production were examined, however, the hydrodynamic performance of a ship and its production are also related. In work such as [Caprace et al. \(2009\)](#); [Caprace and Rigo \(2012\)](#); [Parsons et al. \(1998\)](#); [Rigterink et al. \(2013\)](#) the authors discuss the importance of producibility for naval vessels. If a ship is overly complex to build the structural fabrication cost can increase significantly over the raw steel cost. One of the measures of complexity examined is the curvature of the hull. As shown in [Parsons et al. \(1998\)](#) a hull that has significant amounts of curvatures can be more expensive for shipyards to build due to the process involved in rolling the steel plates. If a vessel, however, is designed or optimized for this alone the resistance can suffer, given that a hull with less curvature may experience higher resistance.

In order to explore these trade-offs an optimization routine was developed comparing the lifetime resistance,  $R_{TE}$ , as shown in equation 2.24 with the build complexity,  $C_B$ , from equation 2.39. As discussed in chapter 2 a lifetime resistance metric can be used to capture the operational profile of a naval vessel. In this work, in order to account for the resistance over the entire operational profile of the vessel a probabilistic mission profile is created. This is a probability density function that represents the probability that the ship will operate at any speed. This profile will differ greatly depending on the type of ship being analyzed and must be generated for each hull form that is optimized. The difference in the mission profile can lead to different trade-offs between the categories of cost. By using a probabilistic approach the objective function is able to account for multiple modes of operation for the vessel being

analyzed. For instance, if a naval vessel will spend the majority of its operational life at a low cruising speed, yet, must be capable of reaching higher speeds during missions the probabilistic profile will account for this and drive the solution towards one that is optimal considering both these modes.

In order to explore the effects of the operational profile on the nature of the trade-spaces two different vessels are examined. The first is a nominal DTMB-5145 naval combatant, from [Benedetti et al. \(2007\)](#), and the second is a container ship based on a SIMMAN KCS hull form, found in [Lee et al. \(1998\)](#). For the naval combatant based on the DTMB-5145 hull form a hypothetical bimodal distribution was used, similar to the one theorized for general high speed naval vessels in [Kramer et al. \(2010\)](#), with the two modes representing an endurance speed, 20 knots, and a mission speed, 40 knots. For the merchant vessel based on the SIMMAN KCS hull form a hypothetical unimodal distribution with the mode at the vessel’s design speed was used. These two mission profiles can be seen in Figures 4.1a and 4.1b.

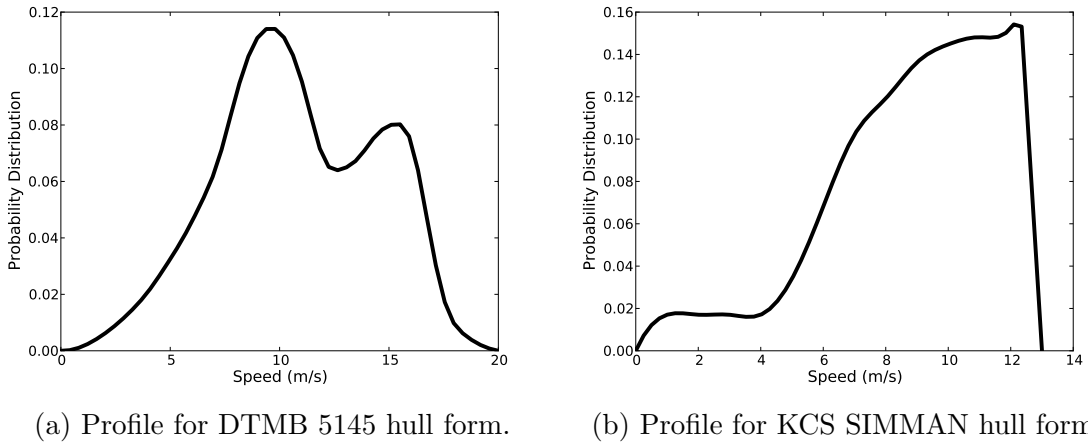


Figure 4.1: Mission profiles for the two vessels

The resistance is calculated using Michells integral, as described in equation 2.12 and Grigson’s friction line from equation 2.18. Once again, a standard NSGA-II is used to develop the trade-spaces between the two categories of cost. An engineer might be eager to minimize the total cost of the vessel and, in theory, a fuel cost

derived from the resistance curves could be combined with a production cost to formulate a single-objective problem, this may not be ideal during the design stage. This type of single-objective approach could lead to design results that are highly dependent on the time-sensitive cost of fuel cost that is historically difficult to estimate. It is important for an engineer to understand the space they are working in so that responses to changes in requirements, mission statements, or other aspects of the vessel can be made quickly and with minimal impact to the overall cost of the ship design. The Pareto-fronts found using the MOGA allows for this information to be developed and used during the ship’s design. Additionally, the assumptions necessary to combine the two objectives, especially the relative prices of oil and steel, would begin to dominate the final solution in a single-objective framework. Using the MOGA allows for an understanding of the design space, from which a final ship can be chosen by an engineer based on their knowledge of the relative importance of the objectives based on variables such as material costs, oil costs, and the shipyard producing the hull.

#### 4.1.1 Transformation Functions

In order to formulate the problem a method had to be chosen to transform the hull form as the optimizer ran. This was done using two transform functions defined along the centerplane of the vessel in the longitudinal and vertical directions. This optimization approach, and the subsequent results can be found in [Temple and Collette \(2015b\)](#). The functions,  $T_l(x)$ , and  $T_v(z)$ , are a function of longitudinal position ( $x$ ) and vertical position ( $z$ ) and define a distance to perturb a station ( $T_l$ ) or a waterplane ( $T_v$ ) at the position indicated.  $T_l$  and  $T_v$  are determined by a set of points,  $(x_1, x_2, \dots, x_n, z_1, z_2, \dots, z_m)$ , within the functions domains and spline functions are used to interpolate between these control points. The function value of the control points are the variables the optimizer is allowed to alter in order to transform the

vessel and minimize the objective functions. Examples of potential transform functions can be seen in Figures 4.2 and 4.3. In these examples there are 5 control points being used to define each of the functions and the optimizer would have control over  $T_l(x_1), \dots, T_l(x_5)$  and  $T_v(z_1), \dots, T_v(z_5)$ .

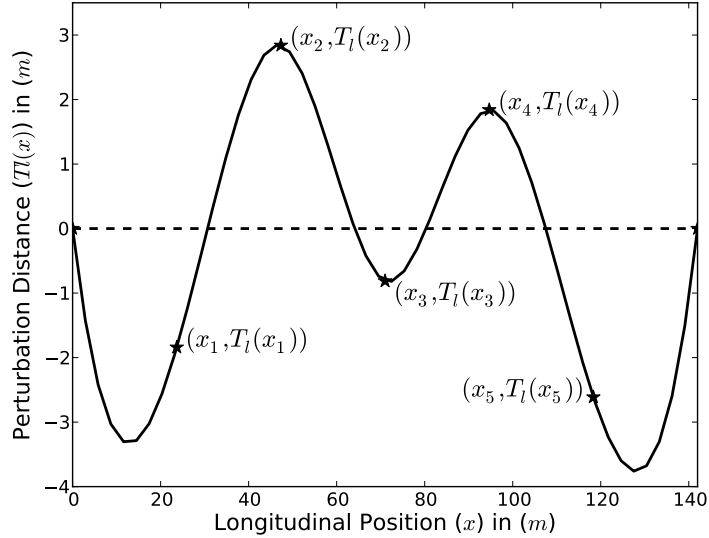


Figure 4.2: A potential function for  $T_l(x)$ . Note that the ends of the domain always map to zero.

In order to transform the hull form using these transform functions equations 4.1 and 4.2 is used.

$$\tilde{S}_i = S_i + T_l(x_i) \text{ for } i = 1, \dots, n \quad (4.1)$$

$$\tilde{W}_i = W_i + T_v(z_i) \text{ for } i = 1, \dots, m \quad (4.2)$$

In equations 4.1 and 4.2  $\tilde{S}_i$  and  $\tilde{W}_i$  are the location of station and waterline  $i$  after the transformation. Likewise,  $S_i$  and  $W_i$  are the locations of the station prior to the transformation. In the optimization performed for this work ten control points were used to determine both transform functions. The optimizer was allowed to manipulate the longitudinal points between  $\pm \frac{L}{5}$  and the vertical points by  $\pm \frac{T}{5}$  without extending the spline beyond the extent of the original hull form. This method of transformation

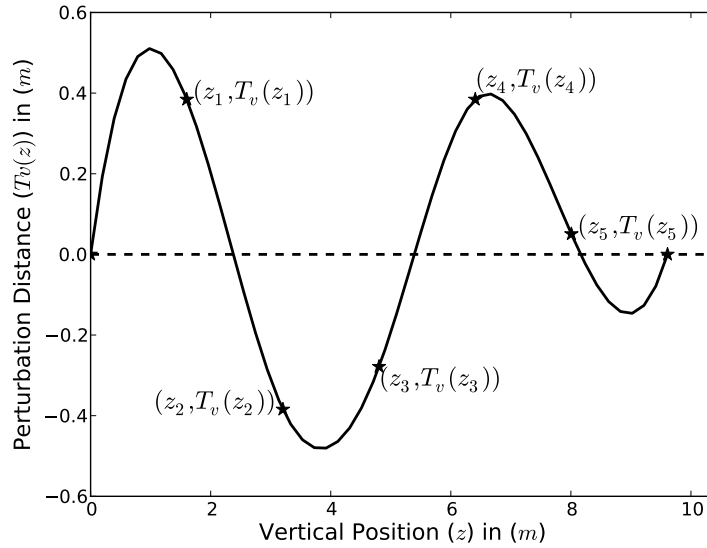


Figure 4.3: A potential function for  $T_v(z)$ . Note that the ends of the domain always map to zero.

allows for significant alterations in a vessel's hull in both a global and local nature. This degree of search power allows the optimization routine to explore enough of the design space to yield trade-spaces which reveal a large amount of information to a designer. The nature of the search method also works well with the objective functions being utilized because they will not fail to converge even on designs that do not resemble conventional ships. This means that the optimizer can search large areas of the design space without having issues in the analysis code failing due to a code error.

#### 4.1.2 Problem Formulation

The transform functions described above are essentially modifying the sectional area curve and the waterplane area curve via the location of the stations and waterplanes. Thus, it was intuitive to constrain the shape of these two curves in order to ensure faired hull forms in the final Pareto front found by the optimizer. In order to formulate the Pareto-front, these constraints points were defined along the two

curves that broke them into regions where certain shape parameters were enforced. The points used to define these regions can be seen in Figures 4.4 and 4.5

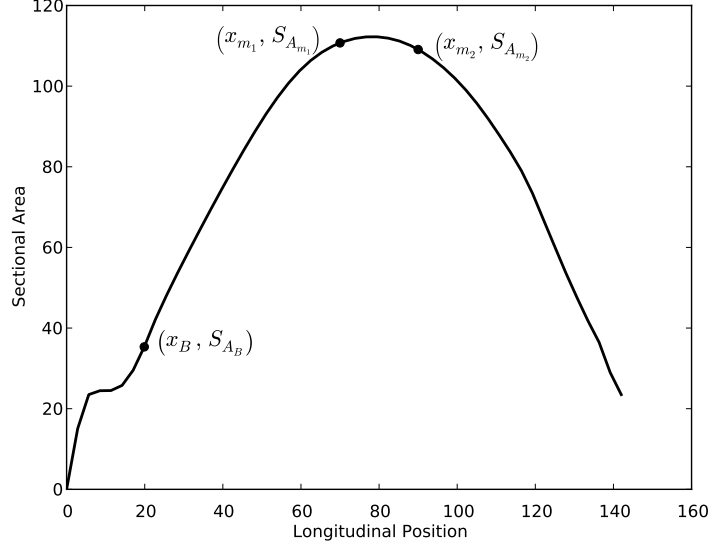


Figure 4.4: The points used to formulate the constraints for the sectional area curve.

In Figure 4.4 the point  $x_B$  is calculated using Equation 4.3, and the points  $x_{m_1}$  and  $x_{m_2}$  represent the start and end of the midbody region, as chosen by the designer.

$$x_b = \{x_i | x_i \leq \frac{L}{2} \text{ and } \underset{2 \leq j \leq n}{\operatorname{argmax}} \left( \frac{dx_j}{dS_{A_j}} \right) = x_i\} \quad (4.3)$$

$$z_p = \{z_i | \underset{2 \leq j \leq n}{\operatorname{argmax}} \left( \frac{dz_j}{dW_{A_j}} \right) = z_i\} \quad (4.4)$$

$$z_m = \{z_i | \underset{1 \leq j \leq n}{\operatorname{max}} (z_j) = z_i\} \quad (4.5)$$

These points are used to control the shape of the sectional area curve. The definition of the points used to define the shape of the waterplane area curve are shown in equations 4.4 and 4.5.

The optimization problem can then be written as:



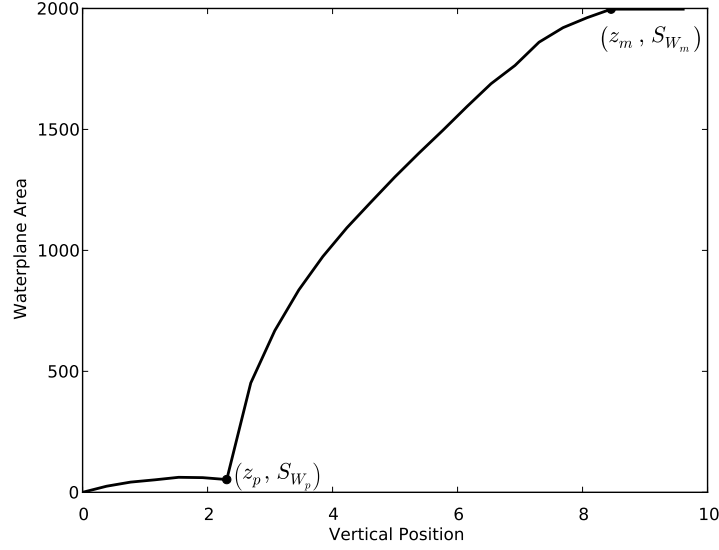


Figure 4.5: The points used to formulate the constraints for the waterplane area curve.

$$\text{minimize: } \mathbf{f}(\mathbf{x}) = (R_L, C_B)$$

$$\text{by varying: } \mathbf{x} = (T_l(x_1), \dots, T_l(x_{10}), T_v(z_1), \dots, T_v(z_{10}))$$

$$\text{within the bounds: } -4\mathbf{S}_s \leq \mathbf{T}_l \leq 4\mathbf{S}_s$$

$$-4\mathbf{W}_s \leq \mathbf{T}_v \leq 4\mathbf{W}_s$$

$$\text{subject to: } g_1 = -2 \leq \tau_{new} \leq 0.01 \text{ meters}$$

$$g_2 = \Delta_T \leq 0.75 \text{ meters}$$

$$g_3 = z_p - z_{pI} \leq 0.05z_{pI},$$

$$g_4 = W_{A_{i-1}} - W_{A_i} \leq \epsilon_1 \quad \forall \{i | i > 1\}$$

$$g_5 = \frac{dz_{i+1}}{dW_{A_{i+1}}} - \frac{dz_i}{dW_{A_i}} \leq \epsilon_2 \quad \forall \{z_i | z_p \leq z_i \leq z_m\}$$

$$g_6 = \frac{dx_{i+1}}{dS_{A_{i+1}}} - \frac{dx_i}{dS_{A_i}} \leq \epsilon_3 \quad \forall \{x_i | x_b \leq x_i \leq a_m\}$$

$$g_7 = \max_{x_{m1} \leq x_i \leq x_{m2}} \left( \frac{d^2 x_i}{dS_{A_i}^2} \right) \leq \epsilon_4$$

$$g_8 = \frac{d^2 x_i}{dS_{A_i}^2} \quad \forall \{x_i | x_{m1} \leq x_i \leq x_{m2}\} \leq \epsilon_5 \quad (4.6)$$

Equation 4.6 is minimizing the resistance and build compexity with respect to the transformation functions. The functions are constrained proportionally to the station spacing,  $S_S$ , and the waterline spacing,  $W_S$ . The two constraints ensure that the transformed hull form does not have excessive trim or change in draft. These two constraints can be altered based on the problem being examined. Different ships may have different requirements with respect to physical characteristics such as draft and trim.

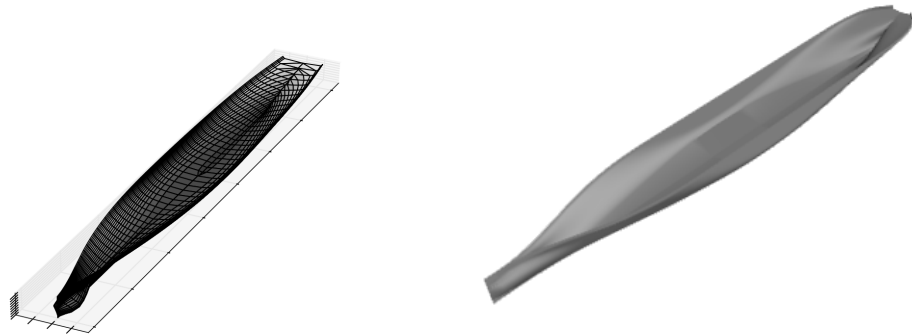
The rest of the constraints ensure that the shape of the sectional area curve and waterplane curve in specific regions follows certain patterns. Constraints  $g_3$  and  $g_4$  ensures that the position of the bulbous bow does not vary too greatly from the original. This is especially important on the *DTMB* design where the bulbous bow protrudes below the hull of the vessel, which can cause the optimizer to find odd shapes for it that exploit Michell’s integral. The 5<sup>th</sup> constraint,  $g_5$ , ensures a degree of monotonicity, controlled by  $\epsilon_2$ , of the waterplane area curve between the bulbous bow and sheer strake of the vessel’s hull. Similarly, the 6<sup>th</sup> constraint,  $g_6$  does the same for the sectional area curve between the bulbous bow and parallel mid-body.  $g_7$  is a constraint that controls the ‘sharpness’ of the midsection of the hull by limiting maximum value of the second derivative of the sectional area curve in the middle of the parallel midbody, the value is constrained by  $\epsilon_4$ . Finally, constraint  $g_8$  ensures that the parallel midbody is flat, to a degree determined by  $\epsilon_5$  Note that these constraints can be relaxed or tightened by the values of  $\epsilon$  depending on the initial hull form being investigated.

By using this type of problem formulation large design spaces can be explored, while ensuring that the resulting vessel’s have shapes within dictated bounds around the original. By tightening or relaxing these constraints, or the proportional constant for  $S_s$  and  $W_s$ , the scope of the exploration can be enlarged or reduced. This allows a designer to understand, at various levels, the trade-offs between these two competing

objectives and how to design with consideration for both.

### 4.1.3 Trade-Spaces

The optimization formulation shown above was applied to two different hull forms. The two hull forms used for the following optimizations can be seen in Figures 4.6a and 4.6b. The naval combatant is a more narrow slender ship; a nominal destroyer, whereas the KCS is a container ship that has been designed to efficiently carry bulk-cargo, and thus it has more parallel mid-body and a higher block coefficient than the destroyer. The difference in the initial design and, especially, the mission profile for these two vessels means they may have significantly different trade-offs between the two objective functions. The principle dimensions for the two vessels can be seen in table 4.1.



(a) The nominal DTMB-5145.

(b) The KCS SIMMAN container ship.

Figure 4.6: The two hull forms used in the optimization routine.

Table 4.1: Principle dimensions for initial hull forms.

Hull Form	$L$ (m)	$B$ (m)	$T$ (m)	$D$ (m)
DTMB-5145	142	18	8.5	9.61
KCS SIMMAN	230	32.2	10.8	12.42

The Pareto fronts found by solving 4.6 for these two vessels can be seen in Figure 4.7. The NSGA-II parameter values used to develop these trade spaces can be seen

in table 4.2. In table 4.2  $|P|$  is the population size,  $N_G$  is the number of generations

Table 4.2: NSGA-II parameters used in the optimization.

$ P $	$N_G$	$p_c$	$\eta_c$	$p_m$	$\eta_m$
192	300	0.9	2.0	0.2	4.0

the optimizer ran until the Pareto-front was stationary,  $p_c$  is the crossover chance,  $\eta_c$  is the crossover exponent,  $p_m$  is the mutation chance, and  $\eta_m$  is the mutation exponent

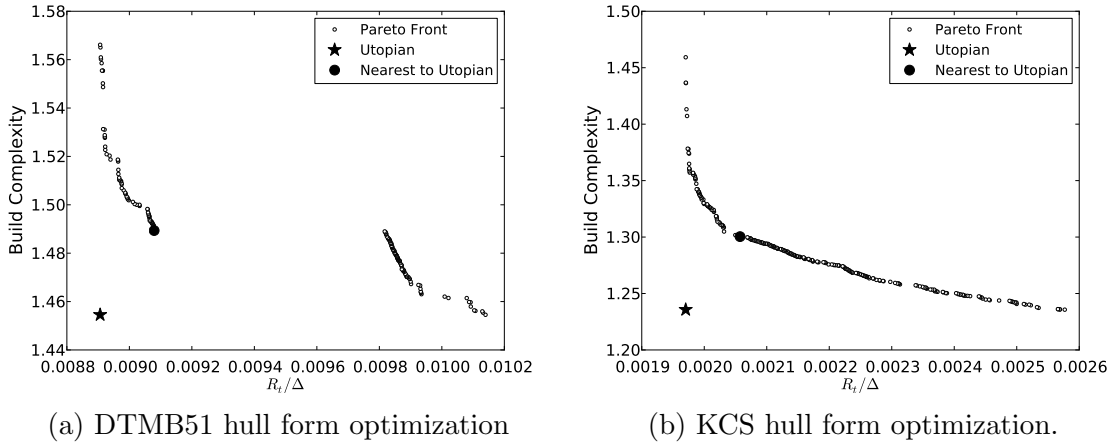


Figure 4.7: Pareto fronts for each vessel type found when solving equation 4.6.

These Figures show the ability of this optimization method to explore large areas of the design space and provide a visualization of the trade-offs. The long, flat ends of the Pareto front show that if designers focus on a single objective a design can be found that performs significantly worse in the other, for only a small gain. For example, if a design was over-optimized for producibility, the resistance can be dramatically increased. However, if a small sacrifice is made in build steelwork complexity, a large gain can be found with respect to resistance; potentially decreasing the overall lifetime costs for the vessel.

It is also interesting to note the differences in the two Pareto fronts. Figure 4.7a shows a sharp, though discontinuous, ‘knee’, indicating a small area of the design space where the objectives are well balanced. In Figure 4.7b there is still a ‘balanced’ region of the front, however, the area is much broader, giving the designer more

freedom to alter designs along the Pareto front and maintain a good trade-off between the objectives. This shows the large effect that the vessel and mission type can have on the nature of the Pareto front. The Pareto front for the destroyer is more difficult to develop; as can be seen in Figure 4.7a. The gap in feasible solutions found in the center of the front show an area of the Pareto front that is difficult to resolve. The differences in the Pareto-front are largely due to differences in the assumed mission requirements of the vessels; represented by the speed profiles. This is why, for a vessel like the KCS, it is possible to resolve more of the Pareto front, yet, for the DTMB-51 it is difficult. It seems to be inherent nature of the ships, as even when the constraints are relaxed, the algorithm still finds difficulty in resolving the Pareto-front. The multi-modal nature of the destroyer’s mission profile; along with the higher top speed it must be capable of reaching, result in a trade space that is more difficult to resolve and has sharper knees. This is in line with results the author’s have found in a similar study with a reduced scope in [Temple and Collette \(2012\)](#). This shows that for a vessel such as a naval combatant, which has a distinct form and a unique operational profile, optimization can be difficult to perform.

It is possible that an optimization algorithm, using some of the principles presented here, could utilize techniques such as multi-disciplinary optimization to resolve these difficult Pareto-fronts more effectively. From a design perspective it can be advantageous to remain in the knees of these fronts in order to ensure balanced trade-offs between these objectives. In order to examine the nature of designs within these areas the hull forms represented by the ‘nearest to the utopian’ points in Figure 4.7 are shown in Figure 4.9. If the furthest ends of a  $k$  dimensional Pareto-front are labeled as  $(f_1^0, \dots, f_k^0)$  then the Utopian point is  $(f_1^0, \dots, f_k^0)^T$ . This point would, clearly, dominate the entire Pareto-front and, unfortunately, is not a feasible design point. However, the ‘nearest to the utopian’ is defined as the point on the Pareto-front that minimizes the Euclidean distance from the utopian point.

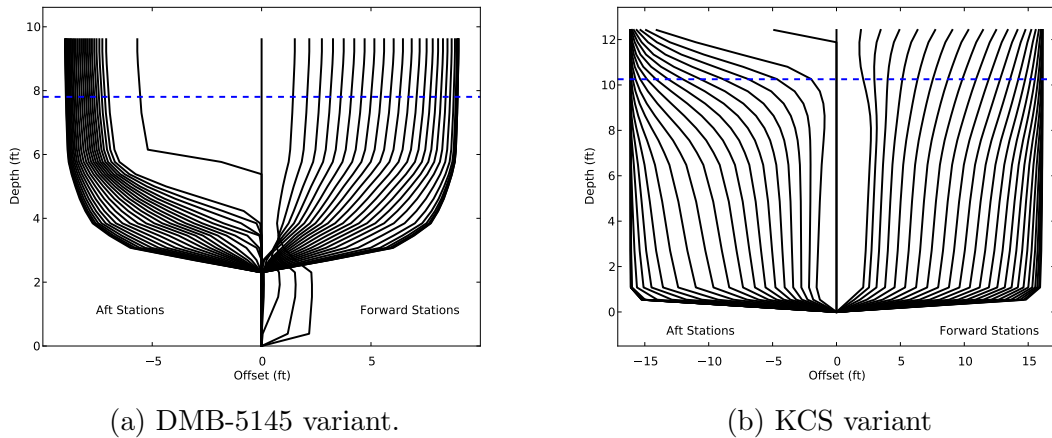


Figure 4.8: Hullforms represented by nearest to utopian point in Figure 4.7.

This Figure shows that by altering specific aspects of the design the optimization is able to find hull-forms that represent good trade-offs between designs. In Figure 4.8a the bulbous bow had its width reduced and length increased, allowing for reduced wave resistance with the blockier, easier to produce hull. This vessel represents a 21% decrease in resistance and 10% decrease in complexity. Similarly the hull form in Figure 4.8b has increased curvature near the stern and entrance to the bow, reducing the drag over the original design. The bulbous bow has also been made less prominent, and the midship coefficient increased; resulting in a vessel with less resistance that is simpler to produce. These changes lead to a 35% decrease in expected resistance and 16% reduction in production complexity. These represent designs that are balanced with respect to the objectives, and superior over the original design in both. For this problem the starting hulls were designed with the intention of meeting many more objectives which may be why such large objective improvements were possible.

These two Pareto-fronts highlight the ability of the optimization routine presented here to aid in the development of designs that can reduce overall lifetime costs. By examining the nature of the vessels at specific areas in the trade-space designers can gain understanding into how to design to minimize these costs. For example; the sectional area curves for the hulls shown in Figures 4.8a and 4.8b can be seen

in Figures 4.9a and 4.9b. These Figures show that the production cost has been

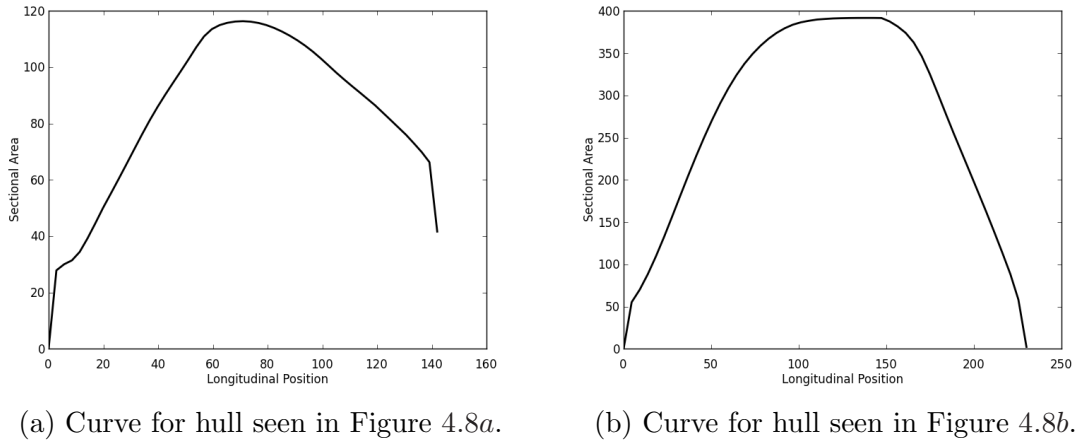


Figure 4.9: Sectional area curves for ‘nearest to utopian’ vessels.

reduced by minimizing the size of the bulbous bow; while altering the entrance and run to reduce drag. They also show that by decreasing the size of the transom on the container ship and increasing it on the combatant both metrics can be improved. It is important to note that these hulls require fine-tuning and fairing to be complete viable options for design; however, by utilizing this type of optimization algorithm the engineer is able to gain an understanding of the trade-space they are working in. This lets the decisions they make in finalizing the hull to be made with reducing overall lifetime costs in mind. By using this as a decision support tool naval vessels can be potentially designed with reduced lifetime costs.

## 4.2 Multi-Disciplinary Optimization of Propeller-Hull Systems

As discussed above, an NSGA-II struggled to resolve the entire Pareto-front even for a problem only involving the hydrodynamic discipline. A multi-disciplinary optimization routine may aid in resolving these types of fronts and, therefore, it is important to show the ability of an MDO algorithm to design in the naval space. In

order to do this a single objective lifetime cost objective is examined, and an MDO implementation is used to reduce it. In traditional naval architecture, the hull is chosen first through the use of hull form ratios and coefficients to satisfy the basic requirements of the vessel while minimizing resistance. Once the hull has been chosen, a propeller-hull matching exercise is then performed at selected vessel operating speeds in order to choose the propeller with the best performance, i.e. the highest possible efficiency at one or multiple design speeds or maximum cavitation-inception speeds.

More recently emphasis has been placed on finding optimal solutions during both of these design steps, however, they are still considered independent problems to solve. It is clear that the interaction of the propeller and hull is substantial; this makes it desirable to design the two simultaneously in order to find solutions that complement each other and reduce the overall fuel consumption of the vessel. Most design optimization routines also only consider a limited number of design points and, hence, may not provide an optimal solution with respect to the total operational envelope of the vessel.

This work proposes a methodology to simultaneously optimize the propeller and hull of a vessel as a coupled system in order to find designs which minimize the total lifetime fuel cost of a vessel. The multi-disciplinary optimization shown in the subsequent sections can be found in [Nelson et al. \(2013\)](#).

The approach is used to optimize the hull form and propeller characteristics of the KCS SIMMAN container ship shown above using a simplistic problem formulation based on basic form ratios. The resistance calculation is, once again, done using Michell's integral and Grigson's friction line. The same operational profile shown in Figure 4.1b is used in the lifetime resistance integral. This aims to show, as discussed in the previous section, the ability of MDO algorithms to effectively optimize in the naval design environment using a simplified multi-disciplinary example. Based on



the results presented in the previous section, a multi-disciplinary tool appears to be the best approach to solving this difficult problem. The subsequently presented optimization aims to show the ability of MDO optimizers to design in the naval space effectively.

### 4.2.1 Vessel Performance

In order to explore the ability of MDO in the marine environment the propeller performance is selected as a second design discipline. Much of the operational performance of a marine propeller is governed by the advance coefficient,  $J$ , which, according to equation 4.7, relates the mean axial advance velocity of the fluid through the propeller plane,  $V_a$ , to the rotational speed of the propeller,  $n$ , and the diameter of the propeller,  $D$ .  $V_a$  is related to the ship velocity,  $V$ , by the wake fraction,  $w$ , as shown in equation 4.8.

$$J = \frac{V_a}{nD} \quad (4.7)$$

$$V_a = V(1 - w) \quad (4.8)$$

The wake fraction is estimated based on block coefficient,  $C_B$ , using equation 4.9 as found in [Manen et. al \(1988\)](#):

$$w = 1.7643C_B^2 - 1.4745C_B + .2574 \quad (4.9)$$

Research conducted in [Bernitsas \(1981\)](#) on the B-series propeller has produced regression equations that can be used to calculate the thrust coefficient,  $K_T$ , and torque coefficients,  $K_Q$ , for a given propeller. The thrust and torque coefficients for the B-Series propellers are expressed as polynomial functions of the pitch to diameter

ratio,  $P/D$ , advance coefficient,  $J$ , expanded blade area ratio,  $A_e/A_o$ , and number of propeller blades,  $z$ .

$$K_T = \Sigma C_{s,t,u,v}^T (J)^s \left(\frac{P}{D}\right)^t \left(\frac{A_e}{A_o}\right)^u (z)^v \quad (4.10)$$

$$K_Q = \Sigma C_{s,t,u,v}^Q (J)^s \left(\frac{P}{D}\right)^t \left(\frac{A_e}{A_o}\right)^u (z)^v \quad (4.11)$$

$C_{s,t,u,v}^Q$  and  $C_{s,t,u,v}^T$  are regression coefficients and  $s$ ,  $t$ ,  $u$ , and  $v$  are power coefficients.

The open water efficiency of the propeller can then be calculated as follows:

$$\eta_{ow} = \left(\frac{J}{2\pi}\right) \left(\frac{K_T}{K_Q}\right) \quad (4.12)$$

Once the open water propeller characteristics have been determined, the required thrust coefficient,  $K_T/J^2$ , for the vessel can be determined as a function of thrust,  $T$ , diameter,  $D$ , water density,  $\rho$ , and the advance speed,  $V_a$  according to equation 4.13. As shown in equation 4.14 the required thrust,  $T$ , is related to the total resistance,  $R_T$ , via the thrust deduction factor,  $t$ , which is related to the wake fraction as given in [Manen et. al \(1988\)](#) and in equation 4.15.

$$\frac{K_T}{J^2} = \frac{T}{D^2 \rho V_a^2} \quad (4.13)$$

$$T = \frac{R_T}{(1-t)} \quad (4.14)$$

$$t = .25w + .14 \quad (4.15)$$

The thrust requirements of the vessel can be matched with the thrust characteristics of the propeller, to find the operating  $J$  value (and, hence, propeller rotational speed,  $n$ ) and corresponding  $\eta_{ow}$  at a given speed, as shown in Figure 4.10. These values determine the powering characteristics of the propeller.

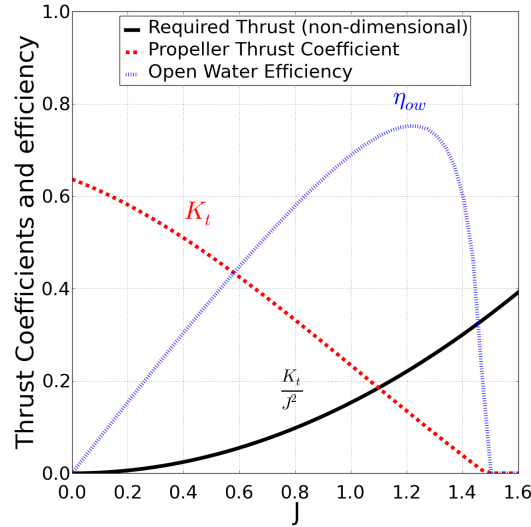


Figure 4.10: An example of a propeller-hull matching exercise showing the required thrust at the endurance speed of  $V = 20$  kts, the open water thrust coefficient, and efficiency curves.

In order to prevent a propeller design from having excessive cavitation, Burrill's 10% back cavitation line [Manen et. al \(1988\)](#) was used. Burrill's cavitation curve depends upon  $\tau_c$ , which is a function of the cavitation number,  $\sigma_{0.7}$ . The formulas for these variables can be seen in equations 4.16 and 4.17.

$$\tau_c = \frac{T/A_p}{\frac{1}{2}\rho(V_r)^2} \quad (4.16)$$

$$\sigma_{0.7} = \frac{P_{atm} + \rho gh - P_v}{\frac{1}{2}\rho(V_r)^2} \quad (4.17)$$

In equation 4.16,  $T$  is the thrust of the vessel,  $A_p$  is the projected area of the propeller (assumed to be equal to the expanded area for B-series propellers), and  $V_r$  is the rotational speed of the propeller at the 0.7 radius. In equation 4.17,  $P_{atm}$  is

the atmospheric pressure,  $h$  is the depth of the propeller hub, and  $P_v$  is the vapor pressure. In this work,  $P_{atm}$  was assumed to be 101.3 KPa and  $P_v$  was assumed to be 1.646 KPa. The rotational speed at the 0.7 radius can be found using equation 4.18.

$$V_r = \sqrt{V_a^2 + (0.7\pi nD)^2} \quad (4.18)$$

In equation 4.18  $V_a$  is the advance velocity,  $n$  is the rpm of the propeller, and  $D$  is the propeller diameter. For a given design, the value of  $\tau_c$  and  $\sigma_{0.7}$  are both found. The maximum  $\tau_{c,max}$  to avoid 10% back cavitation is then found based on  $\sigma_{0.7}$  from Burrill's cavitation curves. The value of  $\tau_c$  can be compared to  $\tau_{c,max}$  to ensure that cavitation will not be an issue for a given propeller choice.

The specific fuel consumption of the engine, SFOC, is provided by engine manufacturers as a function of engine load. In order to determine the fraction of engine load, the power requirements must be known. The effective power of the vessel,  $P_E$ , relates the vessel resistance and speed by

$$P_E = R_T V \quad (4.19)$$

The resulting delivered power,  $P_D$ , required of the propellers can be calculated using equation 4.20:

$$P_D = \frac{P_E}{\text{QPC}} \quad (4.20)$$

where QPC is the quasi-propulsive-coefficient given by the product of three efficiencies affecting the hull and the propeller:

$$\text{QPC} = (\eta_H) (\eta_{RR}) (\eta_{ow}) \quad (4.21)$$

where  $\eta_H$  is the hull efficiency as shown in equation 4.22,  $\eta_{RR} = 1.0$  is the assumed relative rotative efficiency, and  $\eta_{ow}$  is the open water efficiency as calculated in equation 4.12.

$$\eta_H = \frac{1 - t}{1 - w} \quad (4.22)$$

In this work, the losses due to shaft and bearing efficiencies are assumed to be negligible. Once the power is calculated, the specific fuel oil consumption (SFOC) at any speed can be found based on the percentage of load. The SFOC for the L51/60DF engine as a function of engine load taken from [MAN \(2009\)](#) and shown in Figure 4.11, is used in the current work.

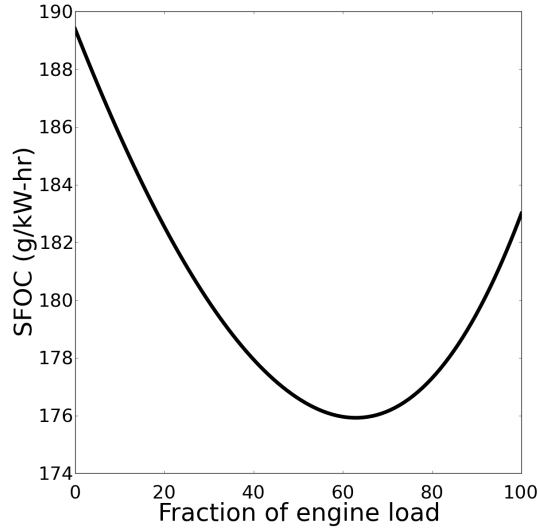


Figure 4.11: Specific fuel consumption as a function of percentage of load for the L51/60DF engine.

A probabilistic integral over an operational profile is used as before, however, since resistance is based off of specific fuel consumption the integral is altered slightly. To calculate the lifetime fuel cost equation 4.23 is used:

$$LFC = \left( \int_V p(V) SFOC(V) P_D(V) dV \right) L_h \quad (4.23)$$

This corresponds to the integral of the fuel flow rate (g/hr) of the engines weighted by the operational PDF, and multiplied by the total number of operational hours,  $L_h$ .

### 4.2.2 Problem Formulation

The goal of this work is to integrate the methods described above with an optimization algorithm in order to simultaneously design the propeller and hull. In order to achieve this, the design vector must contain variables that define the hull, the propeller, and variables that link the two together. For this work, simple form ratios are used to formulate the problem in order to show the potential of the design approach. This algorithm will minimize the LFC with respect to the hull-defining variables beam-to-draft ratio,  $B/T$ , and length-to-beam ratio,  $L/B$ , the propeller geometry variables pitch-to-diameter ratio,  $P/D$ , and blade area ratio,  $A_e/A_o$ , as well as the linked variable diameter-to-draft ratio,  $D/T$ . The beam-to-draft and pitch-to-diameter ratios are given upper and lower bounds based on the range of data available, and the diameter-to-draft ratio is limited by geometric constraints. The blade area ratio is bounded based on cavitation considerations and the upper limit of the B-series.

The nonlinear optimization constraints consist of upper and lower limits on the block coefficient, a cavitation constraint based on the maximum allowable propeller loading at the given cavitation number, and a constraint on the allowable change in draft from the parent hullform. The optimization problem can be summarized as follows:

$$\begin{aligned}
& \text{minimize } LFC \\
& \text{with respect to } 1.2 \leq B/T \leq 3.6 \\
& \qquad \qquad \qquad 0.5 \leq P/D \leq 1.4 \\
& \qquad \qquad \qquad 0.5 \leq D/T \leq 0.9 \\
& \qquad \qquad \qquad 0.55 \leq A_e/A_o \leq 1.05 \\
& \qquad \qquad \qquad 5.0 \leq L/B \leq 8.0 \tag{4.24} \\
& \text{subject to } 0.4 \leq C_b \leq 0.8 \\
& \qquad \qquad \qquad 8.8 \leq T \leq 12 \\
& \qquad \qquad \qquad \tau_c - \tau_{c,max} \leq 0
\end{aligned}$$

Since the objective and constraint functions are continuous and smooth, a gradient-based optimizer, SNOPT [Gill et al. \(2005\)](#), is used. SNOPT is a Sequential Quadratic Programming (SQP) algorithm that solves the Quadratic Programming (QP) subproblems using a reduced-Hessian active-set method. A brief description of the SQP and QP algorithms used in SNOPT is presented below.

Consider a nonlinear optimization problem with objective function,  $f$ , design variables,  $x_k$ , equality constraints,  $c_i$ , and inequality constraints,  $\tilde{c}_j$ , required to be less than or equal to zero. The Lagrangian, with Lagrange multipliers,  $\lambda_i$  and  $\tilde{\lambda}_j$ , and slack variables,  $s_j$ , is defined as:

$$\mathcal{L}(x_k, \lambda_i, \tilde{\lambda}_j, s_j) = f(x_k) + \lambda_i c_i(x_k) + \tilde{\lambda}_j (\tilde{c}_j(x_k) + s_j)$$

The SQP major iterations of SNOPT attempt to satisfy the Karush–Kuhn–Tucker necessary conditions by finding the stationary points of the Lagrangian with respect to  $x_k$ ,  $\lambda_i$ ,  $\tilde{\lambda}_j$ , and  $s_j$ . The quadratic subproblem generated by each major iteration

approximates the Lagrangian as a quadratic and linearizes the constraints. For the approximate Hessian of the Lagrangian, the identity matrix is used initially and subsequent major iterations apply the Broyden–Fletcher–Goldfarb–Shanno (BFGS) update to successively increase the accuracy of the approximation as the optimizer approaches the convex region surrounding the optimum.

The QP solver computes the optimal step from the subproblem generated in each major iteration. The linearized constraints are expressed in a form that separates the set of basic, superbasic, and nonbasic variables, where the basic variables are those used to satisfy the constraints, nonbasic variables are fixed at their bounds, and superbasic variables represent the true degrees of freedom that can be varied to minimize the objective. After a step direction is computed from the reduced Hessian and gradient in terms of the superbasic variables, a line search is used to find a step size that yields a sufficient decrease in the augmented Lagrangian, which is the Lagrangian with an additional quadratic penalty term for each constraint. More details can be found in [Gill et al. \(2005\)](#).

Figure 4.12 illustrates how optimization is used to perform simultaneous hull-propeller optimization over a range of operating conditions. It is a diagram showing both process and data flow, referred to as the eXtended Design Structure Matrix (XDSM) [Lambe and Martins \(2012\)](#). The elements on the diagonal represent distinct processes, the thick, gray lines indicate data dependency, the thin black lines indicate process flow, and the numbers indicate order of execution. A variable on the upper triangular indicates data flow from the process with which it shares a row to the process with which it shares a column, and a variable on the lower triangular indicates data flow from the process in the same row to the process in the same column, which is indicative of feedback present in the system.

The hull and propeller analyses are evaluated in sequence as the hull resistance,  $R_T$ , has no dependence on propeller performance. The propeller analysis computes



the operating advance coefficient based on the value of  $R_T$  it receives, yielding the required propeller rotational speed which is then used in computing the SFOC and the cavitation criterion. To consider the full mission profile, the hull-propeller analysis sequence is run for a range of speeds during each function call and weighted based on the PDF.

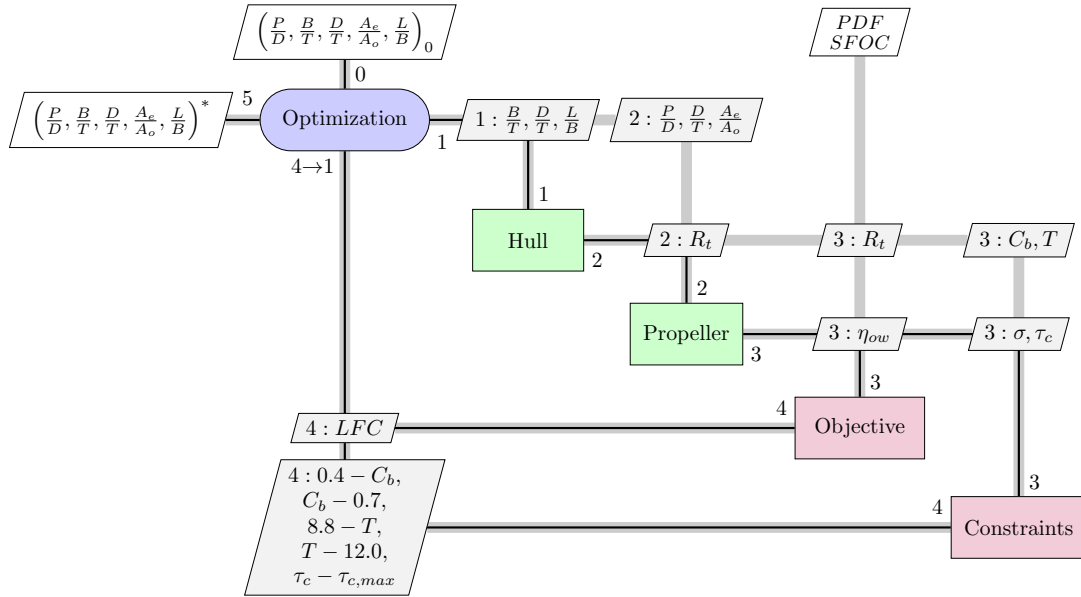


Figure 4.12: Data and process flow diagram for the hull-propeller design optimization process.

Figure 4.12 also explains the sequence in which the hull and propeller analyses are executed within the context of optimization. The algorithm begins at the initial set of design variables,  $(P/D, B/T, D/T, A_e/A_o, L/B)_0$ , executes the hull and propeller analyses in order, and returns the value of the objective and constraint functions to the optimizer. Based on this information, the optimizer internally computes the next iterate — the new set of design variables — and executes the hull-propeller sequence again to obtain the new values of the objective and constraints. This process is repeated until the optimizer determines that the design variables have converged, at which point it exits the loop and returns the optimum,  $(P/D, B/T, D/T, A_e/A_o, L/B)^*$ .

The objective function gradient and constraint Jacobian are evaluated using a

forward difference with a step size determined internally by SNOPT based on the scaling of the problem. Finite-difference methods such as the one used here often suffer from significant truncation error because the amount we can reduce the step size is limited by subtractive cancellation error, which typically begins to dominate at relative step sizes smaller than  $10^{-5}$  [Martins et al. \(2003\)](#). When necessary, the complex-step method and automatic differentiation are two options for circumventing this limitation. However, the low curvature in this design space reduces the impact of truncation error in the problem considered, as Figure 4.13 shows efficient convergence to a gradient norm of  $10^{-10}$ .

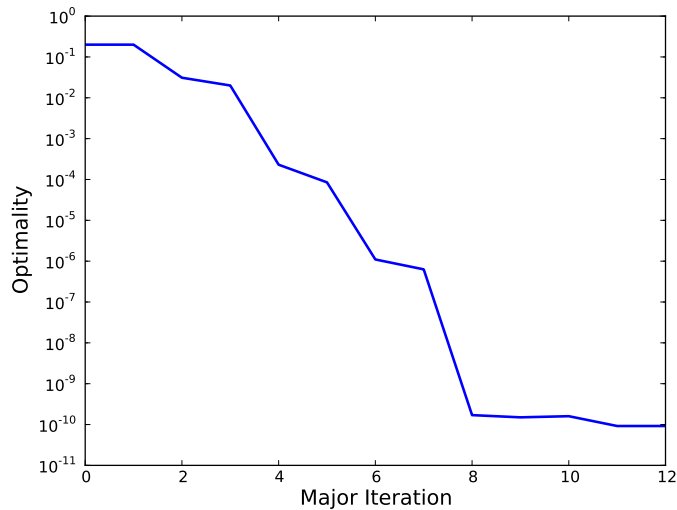


Figure 4.13: Convergence history of the gradient of the Lagrangian plotted against major iteration count.

### 4.2.3 Propeller-Hull Results

The algorithm described in the preceding sections was used to optimize the hull and propeller of a KCS SIMMAN container ship. The original hullform can be seen in Figure 4.14. Through the optimization the length, 230 meters, and the displacement, 49620.6 cubic meters, was kept constant. The vessel is also assumed to have two L51/60DF engines [MAN \(2009\)](#) on board, each with a 5-bladed B-series propeller.



Figure 4.14: Original container ship hullform.

The optimum design vector was  $x^* = \left\{ 3.065 \quad 0.9 \quad 1.066798 \quad 0.878813 \quad 8.0 \right\}$ . This shows that, in the optimal design, the propeller diameter went to its maximum allowable dimension, while the beam went to its minimum. This is expected given the simplistic representation of the hull used in this work. The optimum design vector leads to a lifetime fuel consumption,  $LFC^*$ , of 1.19 million barrels for the ship.

In order to investigate the potential of the simultaneous method proposed in this work it must be compared to a similar exercise using a point-based sequential approach. This is done by formulating two separate optimization problems; one for the hull and one for the propeller, at a given design speed. The optimization problem for the hull is found in equation 4.25.

$$\begin{aligned}
 & \text{minimize} && R_T(x, V') \\
 & \text{with respect to} && 1.2 \leq B/T \leq 3.6 \\
 & && 5.0 \leq L/B \leq 8.0 \\
 & \text{subject to} && 0.4 \leq C_b \leq 0.8 \\
 & && 8.8 \leq T \leq 12
 \end{aligned} \tag{4.25}$$

In equation 4.25  $V'$  is the design speed chosen for the optimization. For this work

a speed of 12.35 meters per second was used. Running this algorithm will produce an optimum beam to draft and length to beam ratio corresponding to a minimum resistance,  $R'_T$ . This resistance is then used to solve the propeller optimization problem seen below in equation 4.26.

$$\begin{aligned}
& \text{minimize} && -N(x, V', R'_T) \\
& \text{with respect to} && 0.5 \leq D/T \leq 0.9 \\
& && 0.5 \leq P/D \leq 1.4 \\
& && 0.55 \leq A_e/A_o \leq 1.05 \\
& \text{subject to} && \tau_c - \tau_{c,max} \leq 0
\end{aligned} \tag{4.26}$$

In equation 4.26  $N$  is the efficiency corresponding with the design vector  $x$ , at the speed  $V^*$  and resistance  $R_T^*$ . Solving the optimization problems given in 4.25 and 4.26 sequentially will produce a design vector which can be used to calculate a corresponding LFC value. When this process is executed on the KCS SIMMAN container ship, a solution,  $x' = \left\{ 2.662 \quad 0.9 \quad 1.115079 \quad 0.882906 \quad 8.0 \right\}$  is found. This leads to a fuel consumption of 1.337 million barrels. A comparison of the two results can be seen in Table 4.3.

Table 4.3: Comparison of results for different optimization methods.

Method	$B/T$	$D/T$	$P/D$	$A_e/A_o$	$L/B$	$C_b$	$T$ (m)	LFC (bbl $\times 10^6$ )
Simultaneous	3.065	0.9	1.07	0.879	8.0	0.8	9.38	1.199
Sequential	2.662	0.9	1.12	0.883	8.0	0.7	10.8	1.337

Table 4.3 shows that there is a 10.36% fuel savings realized when using the simultaneous optimization over the sequential approach. The differences in the two design vectors come from both the simultaneous optimization and the probabilistic approach. The  $B/T$  value of 3.065 for the optimal vessel is the result of optimizing over the entire operational profile, instead of a single design speed. The differences in

the variables describing the propeller,  $P/D$  and  $A_e/A_o$ , are largely the result of the simultaneous optimization. This shows that by considering the propeller and hull as a coupled system, even in the simplified representation shown in this work, considerable fuel savings can be found over the life of a vessel. The two methods also found fairly different hullforms in terms of shape, with the simultaneous method favoring a higher block coefficient and lower draft and the sequential method finding the opposite. This shows that by utilizing multi-disciplinary design techniques it is possible to explore the naval design space and reveal aspects of it that may be difficult to otherwise ascertain. Given the difficulty of the naval lifetime cost problem, the work presented in this section highlights the potential to use multi-disciplinary techniques to facilitate the development of three dimensional trade-spaces comparing different categories of lifetime cost.

### 4.3 Contributions

The work shown in section 4.1 has developed and demonstrated the ability of a novel early-stage design method to develop trade-spaces for build complexity and resistance. This method has been demonstrated by producing these Pareto fronts for two different hullforms; a nominal naval combatant and a container ship. These two hulls differed significantly in both shape and mission and the optimization formulation presented was able to capture these differences and search a large portion of the design space around the original vessels. By utilizing a search method such as this the focus of the optimization becomes informing the designer to the nature of the design space, allowing them to make decisions that support the reduction of lifecycle costs.

While the optimization exercise shown here represent a small portion of the criterion necessary to analyze during ship design, they highlight the potential benefit to understanding this type of trade-space during the time when design decisions can still

be made. It has also been shown that the nature of these trade spaces, while possibly having similar trends, can have varying shapes and may not be entirely intuitive from the outset. The aspects of the design that are changed along this trade-space are also not necessarily evident and this methodology allows these aspects to be explored and better understood. Thus, a tool such as the method presented here could give a designer the ability to make changes to a hull form early in the design process and know how they will impact different life-cycle cost aspects.

It has been shown that, especially for the naval combatant, the trade-space can be difficult to resolve; and the work presented here produced an incomplete Pareto-front. It is believed that this is due to the unique nature of a warship's mission requirement. The shape coupled with the complex operational profile creates a design space that is difficult to explore and, yet, important to understand. This shows that there is a potential to employ more powerful optimization techniques; such as multi-disciplinary optimization methods, to create a framework that is able to resolve Pareto-fronts between competing categories of cost for complex mission types.

Thus, in section 4.2 it has been shown that multi-disciplinary optimization routines can be used effectively in the naval design space. The work presented a new approach to minimize the lifetime fuel consumption of a vessel by simultaneously optimizing the hull and propeller geometry for a vessel. The approach uses a probabilistic mission profile to describe the operation of the vessel in order to avoid optimizing for a single speed. This simultaneous method has shown noticeable improvements in fuel consumption over a traditional sequential point-based approach and converged to different hull and propeller geometries. An algorithm such as the one shown here could aid in the early stage design process, allowing systems to be developed which minimize the lifetime fuel consumption and, therefore, reduced overall ownership costs and emissions.

After performing the optimizations presented in the previous two chapters it is

clear that the lifetime cost space is a difficult one to explore. In chapter 3 the maintenance-production design space, even for a simplified problem, contained a knee in a near-90 degree Pareto-front. In this chapter the Pareto-front found when comparing producibility and resistance was difficult to resolve for the naval vessel. Thus, it is necessary to develop a way to more effectively resolve these fronts to understand the trade-offs between different categories of cost. In the next chapter a method to do this will be presented, utilizing the concepts of multi-disciplinary optimization and specific enhancements to facilitate solving this problem.

## CHAPTER 5

# Enhanced MOCO

### 5.1 Enhanced MOCO Framework (eMOCO)

As was shown in the previous two chapters, the naval lifetime cost design space requires new tools to be able to effectively and accurately resolve the trade-offs. In order to do this an enhanced multi-objective collaborative optimization (eMOCO) framework is created. The eMOCO is a traditional MOCO, as described in chapter 2, with two enhancements that allow it to more effectively solve this category of problem. This problem is difficult for two reasons:

1. The objective spaces themselves differ drastically in nature.
2. The Pareto-fronts are difficult to resolve using traditional optimization methods.

Item 1 means that the use of a distributed MDO architecture, such as CO, can be useful in solving this problem. This is because a distributed architecture utilizes subsystem optimizers that can be tailored to the unique nature of a problem's disciplines. For instance, the hydrodynamic discipline is based on smooth transformation functions and constrained using the area curves of the vessel. This makes it well-suited for gradient-based optimization algorithms, and these will be the most effective tool within this design space. However, due to the nature of both the production and maintenance cost objective functions in the structural design space, different tools



are necessary. In this case a gradient-free optimizer such as a genetic algorithm will be the best approach to solve this discipline problem. This is due to flat regions and regions resembling step functions in this discipline’s objective space. Examples of the structural design space can be seen in Figures 5.1 and 5.2.

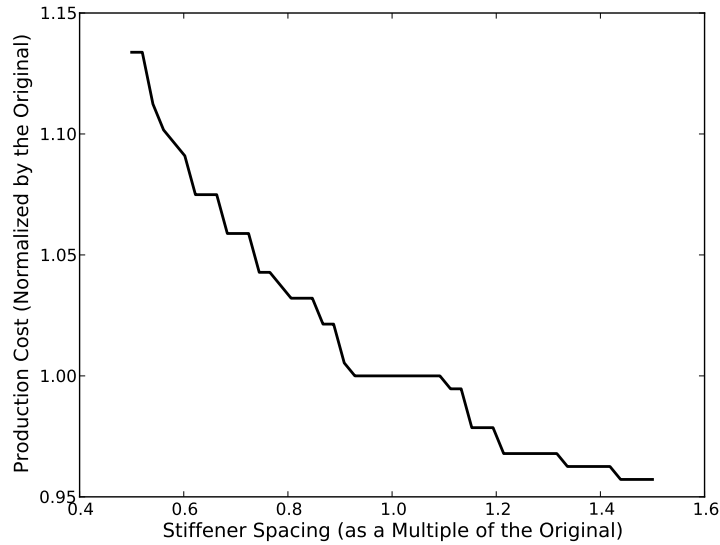


Figure 5.1: The production cost for a structure as a function of the stiffener spacing in a single functional location.

Figure 5.1 shows that the production cost changes with respect to the structure’s stiffener spacing in a fashion resembling a step function. Figure 5.2 has a large flat area in the objective function for a number of stiffener spacings beyond a value of 1.2. This type of objective space, where some sections are flat or near-discontinuous, are not well-suited for algorithms that depend on the problem’s gradient. Thus, these will be best solved with a heuristic algorithm such as a single-objective genetic algorithm.

In order to address these differences between the different design spaces, a decision support process, goal programming, is employed at the discipline level to minimize objective functions with respect to discipline variables during every analysis at the sub-system level. This aids in pushing the Pareto-front through flat portions of the design space or weak local minima at the system level.

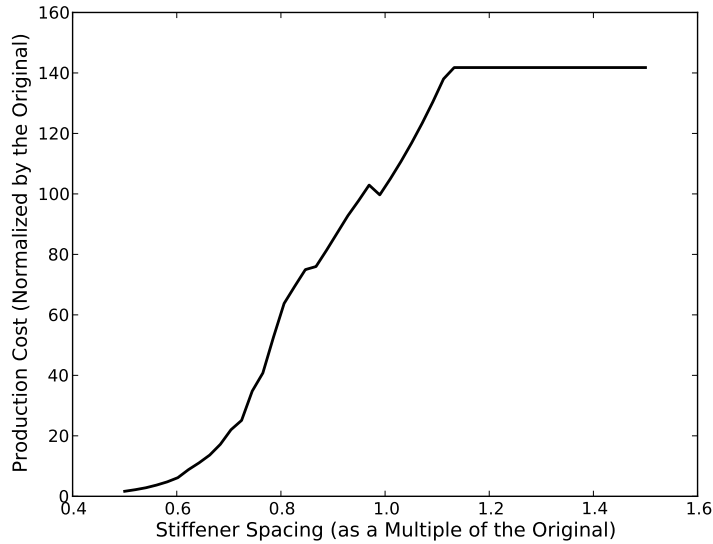


Figure 5.2: The maintenance cost for a structure as a function of the stiffener spacing in a single functional location.

A problem, however, arises when using population-based algorithms at the sub-system level. In current literature, when an optimizer such as a SOGA is used to solve the discipline problem a small design of experiments around each point in the system level population is performed, and using this as an initial population for the discipline optimizer. This can become quickly intractable given the number of genetic algorithms that must be executed. In order to address this a new single-objective optimizer, the locally-elitist genetic algorithm (LEGA) is proposed.

### 5.1.1 Goal Programming at the Discipline Level

Goal programming is a decision support process (DSP) that has been used within engineering optimization to handle competing objectives of varying importance. In goal-programming different objectives are satisfied in an order based on their relative importance. This work utilizes lexicographical goal-programming in which each objective is satisfied completely before the optimizer begins working on the next one.

This formulation can be expressed as shown in equation 5.1.

$$\begin{aligned}
& \text{minimize: } F(\mathbf{x}) = [d_1^+, d_2^+, \dots, d_n^+] \\
& \text{subject to: } \mathbf{g}(\mathbf{x}) \leq \mathbf{0} \\
& f_i(\mathbf{x}) + d_i^+ - d_i^- = b_i \quad \forall i = 1, \dots, n
\end{aligned} \tag{5.1}$$

In equation 5.1 each objective,  $f_i$  is being minimized towards a goal,  $b_i$ , according to their respective priority. This manifests in the variables  $d_i^+$  and  $d_i^-$ , which represent the positive or negative variance from the goal of the objective. In the lexicographical approach to goal-programming the constraints ensure that it does not increase the objective functions that have higher priority [Tamiz et al. \(1998\)](#).

This work uses goal-programming in a novel approach to allow the sub-system problems to reduce the local objective functions while maintaining the inter-discipline feasibility. This lets them act as a local decision maker, ensuring that solutions passed back to the system-level optimizer represent areas of the design space that are locally optimal. By utilizing this technique, along with the inter-disciplinary feasibility metrics inherent to collaborative optimization, the system-level optimizer can efficiently resolve difficult Pareto-fronts involving sub-spaces of drastically different natures.

Collaborative Optimization (CO) separates a system-level problem and discipline-level ones by introducing copies of coupling and shared design vectors and passing them to the sub-system optimizers ?. The system-level optimizer then focuses on minimizing the objective vector,  $\mathbf{f}(\mathbf{x})$ ; while the sub-system problem then ensures all local constraints are satisfied while minimizing discrepancy between local design variables and the copies sent from the system-level optimizer. The system- and sub-

system level problems can be seen in 5.2 and 5.3:

**System Level:**

$$\begin{aligned} &\text{minimize: } \mathbf{f}(\mathbf{x}) = (f_0, f_1, \dots, f_N) \\ &\text{with respect to: } \mathbf{x} = (x_0, \hat{x}_1, \dots, \hat{x}_N, \hat{y}) \\ &\text{subject to: } g_0(\mathbf{x}) \geq 0 \end{aligned}$$

$$\begin{aligned} J_i^* = & \|\hat{x}_{0_i} - x_0\|_2^2 + \|\hat{x}_i - x_i\|_2^2 + \\ & \|\hat{y}_i - y_i\|_2^2 = 0 \text{ for } i = 1, \dots, N \end{aligned} \quad (5.2)$$

**Sub-System Level:**

$$\begin{aligned} &\text{minimize: } J_i = \|\hat{x}_{0_i} - x_{0_i}\|_2^2 + \\ & \|\hat{x}_i - x_i\|_2^2 + \|\hat{y}_i + y_i\|_2^2 \\ &\text{with respect to: } \hat{x}_{0_i}, x_i \\ &\text{subject to: } g_i(\hat{x}_{0_i}, x_i, y_i) \geq 0 \end{aligned} \quad (5.3)$$

In equation 5.2,  $x_0$  represents the vector of variables shared between disciplines,  $x_i$  represent design variables unique to the  $i^{th}$  discipline, and  $y_i$  represents coupling variables from discipline  $i$  to a subset of disciplines  $j \neq i$ . The coupling variables may be specific design variables themselves or, more often, state vectors that are calculated based on the other design variables. Variables marked with a  $\hat{\phantom{x}}$  represent copies passed between the system and sub-system problems. By having local copies of each variables within the various problems, the algorithms can work in parallel to reduce local objectives and constraints. The inter-disciplinary feasibility function,  $J_i$  for each discipline ensures that, when the system-level optimizer converges, each discipline agrees on the optimal design vectors.

Due to the distributed nature of the MOCO architecture it is possible to utilize the sub-system optimizers in the development of the Pareto-fronts. By enhancing the MOCO with the goal-programming DSP outlined above at a sub-system level the local objective function value can be reduced. The sub-system populations passed back to the system level optimizer then represent design vectors that are minimized with respect to their disciplines, facilitating the movement of the Pareto-front towards the optimum. This leads to the revised sub-system problem formulations in equation 5.4:

$$\begin{aligned}
& \text{minimize: } \mathbf{F}(\mathbf{x}) = [d_{i_J}^+, d_{i_{f_1}}^+, \dots, d_{i_{f_N}}^+] \\
& \text{with respect to: } \hat{x}_{0_i}, x_i \\
& \text{subject to: } g_i(\hat{x}_{0_i}, x_i, y_i) \geq 0 \\
& \quad J_i(\hat{x}_0, x_i, y_i) + d_{i_J}^- - d_{i_J}^+ = 0 \\
& \quad f_{i_1}(\hat{x}_0, x_i, y_i) + d_{i_{f_1}}^- - d_{i_{f_1}}^+ = 0 \\
& \quad \vdots \\
& \quad f_{i_N}(\hat{x}_0, x_i, y_i) + d_{i_{f_N}}^- - d_{i_{f_N}}^+ = 0 \tag{5.4}
\end{aligned}$$

The system level problem remains as shown in equation 5.2. The vector of objective functions is reduced while satisfying any shared constraints; and ensuring that there is inter-disciplinary feasibility. However, at a sub-system level a lexicographical goal-programming approach is used to accomplish two goals:

1. Minimize the discipline infeasibility for the local design variables.
2. Reduce any local objective functions.

This means the sub-system problem first minimizes the local  $J$  function; then, secondarily, reduces the local objectives. This can aid the system-level optimizer in resolving difficult Pareto-fronts by ensuring that discipline design variables are pushed towards the front. Note that  $N$  number of discipline objectives can be minimized

during the goal-programming routine. This allows the engineer using the algorithm to set a hierarchy to different objectives, allowing their engineering experience and intuition to play a part in the outcome of the optimizer. Note that the formulation shown in equation 5.4 assumes the local objective functions are being minimized towards zero; however, this could be changed to reflect the nature of whatever problem is being solved.

Since the interdisciplinary feasibility functions can be optimized with any type of algorithm, the sub-system problems can utilize optimization techniques tailored to the local objectives. For instance, if the space is discontinuous or multi-modal a gradient-free algorithm such as a genetic algorithm or particle swarm optimizer can be used; however, if it is  $C_1$  continuous a more effective gradient-based method can be used. Thus, the system-level can employ a multi-objective genetic algorithm to resolve the full-Pareto front, yet, the specific nature of each discipline can still be exploited by the sub-system problem to aid the system-level optimizer. This also allows various optimizers to be implemented at a sub-system level at the designers will with relative ease depending on the problem being solved.

### **5.1.2 Locally Elitist Genetic Algorithm (LEGA)**

In order for the goal-programming enhanced MOCO to effectively optimize non-continuous sub-spaces; a gradient-free algorithm must be utilized at a sub-system level. In current literature sub-system genetic algorithms have been developed for a MOCO framework by using a design-of-experiments method to sample points in the local vicinity around each point in the system-level population. These sample points are then used as the initial population for a single-objective genetic algorithm (SOGA). This means that for every candidate solution in the system-level a full genetic algorithm must be performed. While this approach is conceptually intuitive, it is also computationally expensive. It would be advantageous if a single execution

of a genetic algorithm could be done at the sub-system level.

However, each candidate solution in the system-level population will have different values of  $\hat{x}_i$ ,  $x_0$ , and  $\hat{y}_i$ . Since these vectors do not change throughout the discipline-level optimization they will be referred to as *static vectors*. Since the static vectors are fundamental to  $i^{th}$  sub-system's  $J_i$  function, the discipline-level problem associated with each candidate solution is actually slightly different. This makes it difficult to use the standards evolutionary operators such as crossover; since each solution represents a slightly different optimization problem based on its location in the design space. The problem lies in that if the standard operators are used the discipline-level SOGA will quickly move each solution to whichever candidate is nearest to the feasible domain, drastically diminishing the genetic diversity in the population. In order to avoid this the diversity of the static vectors within a population must be maintained throughout the genetic algorithm. This can be done by defining new crossover and selection functions that are elitist *locally* with respect to solutions with identical static vectors; however, highly non-elitist with respect to the entire population. The crossover function can be seen in algorithm 1:

---

**Algorithm 1** Crossover For LEGA

---

**Require:** Two parent solutions,  $x_1$  and  $x_2$ , with corresponding state vectors,  $\mathbf{y}_{i_1}$  and  $\mathbf{y}_{i_2}$ , discipline-specific copies,  $\hat{\mathbf{x}}_{i_1}$  and  $\hat{\mathbf{x}}_{i_2}$ , and shared copies,  $\mathbf{x}_{0_1}$  and  $\mathbf{x}_{0_2}$

```

1: function LEGA-CROSSOVER( $x_1|_{y_1}, x_2|_{y_2}$ )
2:    $\theta_1 \leftarrow (\mathbf{x}_{0_1}, \hat{\mathbf{x}}_{i_1}, \mathbf{y}_{i_1})$ 
3:    $\theta_2 \leftarrow (\mathbf{x}_{0_2}, \hat{\mathbf{x}}_{i_2}, \mathbf{y}_{i_2})$ 
4:    $c_1|_{\theta_1}, c_2|_{\theta_1}, c_1|_{\theta_2}, c_2|_{\theta_2} \leftarrow \mathbf{crossover}(x_1|_{\theta_1}, x_2|_{\theta_2})$ 
5:    $w_1 \leftarrow \min(\min(f(c_1|_{\theta_1}), f(c_2|_{\theta_1})), f(x_1|_{\theta_1}))$ 
6:    $w_2 \leftarrow \min(\min(f(c_1|_{\theta_2}), f(c_2|_{\theta_2})), f(x_2|_{\theta_2}))$ 
7:   return  $w_1, w_2$ 

```

---

In algorithm 1 the static vectors from each parent solution are stored in:  $\theta_1$  and  $\theta_2$ . A crossover method is then used to produce two children from the parents; and each candidate child solution is given both parents  $\theta$  vectors, producing four unique

solutions. All solutions associated with a given  $\theta$  vector are then compared; and the winner from these comparisons is added to the child population. Note that this means the LEGA has more objective function evaluations per generation, however, this cost is significantly less than the cost of solving an individual genetic algorithm for each point in the system-level population. This ensures that the a strong-candidate solution corresponding to *each* static  $\theta$  vector is added to the child population; thus helping to preserve genetic diversity with respect to the static vectors.

In order to ensure the diversity of the static vectors remains from each generation to the next; a selection method is also utilized that focuses on maintaining this diversity.

---

**Algorithm 2** Selection of continuing population for LEGA

---

**Require:** Population of children  $W$  and parents,  $P$

```

1: function LEGA-SELECTION( $W, P$ )
2:   for all  $c \in W$  do
3:     for all  $x \in P$  do
4:       if  $c$  is offspring of  $x$  then
5:          $x \leftarrow \min(f(c), f(x))$ 
6:   return  $P$ 

```

---

Algorithm 2 will only ever compare a child candidate solution (the population of which is generated using algorithm 1) to one of the parent solutions that produced it. Therefore, even if a small number of static variable vectors make up the mating pool, or child pool, the diversity of static vectors will not degenerate from one generation to the next. This creates an algorithm that, from a population perspective, is highly non-elitist; since poor solutions can remain in the population to preserve the diversity of static vectors, however, it is quite elitist locally in improving the solutions attached to each of the static vectors.

The primary reason this must be done is that the discipline level SOGA is seeking to improve the *entire* system-level population in a single run; meaning that the entire final population must be significant to the system-level optimizer, not only a single



optimum solution. While this approach is not as intuitive as designing an entire SOGA run around each system-level individual, it functions well within the MOCO framework and saves significantly on computational effort.

The eMOCO presented in this section is developed mainly using the Python Programming language. This includes the system-level optimizer, the LEGA discipline optimizer, and the interface between the system and sub-system levels. In order to increase the computational efficiency both the system and sub-system optimizers are designed to run in parallel across multiple processors.

## 5.2 Test Problems

In order to show the ability of the enhanced MOCO to solve multi-objective and multi-disciplinary engineering problems multiple test cases will be analyzed. First, a set of standard multi-objective problems that have been used to test algorithms such as the NSGA-II will be used to show the eMOCO's ability to find the solution to basic multi-objective problems. Second, a test-problem based on one presented in other literature on multi-disciplinary optimization is then solved using both the eMOCO and a traditional MOCO (tMOCO) in order to show the computational benefit of the enhanced algorithm.

### 5.2.1 Multi-Objective Test Problems

Two mathematical problems are used to show the algorithm's ability to resolve different Pareto-fronts. These are defined by equations 5.5 and 5.6. They are called CONSTR and TNK respectively. Both of these are taken from [Deb et al. \(2002\)](#) and

have been used in the validation of many multi-objective optimization algorithms.

$$\begin{aligned}
& \text{minimize: } \mathbf{f}(\mathbf{x}) = \left(x_1, \frac{1+x_2}{x_1}\right) \\
& \text{subject to: } g_1(\mathbf{x}) = -x_2 + 9x_1 - 1 \geq 0 \\
& \qquad \qquad g_2(\mathbf{x}) = \frac{x_2 + 9x_1 - 6}{6} \geq 0
\end{aligned} \tag{5.5}$$

$$\begin{aligned}
& \text{minimize: } \mathbf{f}(\mathbf{x}) = (x_1, x_2) \\
& \text{subject to: } g_1(\mathbf{x}) = x_1^2 + x_2^2 - 1 - 0.1 \cos(16 \arctan(\frac{x_1}{x_2})) \geq 0 \\
& \qquad \qquad g_2(\mathbf{x}) = \frac{-(x_1 - 0.5)^2 - (x_2 - 0.5)^2 + 0.5}{0.5} \geq 0
\end{aligned} \tag{5.6}$$

The problem in 5.5 is driven largely by the second objective function and first constraint; whereas the problem in 5.6 is clearly driven entirely by the constraints.

In order to test the enhanced MOCO using these problems they were divided into two disciplines each; where  $x_1$  is the discipline variable for the first discipline,  $x_2$  is the discipline variable for the second, and there are no shared variables. Equation 5.5 can be transformed into the following system-level and sub-system problems:

**System Level:**

$$\begin{aligned}
& \text{minimize: } \mathbf{f}(\mathbf{x}) = \left(\hat{x}_1, \frac{1+\hat{x}_2}{\hat{x}_1}\right) \\
& \text{subject to: } \|\hat{x}_1 - x_1\|_2^2 + \|\hat{x}_2 - x_2\|_2^2 = 0
\end{aligned} \tag{5.7}$$

**Discipline 1:**

$$\begin{aligned}
&\text{minimize: } F(x) = [d_{1_j}^+, d_{1_f}^+] \\
&\text{subject to: } g_1(x) = -\hat{x}_2 + 9x_1 - 1 \geq 0 \\
&\quad g_2(x) = \|\hat{x}_1 - x_1\|_2^2 + d_{1_j}^+ - d_{1_j}^- = 0 \\
&\quad g_3(x) = x_1 + d_{1_f}^+ - d_{1_f}^- = 0
\end{aligned} \tag{5.8}$$

**Discipline 2:**

$$\begin{aligned}
&\text{minimize: } F(x) = [d_{2_j}^+, d_{2_f}^+] \\
&\text{subject to: } g_1(x) = \frac{x_2 + 9\hat{x}_1 - 6}{6} \geq
\end{aligned} \tag{5.9}$$

$$\begin{aligned}
&\quad g_2(x) = \|\hat{x}_2 - x_2\|_2^2 + d_{1_j}^+ - d_{1_j}^- = 0 \\
&\quad g_3(x) = \left( \frac{1 + x_2}{\hat{x}_1} \right) + d_{2_f}^+ - d_{2_f}^- = 0
\end{aligned} \tag{5.10}$$

By breaking equation 5.5 into equations 5.7, 5.8 and 5.10 it can be solved using the enhanced-MOCO algorithm. The goal-programming is lexicographical in approach; this means that the sub-system optimizers will first minimize the disciplinary infeasibility as much as possible; and then focus on reducing the local objective function; without increasing the value of  $J_i$ . This allowed the algorithm to ensure the inter-disciplinary infeasibility, and also allow the sub-system optimizers to reduce the objectives specific to their subspaces.

The problem shown in 5.6 can be broken down similarly as seen in equations 5.11, 5.12,

and 5.14.

**System Level:**

$$\text{minimize: } \mathbf{f}(\mathbf{x}) = (\hat{x}_1, \hat{x}_2)$$

$$\text{subject to: } \|\hat{x}_1 - x_1\|_2^2 + \|\hat{x}_2 - x_2\|_2^2 = 0 \quad (5.11)$$

**Discipline 1:**

$$\text{minimize: } F(x) = [d_{1_j}^+, d_{1_f}^+]$$

$$\text{subject to: } g_1(\mathbf{x}) = x_1^2 + \hat{x}_2^2 - 1 - 0.1 \cos(16 \arctan(\frac{x_1}{\hat{x}_2})) \geq 0$$

$$g_2(x) = \|\hat{x}_1 - x_1\|_2^2 + d_{1_j}^+ - d_{1_j}^- = 0$$

$$g_3(x) = x_1 + d_{1_f}^+ - d_{1_f}^- = 0 \quad (5.12)$$

**Discipline 2:**

$$\text{minimize: } F(x) = [d_{2_j}^+, d_{2_f}^+]$$

$$\text{subject to: } g_1(x) = \frac{-(\hat{x}_1 - 0.5)^2 - (x_2 - 0.5)^2 + 0.5}{0.5} \geq 0 \geq \quad (5.13)$$

$$g_2(x) = \|\hat{x}_2 - x_2\|_2^2 + d_{1_j}^+ - d_{1_j}^- = 0$$

$$g_3(x) = x_2 + d_{2_f}^+ - d_{2_f}^- = 0 \quad (5.14)$$

It is important to note that the division of this problem into two disciplines is arbitrary; and the coupling between them is high. This means it is not expected for the enhanced-MOCO to outperform more traditional algorithms, however, it is important that the algorithm is able to resolve these Pareto-fronts.

The Pareto-fronts for these problems using both the enhanced-MOCO and a traditional genetic algorithm (in this case an implementation of the NSGA-II [Deb et al.](#)

(2002)) are shown in Figures 5.3 and 5.4. In both cases the optimizer evolved a population of 50 individuals over 50 generations. Both discipline optimizers used to produce the results are the LEGA presented above; however, similar ones were found using an SQP algorithm at the discipline level.

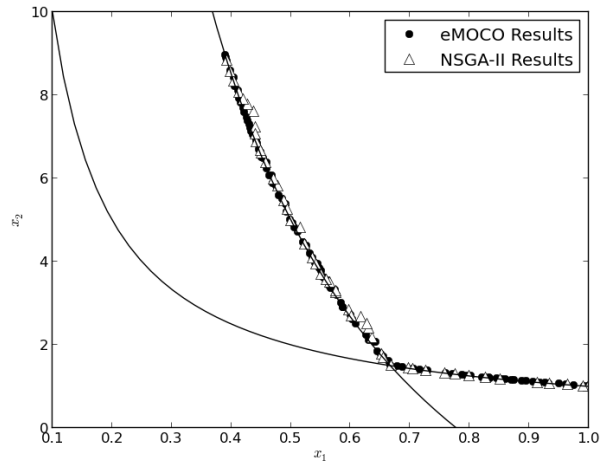


Figure 5.3: CONSTR Problem - solved with eMOCO and NSGA-II.

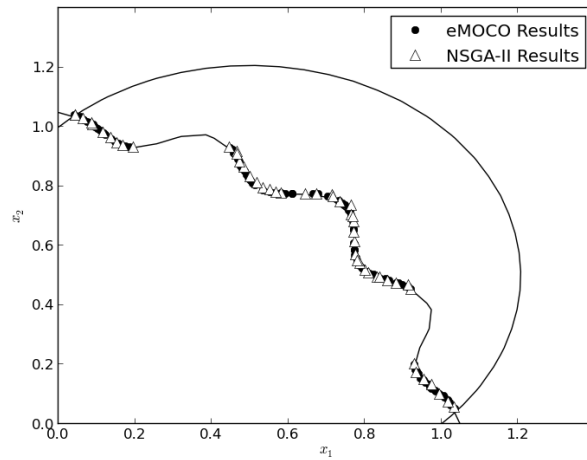


Figure 5.4: TNK Problem - solved with eMOCO and NSGA-II.

Figures 5.3 and 5.4 show that the eMOCO is able to resolve both pareto fronts as well or better than a traditional NSGA-II. The TNK problem is a constraint-dominated function with a highly non-linear Pareto-front, while the CONSTR prob-

lem is objective-dominated in one region and constraint-dominated in another. For both these problems the eMOCO performs well.

## 5.2.2 Multi-Disciplinary Test Problem

In order to test the algorithm on an intentionally multi-disciplinary problem a test problem based on one shown in [Ruiyi et al. \(2011\)](#) is used. The problem involves three variables and two disciplines; each of which has a state variable that is passed to the other. An outline of the problem can be seen in Figure 5.5.

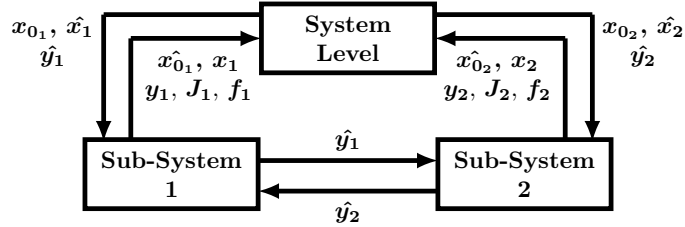


Figure 5.5: Basic data flow for the two-discipline example.

The problem involves one shared variable, two discipline variables, and two state variables that are passed between the disciplines. The system and discipline formulations are shown in in 5.15.

### System Level:

$$\text{minimize: } f_1(\mathbf{x}) = x_1 + \sqrt{x_2} + \frac{y_2^2 - y_1^3}{10^4} + 150,$$

$$f_2(\mathbf{x}) = x_2^2 + x_3 + y_1 + e^{-y_1}$$

with respect to:  $x_1, \hat{x}_2, \hat{x}_3, \hat{y}_1, \hat{y}_2$

$$\text{subject to: } \sum_{i=1}^3 \|x_i - \hat{x}_i\|_2^2 + \sum_{i=1}^2 \|y_i - \hat{y}_i\|_2^2 = 0 \quad (5.15)$$

**Discipline 1:**

$$\text{minimize: } F(\mathbf{x}) = [d_{1_j}^+, d_{1_f}^+]$$

$$\text{with respect to: } \hat{x}_1, x_2, y_1$$

$$\text{subject to: } (\hat{x}_1^2 + x_2 - 0.2\hat{y}_2) - y_1 = 0$$

$$\|x_1 - \hat{x}_1\|_2^2 + \|x_2 - \hat{x}_2\|_2^2 + \dots$$

$$\dots \|y_1 - \hat{y}_1\|_2^2 + d_{1_j}^+ + d_{1_j}^- = 0$$

$$f_1(\mathbf{x}) + d_{1_f}^+ - d_{1_f}^- = 0 \tag{5.16}$$

**Discipline 2:**

$$\text{minimize: } F(\mathbf{x}) = [d_{2_j}^+, d_{2_f}^+]$$

$$\text{with respect to: } \hat{x}_1, x_3, y_2$$

$$\text{subject to: } (\hat{x}_1 + x_3 + \sqrt{\hat{y}_1}) - y_2 = 0$$

$$\|x_1 - \hat{x}_1\|_2^2 + \|x_3 - \hat{x}_3\|_2^2 + \dots$$

$$\dots \|y_2 - \hat{y}_2\|_2^2 + d_{2_j}^+ + d_{2_j}^- = 0$$

$$f_2(\mathbf{x}) + d_{2_f}^+ - d_{2_f}^- = 0 \tag{5.17}$$

In equations 5.15 through 5.17  $x_1$  is a shared variable,  $x_2$  is specific to discipline 1 and  $x_3$  is specific to discipline 2. Both disciplines have state variables  $y_1$  and  $y_2$  that are dependent on each other and the entire vector of design variables. The objective function also involve both disciplines and their respective state variables. This is an example problem that is somewhat representative of the naval design situations this algorithm is being developed for. The design vector and, more specifically, the number of state variables are small, yet they are critical to resolving the front. In order to show the benefit of using the enhanced MOCO this problem will be solved

using both a traditional MOCO and the eMOCO.

Though the MDO example is more complex than the problems shown in the previous section, it is still mathematically simple enough that both the enhanced MOCO and a traditional one can solve it. Thus, it is necessary to have a measurement of convergence in order to analyze the speed at which they solve the problem. Measuring the speed of convergence in a multi-objective problem is not as straight forward or standardized as in single-objective optimization, however, different approaches have been proposed. In [Collette and Siarry \(2005\)](#) a convergence speed metric was proposed based on a threshold frontier. In this metric a true Pareto front is offset by a vector,  $v$  as seen in Figure 5.6.

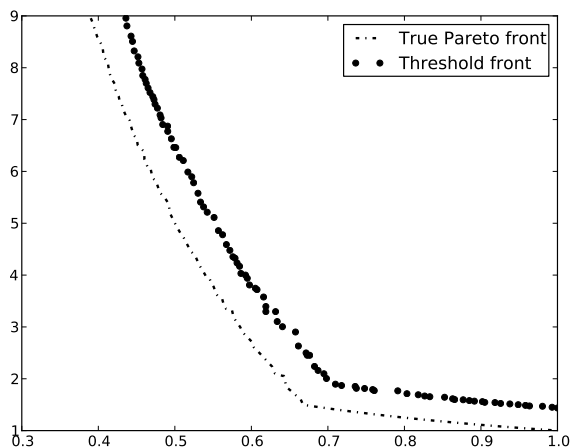


Figure 5.6: An example of a true Pareto front and threshold front.

In the metric proposed in [Collette and Siarry \(2005\)](#) convergence is measured as the portion of a population that falls between the true Pareto front and threshold front at a given generation. This work proposes a similar metric to compare the convergence of the two different MOCO algorithms. A metric such as the threshold front is useful, however, it is possible to report unrealistic convergences where a candidate population is clustered in a small portion of the Pareto-front. Therefore a metric is proposed that combines a threshold measurement with a Pareto-span metric.



The convergence at the  $i^{th}$  generation, denoted as  $\hat{e}(i) \in (0, 1)$ , is calculated using equation 5.18.

$$\hat{e}(i) = \frac{1}{2} \left( \frac{W_{TH}(S_i)}{|S_i|} + \frac{f_{i_1}(x)_{max} - f_{i_1}(x)_{min}}{f_{F_1}(x)_{max} - f_{F_1}(x)_{min}} \right) \quad (5.18)$$

In equation 5.18  $W_{TH}(S)$  is the number of individuals in the  $i^{th}$  solution set that fall under the threshold front and  $|S_i|$  is the size of the  $i^{th}$  solution set.  $f_F(X)$  is the threshold (or ‘true’) Pareto front, and  $f_i(x)$  is the Pareto frontier during the  $i^{th}$  generation. The maximum value  $\hat{e}(i)$  can take is 1.0. Both the eMOCO and traditional MOCO are run until the Pareto front reaches a convergence value of 0.95.

The first term in this metric measures the amount of the population below the threshold frontier, where the second term measures the span of the current front relative to the final one. By utilizing both these concepts a more complete picture of convergence can be determined.

The Pareto front found using a traditional MOCO (tMOCO), an overview of which can be found in ?, and the eMOCO can be seen in Figure 5.7. A population size of 200 was used for all runs.

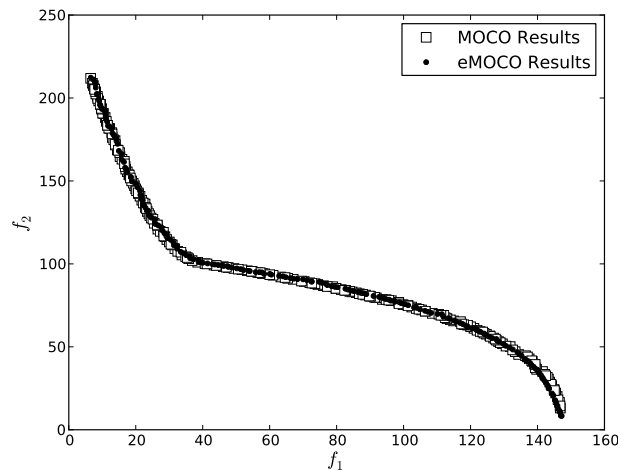


Figure 5.7: The results for th MDO test problem for both the traditional and enhanced MOCO.

Figure 5.7 shows that both algorithms converge to the same Pareto front. This

Table 5.1: Average generations to converge for the traditional (*tMOCO*) and enhanced (*eMOCO*) MOCO over 100 samples.

Algorithm	Average Generations
tMOCO	148.9
eMOCO	109.1

is expected as the problem is a relatively straight-forward MDO example. However, it is important to examine the speed at which both algorithms converge. In order to compare the two algorithms 100 runs of each were done and the average generations to convergence was examined. These values can be seen in Table 5.1.

In order to ensure the validity of the mean shift seen in table 5.1 Welch’s T-Test was performed and the null hypothesis was rejected with a  $p$ -value of 0.00653, showing that the two samples of test runs are statistically different. Table 5.1 shows that the enhanced MOCO is able to consistently solve the test problem in less generations than the traditional one. In fact, it shows that even on this simple example problem the enhanced MOCO is able to converge in 27% less generations than a traditional one over 100 sample runs. This represents a substantial increase in speed; especially for engineering problems where objective calculation can be computationally expensive. This shows that this type of problem; multi-disciplinary problems with important, yet small in dimension, coupling can be much more challenging for traditional MDO techniques to solve than expected. These results show the enhanced MOCO is specifically well suited to solve problems with difficult to resolve Pareto fronts that have small degrees of coupling between their discipline objective functions.

### 5.3 Naval Design Case Study

In order to show the ability of the enhanced MOCO to develop the trade-spaces between different facets of lifetime cost a nominal DTMB-5145 is optimized for both resistance and production. A simplified version of the structure found in [Ashe et al.](#)

(2009) and hull form found in [Benedetti et al. \(2007\)](#) are used. This is the type of problem that the resistance-production trade-space represents; as these two objectives are competing and coupled, however, the coupling is small between the objectives themselves. It is also a relationship representing the cost during two drastically different phases of the vessel's life (production and operation); this is difficult to understand intuitively, making it a good test case for this framework.

### 5.3.1 Objective Function Calculation

In order to calculate the resistance at a single design speed the thin-ship theory as outlined in chapter 2 is used. Frictional resistance is calculated using the ITTC-57 friction line, as described in equation 2.19. These two values are summed together for an estimate of the ship's total resistance at its design speed. Production cost is calculated using equation 2.25, also explained in chapter 2. These two equations incorporate both the hydrodynamic and structural design spaces for a naval vessel and are used within the proposed multi-disciplinary optimization framework.

### 5.3.2 Optimization

The two objective functions used here are prime examples of design spaces whose nature differ significantly. Various researchers have used fast gradient-based optimizers to reduce drag as calculated by Michell's integral successfully and efficiently. However, the production cost is non-smooth due to the nature of the ship's structure. This makes it well suited for an evolutionary based optimizer such as the genetic algorithm. Therefore; developing trade-spaces between these two objectives lends itself well to the enhanced MOCO presented in this work.

The transformation method that is used is described in chapter 4. This method defines a spline across the centerplane of the vessel dictated by control points  $\hat{T}_{l_1}, \dots, \hat{T}_{l_n}$ . However, the scale of the transformation is reduced; in this work, in order to simplify

the problem there is no vertical transform function applied and the maximum perturbation distance is reduced. This is representative of work published in [Temple and Collette \(2012\)](#). The scantlings are defined using a structural discretization based on stiffened panels within various functional locations of the hull. This optimization method is formulated along the same lines as the one presented in equation 3.10. However, similarly to the hydrodynamic portion the scale is reduced, and the problem is similar to the one presented in [Temple and Collette \(2013\)](#)

This leads to the following multi-disciplinary problem being developed.

**System Level:**

$$\begin{aligned}
& \text{minimize: } \mathbf{f}(\mathbf{x}) = (R_L(\mathbf{x}), C_P(\mathbf{x})) \\
& \text{with respect to: } \hat{\mathbf{x}}_H = \hat{T}_{l_1}, \dots, \hat{T}_{l_N} \\
& \hat{\mathbf{x}}_S = \Delta, (t_p, t_w, t_f, h_w, b_f)_i \text{ for } i = 1 \text{ to } n_f \\
& \text{subject to: } \sum_{i=1}^N \|x_{H_i} - \hat{x}_{H_i}\|_2^2 + \sum_{j=2}^5 \sum_{i=1}^{n_f} \|x_{S_{j_i}} - \\
& \quad x_{\hat{S}_{j_i}}\|_2^2 + \|\Delta - \hat{\Delta}\|_2^2 = 0
\end{aligned} \tag{5.19}$$

**Hydro Discipline:**

$$\begin{aligned}
& \text{minimize: } F(\mathbf{x}) = [d_{H_j}^+, d_{H_f}^+] \\
& \text{with respect to: } T_{l_1}, \dots, T_{l_N} \\
& \text{subject to: } |T_{new} - T| \leq 2 \\
& \sum_{i=1}^N \|x_{1_i} - \hat{x}_{1_i}\|_2^2 + d_{H_j}^+ + d_{H_f}^- = 0 \\
& R_T(\mathbf{x}_H) + d_{H_f}^+ - d_{H_f}^- = 0
\end{aligned} \tag{5.20}$$

**Structure Discipline:**

$$\begin{aligned}
& \text{minimize: } F(\mathbf{x}) = [d_{S_J}^+, d_{S_f}^+] \\
& \text{with respect to: } \Delta, (t_p, t_w, t_f, h_w, b_f)_i \text{ for } i = 1 \text{ to } n_f \\
& \text{subject to: } |\Delta - \Delta_i| = 0 \\
& W_S - 1.5W_{S_I} \geq 0 \\
& S_{M_V} - S_{M_{V_I}} \leq 0 \\
& U_{cs_p} - U_{cs_{p_I}} \leq 0 \quad \forall p \\
& SM_p - SM_{p_I} \leq 0 \quad \forall p \\
& d(x_i, x_j) < 0.06 \quad \forall j, i \\
& \sum_{j=2}^5 \sum_{i=1}^{n_f} \|x_{2_{j_i}} - \hat{x}_{2_{j_i}}\|_2^2 + \dots \\
& \dots \|\Delta - \hat{\Delta}\|_2^2 + d_{S_J}^+ + d_{S_f}^- = 0 \\
& C_P(\mathbf{x}_s) + d_{S_f}^+ - d_{S_f}^- = 0 \tag{5.21}
\end{aligned}$$

In this formulation the system level optimizer is minimizing production steelwork cost and the resistance at the vessel’s design speed while ensuring that interdisciplinary feasibility is maintained. The hydrodynamic discipline problem is minimizing the difference between its design variables and the corresponding system level variables as a primary goal and the resistance as a secondary one. As the ship’s hull is transformed the displacement remains constant and, thus, the draft is altered. This discipline constraint ensures that the draft does not change more than 2 meters.

The structural discipline also minimized the difference between its design variables and the associated ones at the system level as well as the production cost of the structure. The constraints satisfied here are that the weight does not increase more than 50% and that the section modulus of the entire structure, the ultimate compressive strength as well as the section modulus of each individual panel is not

reduced. This discipline also ensures that the the components of the different panels do not come within  $6mm$  of each other.

The hydrodynamic discipline uses an SQP (sequential quadratic programming) optimizer included in the Python-based optimization suite pyOpt [Perez et al. \(2012\)](#) This algorithm is a gradient based optimizer that is effective at minimizing functions that are  $C_1$  continuous with well defined minima. The structural discipline uses the LEGA described in section 5.1.2. This algorithm has been specifically designed for sub-problems such as this that are not continuous and may be multi-modal in objective space with weak minima. It is also designed to minimize computation time by only requiring one run for an entire population.

To demonstrate the ability of the enhanced MOCO to develop these Pareto fronts in the naval design space a nominal DTMB5145 naval combatant is used as the initial design. The bodyplan for the initial vessel can be seen in Figure 5.8 and its structure is shown in Figure 5.9.

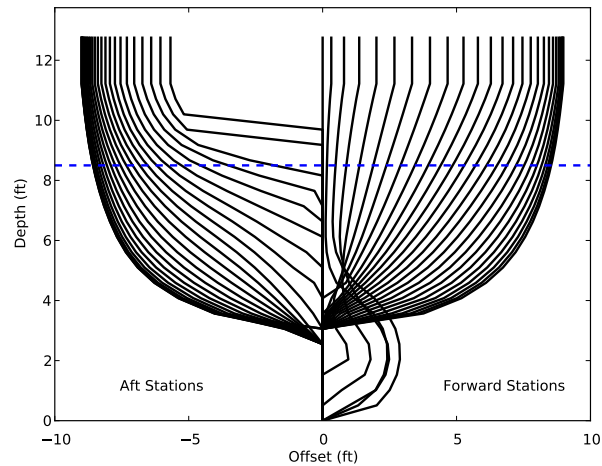


Figure 5.8: Bodyplan for nominal naval combatant

In order to test the ability of the eMOCO to find lifetime cost trade-offs in the naval design space it will be used, along with a traditional optimization method to find a Pareto-front between steelwork production cost and resistance. The multi-

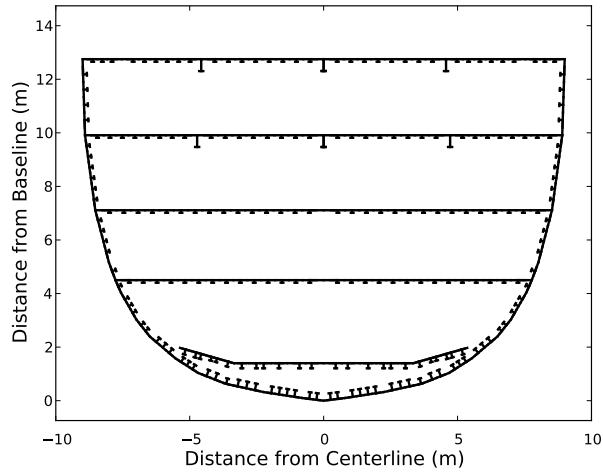


Figure 5.9: Internal structure for nominal combatant.

objective optimizer used for comparison is an NSGA-II implementation solving both disciplines at once. This means it is using an entirely population-based approach without the benefit of any gradient information for the hydrodynamic discipline. The lower resistance will lead to less operational costs, and historically has been the driver behind most naval design optimization. However, by considering multiple cost aspects the designer can focus on reducing total ownership costs from both a structural and hydrodynamic perspective. In the aforementioned work a traditional optimization algorithm was unable to find the complete Pareto front, and specifically struggled to resolve the resistance portion.

### 5.3.3 Results

The Pareto front found using both the enhanced MOCO and an NSGA-II can be seen in Figure 5.10.

In this figure both objectives are normalized by their respective values for the initial hull. As can be seen both optimizers are able to produce fronts with design solutions that dominate the original design with respect to both objective functions. However, the results here show a similar trend as the author's previous work - namely,

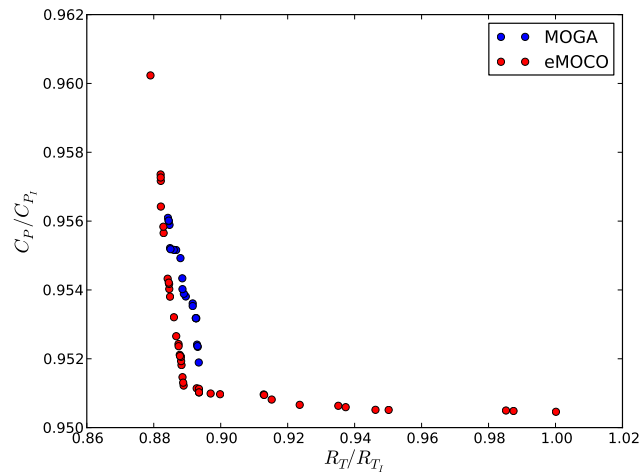
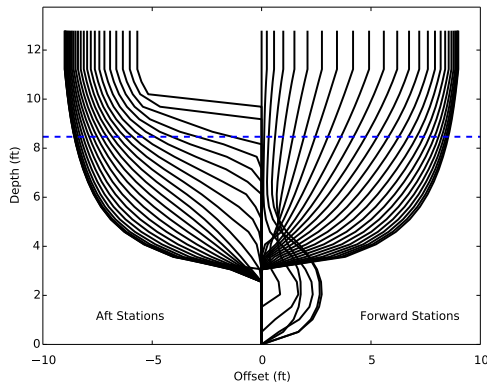


Figure 5.10: Pareto front for nominal naval combatant

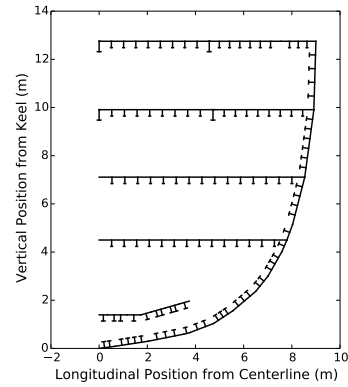
that traditional optimization routines cannot resolve the full front.

Even for this highly simplified test case for the enhanced MOCO the MOGA is only able to resolve the production end of the Pareto front, showing no solutions along the resistance side of the front. This is in line with the results found in [Temple and Collette \(2015b\)](#). Meanwhile, the eMOCO is able to resolve solutions in both respective regions that entirely dominate the front found by the MOGA. It is important to note that the shape of the Pareto-front is similar to the one seen in Figure 3.5. This means that, once again, a single-objective optimizer may end up sacrificing a significant amount in one objective for a small gain in the other. It also means that the inability of the MOGA to resolve the front results in a loss of critical information regarding the nature of the problem. In this type of front, missing the ‘knee’ leads to an understanding of the design space that is fundamentally flawed and may lead to poor design choices being made. This gives the designer a better understanding of the design space and ensures that the information garnered from the Pareto-front is truly aiding them in reducing lifetime ownership costs. Given that the purpose of this type of optimization is to understand trends in the design space, capturing that space is critical. When only small portions of it are resolved valuable information

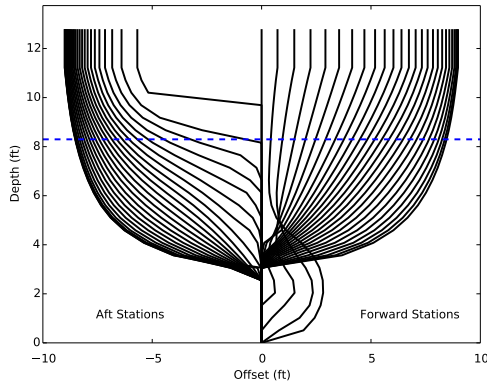




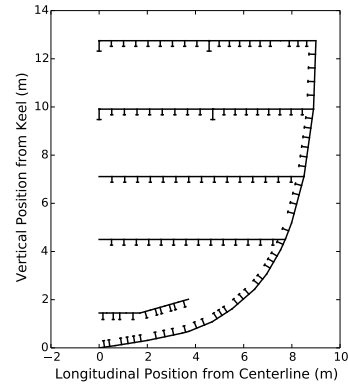
(a) Hull form for vessel with highest resistance.



(b) Structure for vessel with highest resistance.



(c) Hull form for vessel with highest production cost.



(d) Structure for vessel with highest production cost.

Figure 5.11: The hull forms and structures for the vessels at the extreme ends of the Pareto front.

can be missed. For instance: the ends of the Pareto front (the portions missed by traditional optimization) are examined in Figure 5.11.

From Figure 5.11a it can be seen that in the structure that is the cheapest to produce, the bulbous bow of the original vessel is simplified. Along the Pareto front - as the knee is approached - the bulbous bow becomes wider and the stern shallower - reducing the overall resistance. This can be seen in Figure 5.11c where the resistance is minimized. Along the edges of the Pareto front between these points and the 'knee' the evolution of these trends can be seen. It is this information that it is critical to the engineer - as understanding the trends in both the hydrodynamic and structural

space and, specifically, how they influence each other is vital to reducing the overall ownership costs. The proposed enhanced collaborative optimization framework is able to resolve these Pareto-fronts and reveal this information.

## 5.4 Contributions

In this chapter a novel multi-disciplinary design framework has been presented. The framework is based on a MOCO algorithm with two enhancements to tailor it to solving the naval lifetime cost problem. The first enhancement is the use of goal-programming in the discipline optimizer to facilitate finding the Pareto-fronts given the inherent flatness and weak minima present in this problem. By utilizing goal-programming the discipline optimizers are able to aid the system-level optimizer by finding points that are optimal with respect to their local objective functions. The nature of goal-programming as a decision support process also allows a designer to encode some of their intent and intuition into the algorithm by supplying a hierarchy of objective functions to each sub-space. This aids in ensuring that the trade-spaces found are both optimal and represent the engineers vision for the vessel being designed. The second enhancement is a locally-elitist genetic algorithm (LEGA) for use in sub-spaces that are best suited to be optimized using a heuristic population-based algorithm. This novel single-objective genetic algorithm allows the discipline-level problem to be solved in a single execution rather than multiple, greatly reducing computational effort. These two separate enhancements work together to allow the eMOCO to effectively solve the lifetime cost problem.

The eMOCO has been tested on standard multi-objective test problems and been shown to successfully solve them. It has also been used to solve a MDO test problem that has been used in other literature and has been shown to solve the problem more effectively than a traditional MOCO. Finally, it has been used to solve a simplified

naval design example and was far more capable than a traditional MOGA. The results shown in the naval design example show the ability of the eMOCO to solve for the fronts in these trade-spaces and identify the ‘knee’, which is the critical point for a designer. These results re-iterate the concepts found in chapters 3 and 4; that these Pareto-fronts have sharp corners with a knee that is hard to resolve. This means that this is not a problem suited for either single objective optimization routines or traditional multi-objective algorithms. Thus, the eMOCO presented here is a way to resolve these Pareto fronts, locate the knee regions, and give designers a way to understand the trade-offs between the different cost categories.

## CHAPTER 6

# Three Dimensional Trade Spaces

### 6.1 Resistance-Maintenance-Production

The primary goal of developing the eMOCO presented in the previous chapter is to solve harder and larger problems in the naval lifetime cost design space. Based on the results in chapters 3, 4, and 5 it is expected that traditional multi-objective optimization algorithms are unable to resolve the three-dimensional design space. Using the proposed multi discipline approach can yield a better understanding can be gained regarding the impact design decisions have on the lifetime cost of naval vessels. The problem that is solved here is a combination of the smaller problems discussed in the previous chapters. It is broken down into two disciplines: a structural one and a hydrodynamic one. The structural discipline is focused on the maintenance cost objective function, as well as ensuring that that the overall strength of the ship is satisfactory. The hydrodynamic discipline aims to minimize the lifetime resistance of the vessel while ensuring operational performance does not suffer. The production objective is addressed in a somewhat different manner. It is designed in a decomposable manner to utilize both disciplines.

In chapter 2 two different production metrics were introduced. The first was a steelwork and labor costing metric taken from [Rahman and Caldwell \(1995\)](#) and

described in equation 2.25. For reference the equation was:

$$C_P = \sum_{i=1}^n \sum_{j=1}^9 C_{j_i} \quad (6.1)$$

Equation 2.25 is a summation over structural panels alone, meaning it can be calculated entirely using design variables from the structural discipline. A second metric introduced was based on the fuzzy metric proposed in [Parsons et al. \(1998\)](#) and attempts to measure the ‘producibility’ of a vessel based on the Gaussian curvature of her hull. The equation is described in 2.39 and shown again here:

$$C_B = \frac{\sum_{i=1}^{S_n} \sum_{j=1}^{W_n} C_R(i, j) \cdot P_A(i, j)}{SA} \quad (6.2)$$

This equation is based on the curvature of the hull form, and thus is only dependent on shape variables. It is important to note that the fuzzy metric originally proposed in [Parsons et al. \(1998\)](#) was a multiplier on a given raw cost for a steel plate. This was largely due to shipyards wanting to keep the actual costs they incur to cold roll steel proprietary. However, this allows a new combined metric to be developed in a simple manner. If the producibility metric is used as a multiplier for the steelwork and labor costing equation a final production metric,  $C_{P_T}$  can be developed:

$$C_{P_T} = C_B \times C_P \quad (6.3)$$

This formulation allows the single production metric to be decomposable with respect to the two disciplines being analyzed. The system level optimizer can minimize the combined objective presented in equation 6.3 while the structural and hydrodynamic discipline optimizers will only minimize equations 2.25 and 2.39 respectively.

This allows the system and sub-system problems to be formulated as follows:

**System Level:**

$$\begin{aligned}
& \text{minimize: } \mathbf{f}(\hat{\mathbf{x}}, \hat{\mathbf{T}}) = \left( C_T(\hat{\mathbf{x}}), R_{T_E}(\hat{\mathbf{T}}), C_{P_T}(\hat{\mathbf{x}}, \hat{\mathbf{T}}) \right) \\
& \text{with respect to: } \hat{\mathbf{x}} = (\hat{t}_p, \hat{t}_w, \hat{t}_f, \hat{h}_w, \hat{b}_f, \hat{m}_s)_i \text{ for } i = 1 \text{ to } n_f \\
& \hat{\mathbf{T}} = \left( T_l(\hat{x}_1), \dots, T_l(\hat{x}_{n_t}), T_v(\hat{z}_1), \dots, T_v(\hat{z}_{n_t}) \right) \\
& \text{subject to: } \sum_{i=1}^{n_f} \sum_{j=1}^6 \|\hat{x}_{ij} - x_{ij}^2\|_2^2 = 0 \\
& \sum_{i=1}^{n_{t_l}} \|\hat{T}_i - T_{l_i}\|_2^2 + \sum_{i=1}^{n_{t_v}} \|\hat{T}_i - T_{v_i}\|_2^2 = 0 \tag{6.4}
\end{aligned}$$

**Structural Discipline:**

$$\begin{aligned}
& \text{minimize: } F(\mathbf{x}) = [d_{S_J}^+, d_{S_{f_1}}^+, d_{S_{f_2}}^+] \\
& \text{with respect to: } \mathbf{x} = (t_p, t_w, t_f, h_w, b_f, m_s)_i \text{ for } i = 1 \text{ to } n_f \\
& \text{subject to: } |\Delta - \Delta_t| = 0 \\
& W_S - 1.5W_{S_I} \geq 0 \\
& S_{M_V} - S_{M_{V_I}} \leq 0 \\
& U_{csp} - U_{csp_I} \leq 0 \quad \forall p \\
& S_{M_p} - S_{M_{p_I}} \leq 0 \quad \forall p \\
& d(x_i, x_j) < 0.06 \quad \forall j, i \\
& \sum_{j=2}^5 \sum_{i=1}^{n_f} \|x_{2j_i} - \hat{x}_{2j_i}\|_2^2 + \dots \\
& \dots \|\Delta - \hat{\Delta}\|_2^2 + d_{S_J}^+ + d_{S_J}^- = 0 \\
& C_T(\mathbf{x}) + d_{S_{f_1}}^+ - d_{S_{f_1}}^- = 0 \\
& C_P(\mathbf{x}) + d_{S_{f_2}}^+ - d_{S_{f_2}}^- = 0 \tag{6.5}
\end{aligned}$$

### Hydro Discipline:

$$\begin{aligned}
& \text{minimize: } F(\mathbf{T}) = [d_{H_J}^+, d_{H_{f_1}}^+, d_{H_{f_2}}^+] \\
& \text{with respect to: } \mathbf{T} = (T_l(x_1), \dots, T_l(x_{n_t}), T_v(z_1), \dots, T_v(z_{n_t})) \\
& \text{subject to: } |T_{new} - T| \leq 2 \\
& \quad -2 \leq \tau_{new} \leq 0.01 \text{ meters} \\
& \quad z_p - z_{p_I} \leq 0.05 z_{p_I}, \\
& \quad W_{A_{i-1}} - W_{A_i} \leq \epsilon_1 \quad \forall \{i | i > 1\} \\
& \quad \frac{dz_{i+1}}{dW_{A_{i+1}}} - \frac{dz_i}{dW_{A_i}} \leq \epsilon_2 \quad \forall \{z_i | z_p \leq z_i \leq z_m\} \\
& \quad \frac{dx_{i+1}}{dS_{A_{i+1}}} - \frac{dx_i}{dS_{A_i}} \leq \epsilon_3 \quad \forall \{x_i | x_b \leq x_i \leq a_m\} \\
& \quad \max_{x_{m_1} \leq x_i \leq x_{m_2}} \left( \frac{d^2 x_i}{dS_{A_i}^2} \right) \leq \epsilon_4 \\
& \quad \frac{d^2 x_i}{dS_{A_i}^2} \forall \{x_i | x_{m_1} \leq x_i \leq x_{m_2}\} \leq \epsilon_4 \\
& \quad \sum_{i=1}^N \|x_{1_i} - \hat{x}_{1_i}\|_2^2 + d_{H_J}^+ + d_{H_J}^- = 0 \\
& \quad R_{TE}(\mathbf{T}) + d_{H_{f_1}}^+ - d_{H_{f_1}}^- = 0 \\
& \quad C_B(\mathbf{T}) + d_{H_{f_2}}^+ - d_{H_{f_2}}^- = 0 \tag{6.6}
\end{aligned}$$

In equation 6.4 the system level optimizer is minimizing the total maintenance cost, as described in section 3.1 with respect to the structural design vector,  $\mathbf{x}$ . As in equation 3.10 the design vector  $\mathbf{x}$  represents the scantlings for the  $n_f$  functional locations used in the top tier of structural discretization. The system level also minimized the lifetime resistance,  $R_L$  by varying the control points for the two transformation functions, as described in equation 4.6. Equation 6.3 is a function of both the transformation variables and structural ones, however, it is decomposable at the system

level as previously mentioned. The constraints ensure that the discipline level optimizers converge to the same final solution. This problem represents three large, and possibly conflicting, measures of lifetime cost that a designer could potentially be concerned with. By developing this trade space insight into how to reduce the overall cost can be gained.

The structural sub-system problem, seen in equation 6.5 has three goals, ordered by priority. The primary goal of this problem is to reduce the interdisciplinary infeasibility,  $J$ , at the discipline level. However, as a secondary goal the optimizer is reducing the total maintenance cost, and as a third goal it is reducing the portion of the production metric dependent on the structural variables. Similarly the hydrodynamic sub-problem focuses on minimizing its local  $J$  function first, then reduces the lifetime resistance, and finally minimizing the portion of the production metric dependent on the transformation functions. The production metric is set as a lower priority over the resistance and maintenance due to the simpler nature of the objective function and its smaller impact on the lifetime cost for the vessel. However, depending on the designers intent and engineering intuition the priorities of different objectives in the goal-programming can be altered.

During this execution of the optimizer the maintenance framework described in chapter 3 is slightly altered. In the originally presented framework the cost term,  $C_{M_i}$  is calculated by performing a smith-type progressive collapse analysis to find the ultimate moment of the vessel in both sagging and hogging. If these moments are below a pre-determined threshold, then panels are replaced until the threshold is met. However, that method becomes computationally time consuming in the larger problem formulation. In order to reduce the computational burden for the problem the global cost term is calculated by checking the following two criteria:

1. The ultimate compressive strength (UCS) for each panel is not less than a predetermined fraction of that panel's original UCS.



2. The total section modulus for the vessel is not below a predetermined fraction of its original.

If either of these two criteria fail, panels are replaced until they once again are met. This allows the maintenance framework to check the ‘global’ strength of the vessel during each year of operation, but do so at a smaller computational burden to increase the speed at which this problem can be solved.

The system level optimizer is an implementation of the NSGA-II, with the run parameters shown in Table 6.1. The structural discipline is optimized using the LEGA described in chapter 5, and the hydrodynamic discipline is optimized using a gradient-based SQP optimizer. This shows that the eMOCO framework can successfully combine different types of optimizers to take advantage of unique design spaces and develop Pareto-fronts. In Table 6.1  $|P|$  is the size of the population,  $N_G$  is the

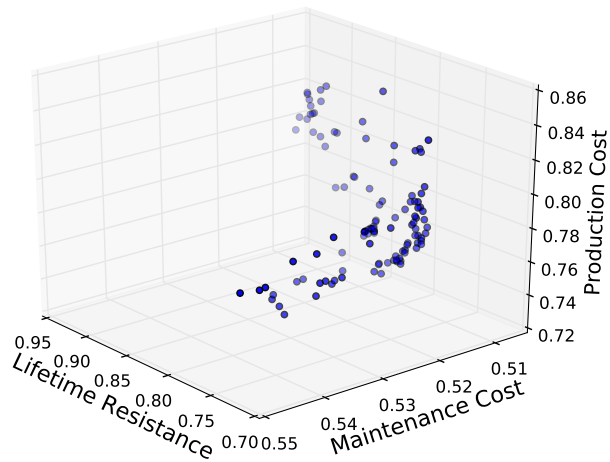
Table 6.1: Run Parameters for System-Level Optimizer.

$ P $	$N_G$	$p_c$	$\eta_c$	$p_m$	$\eta_m$
224	200	.95	2.0	0.1	2.0

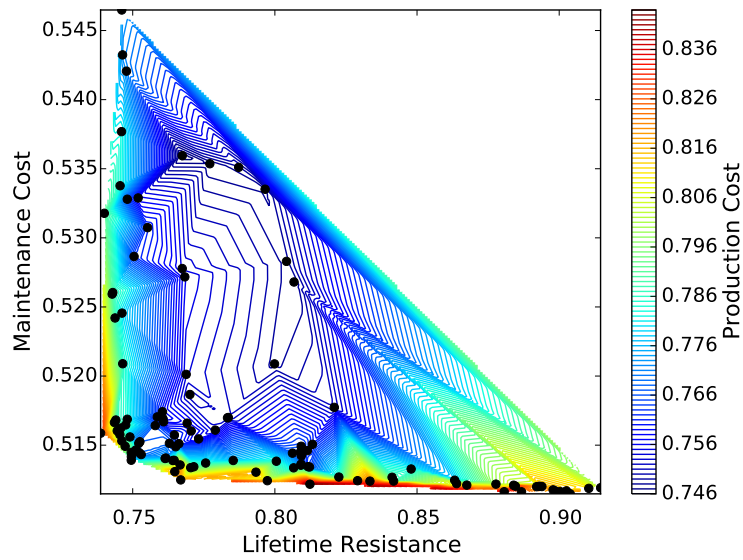
number of generations the optimizer is run for,  $p_c$  and  $p_m$  are the crossover and mutation percentages, and  $\eta_c$  and  $\eta_m$  are the crossover and mutation exponents. Using this formulation for the naval lifetime cost problem three dimensional trade-spaces between production cost, resistance, and maintenance cost are able to be developed. These results are novel, the nature of this type of trade-space has not be explored in current literature, and it will be shown that it can give valuable insight to an engineer.

### 6.1.1 Pareto Fronts

The three dimensional Pareto-front found using this method is presented in Figure 6.1. Figure 6.1a shows the front found by the eMOCO in three dimensional space, while 6.1b shows the same front projected onto a topographical contour plot of the



(a) Multi-disciplinary front in three dimensional space.



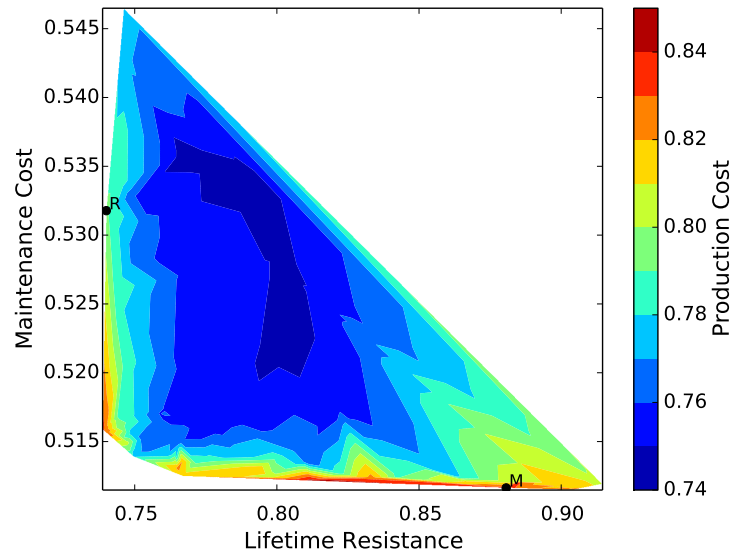
(b) Projected contours for three dimensional front.

Figure 6.1: Three dimensional Pareto front for resistance, maintenance, and production.

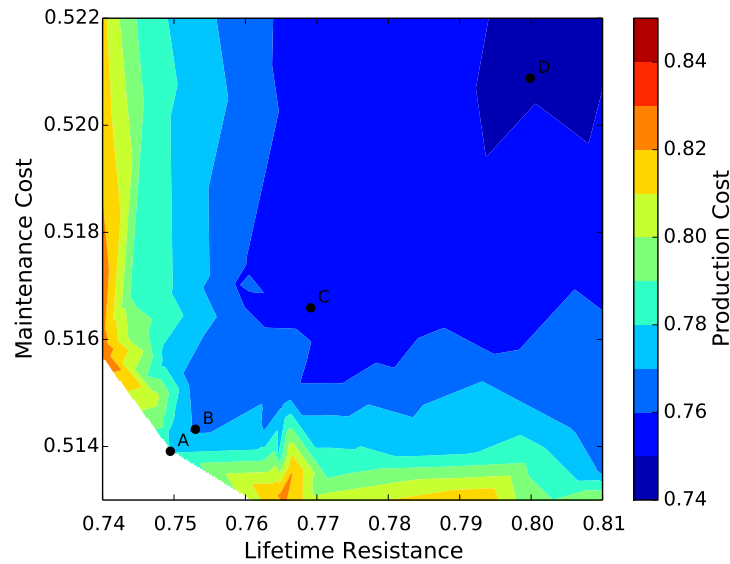
production cost metric. Figure 6.1 shows that the three dimensional front follows the same trend with respects to shape as the results seen in chapters 3 and 5. That is, the ‘knee’ of the front comes at a sharp right angle, with steep sides going in each of the respective objective directions. This, once again, shows that using single-objective, or sequential optimization on this type of problem could lead to inadvertent and unnecessary losses in some objectives for the sake of small gains in one. This highlights the importance of understanding the nature of these trade-offs for a designer, and the benefit of having a tool to visualize them. By having this ability an engineer can get an idea as to the location of the knee in this design space and ensure that the vessel they develop has reduced lifetime costs with respect to each category.

In order to better understand the trade-offs between these different categories of cost, and the impact of design decisions in this space, similar contour plots are shown in Figure 6.2. These contours represent ‘Pareto Zones’ for the final Pareto front, where the production cost will be similar within the zone. The shape of these zones represent the trade-off between lifetime resistance and maintenance cost for that respective production zone. In this way it is simpler to see the way that the trade-offs between two objectives changes with a change in the third. In Figure 6.2a the entire front is shown. In this figure two points are highlighted and labeled  $R$  and  $M$  respectively. These points represent designs that are optimized more rigerously for one objective, resistance or maintenance, without as much care to the other two. It is also important to understand the ‘knee’ region of this front, given that a designer would be most interested in this are. Therefore, Figure 6.2b shows the same contour plot zoomed in around the ‘knee’ region. This region has four highlights points,  $A$ ,  $B$ ,  $C$ , and  $D$ . These points are all near the ‘knee’ of the trade-space in various Pareto zones and show how the designs change for vessels that are balanced between resistance and maintenance for different production cost values.

Figure 6.2 shows more clearly the sharp angle near the ‘knee’ of the Pareto front.



(a) Contour Plot for Entire Front



(b) Contour Plot Focused on 'Knee' Region.

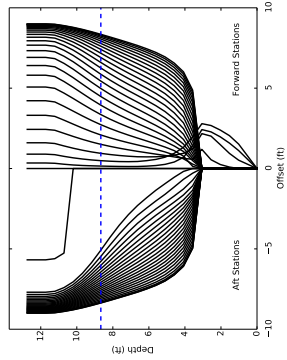
Figure 6.2: Contour plots for the Pareto-front shown in Figure 6.1.

Note that the jagged edges of the Pareto zone is due to the points found by the system-level genetic algorithm, as they don't represent a perfect spread over this front. However, their shape is still representative of the trade-offs in this design space. First it is important to note that the entire front represents multi-disciplinary designs that dominate the original hull significantly. This shows the capability of

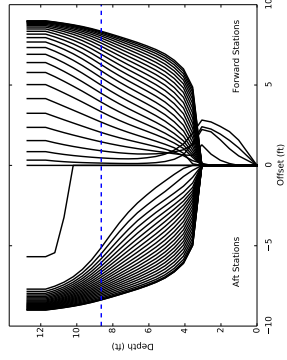
this optimization algorithm to aid designers in developing vessels that have reduced lifetime cost, while maintaining their safety and operational requirements. More importantly, however, is the change in the Pareto zones as the production cost changes. Given different levels of production cost, the trade-offs between lifetime resistance and maintenance also changes. This can be seen by the translation in the ‘knee’ of the front across the different Pareto zones. This highlights the significant benefit of using multi-disciplinary optimization tools when approaching this type of problem. If sequential tools were used, the end result may represent a design that was only locally optimal with respect to the previous optimization. However, when using a tool that simultaneously reduces the three objectives designs can be found that represent balanced trade-offs between different categories of cost.

### 6.1.2 Design Comparisons

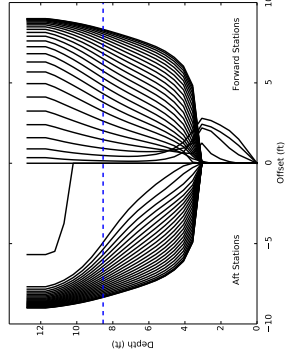
In order to better understand the results presented in Figure 6.2 the specific labeled designs will be explored in further detail. First the designs labeled *A*, *B*, *C*, and *D* will be examined. These designs, as can be seen in Figure 6.2*b* represent vessels located near the ‘knee’ of subsequent Pareto zones. That means that for different levels of production cost they are reasonable balanced between the other two objectives: lifetime resistance and maintenance cost. In order to compare the different designs the bodyplan, structure, and yearly maintenance cost for each one will be shown. To show the difference in structure somewhat better, the change in structural volume as a percent of the original,  $V_S$ , is shown for each structural image.



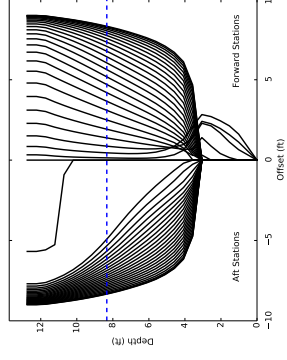
(a) Bodyplan for Vessel 'A'.



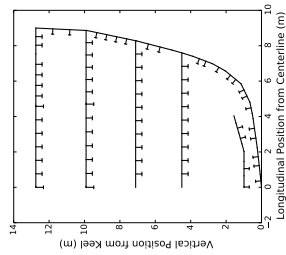
(b) Bodyplan for Vessel 'B'.



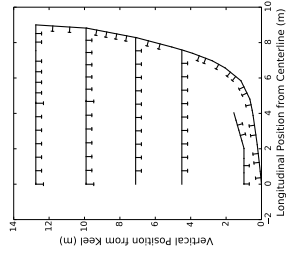
(c) Bodyplan for Vessel 'C'.



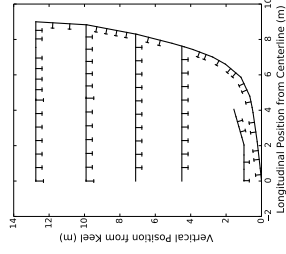
(d) Bodyplan for Vessel 'D'.



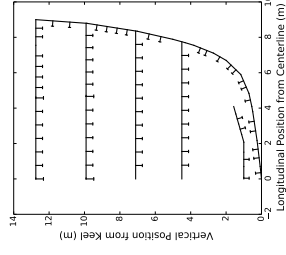
(e) Structure for Vessel 'A'.  
 $V_S = 1.26$ .



(f) Structure for Vessel 'B'.  
 $V_S = 1.25$ .



(g) Structure for Vessel 'C'.  
 $V_S = 1.20$ .



(h) Structure for Vessel 'D'.  
 $V_S = 1.12$ .

Figure 6.3: Bodyplans, structure, and yearly maintenance for vessels in 'knee' regions of various Pareto zones.

An important aspect of Figure 6.3 to note is the differences, and similarities, between the hull form and structures. The hullforms themselves are all relatively similar, showing that throughout the design space certain changes to the shape of the vessel will result in a better trade-off between the other categories of cost. For instance, all the vessels in Figure 6.3 have an increased parallel midbody, a larger flat bottom, and a smaller bulbous bow. Similarly, each of the structures has increased volume over the original, however, each of the structures has fewer components overall via larger stiffener spacing. By increasing the structural volume the maintenance cost is able to be reduced, and by reducing the curvature and number of stiffeners, the production cost able to be reduced. This shows that the idea of structures solely as weight may lead to higher overall lifetime costs for naval vessels. This is important to see that these similarities exist, since one of the assumptions regarding the LEGA presented in chapter 5 is that there are similar trends between the design variables and objective functions throughout the design space. Therefore, the fact that the similarities exist shows the ability of the LEGA to function as a discipline optimizer in the naval lifetime cost problem.

However, there are still differences between these hull forms. The bow region changes slightly from one design to the next as can be seen in Figure 6.4. This figure shows that the bow and entrance for each vessel becomes shallower from each knee region to the next. The entrance to the run, specifically, becomes a shallower angle, reducing production cost. However, as the angle of the entrance becomes shallower, the bulbous bow becomes slightly wider with a steeper bottom half, which helps maintain the reduced resistance as production cost is minimized. The differences in these hull forms can be seen further in Figures 6.5 and 6.6. These figures show specific regions of the sectional and waterplane area curves for vessels *A* through *D*.

Figure 6.5 shows similar trends to Figure 6.4. Figures 6.5*a* and 6.5*b* show that

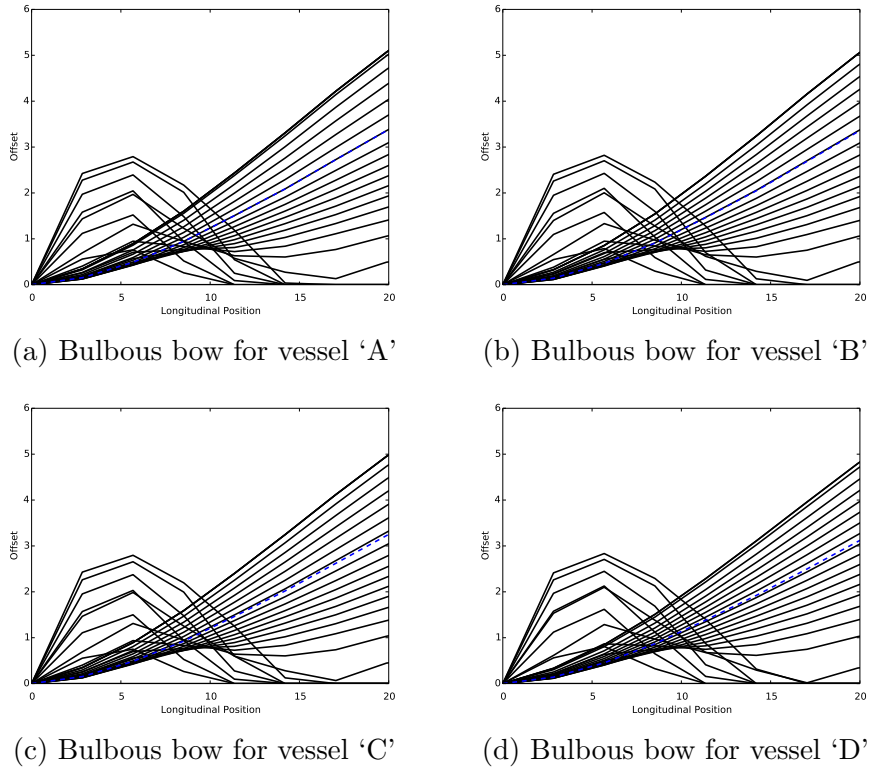
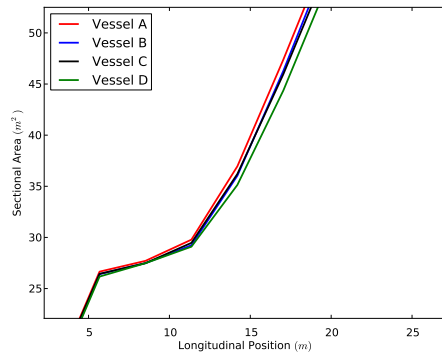


Figure 6.4: Bulbous bows for vessels in the 'knee' region.

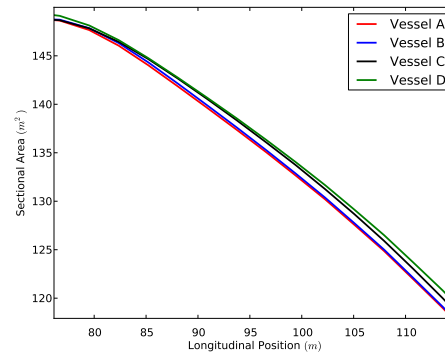
from vessel *A* through *D* the angles into and out of the midbody of the vessel become shallower. This reduces complexity, resulting in the lower production cost, however, comes at the cost of increased resistance. Similarly vessel Figure 6.5c shows that *D* has a wider transom than either of the other three vessels, once again reducing the complexity of the hull. Figure 6.6 also shows the reduced curvature through the 'knee' regions of Figure 6.2b. In Figure 6.6a it can be seen that Vessel *A* has more vertical curvature near the bottom of the hull than vessel *D*, which has a flatter bottom. Similarly, Figure 6.6b show the curvature below the sheer strake is reduced in vessels *C* and *D*, resulting in a less complex vessel. The differences in these hulls shows a designer how to change a hull form to remain balanced between the three different categories of cost. These trends highlight the benefit of being able to develop this type of three-dimensional front.

The structural differences between the two vessels is also important. These are

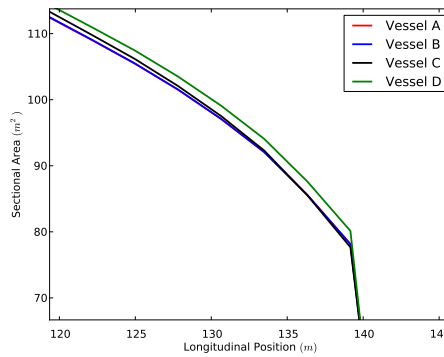




(a) Bow region for different vessels.

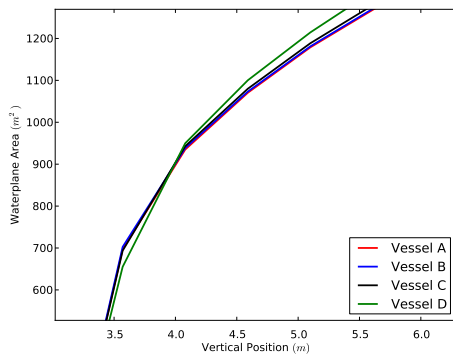


(b) Midbody region for different vessels.

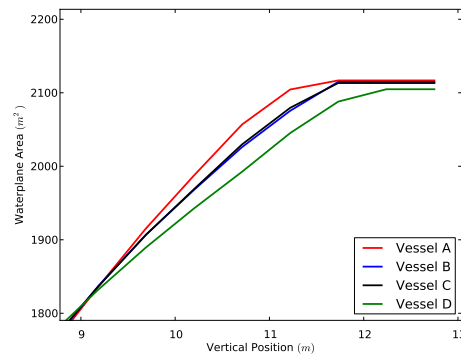


(c) Stern region for different vessels.

Figure 6.5: Different regions of the sectional area curves for vessels A through D.



(a) Flat bottom region for different vessels.



(b) Sheer strake region for different vessels.

Figure 6.6: Different regions of the waterplane area curves for vessels A through D.

especially difficult to see in Figure 6.3 as the thicknesses of the various structural components cannot be shown in a two dimensional plot. However, similarly to the hull forms, the global trends of this design space are clear. In order to develop structures with reduced weight to maintain hydrodynamic performance; yet, also find a balance between production and maintenance, structures were developed with larger spacing between components and thicker scantlings. To see this more clearly the scantlings for the different functional locations can be seen in Tables 6.2 and 6.3.

Table 6.2: Scantlings for vessels A, B, C, and D ( $t_P$ ,  $t_w$ ,  $t_f$ ). Units are all  $m$ .

Functional Location	$t_p$				$t_w$				$t_f$			
	A	B	C	D	A	B	C	D	A	B	C	D
BSBT	0.009	0.010	0.009	0.010	0.008	0.008	0.008	0.009	0.007	0.007	0.008	0.007
SBBT	0.012	0.012	0.013	0.013	0.008	0.008	0.008	0.009	0.007	0.007	0.008	0.007
SBIH	0.012	0.012	0.013	0.013	0.008	0.008	0.008	0.009	0.007	0.007	0.008	0.007
SAIH	0.012	0.012	0.013	0.013	0.008	0.008	0.008	0.009	0.007	0.007	0.008	0.007
DIBT	0.013	0.013	0.013	0.013	0.008	0.008	0.008	0.009	0.007	0.007	0.008	0.007
WTDK	0.010	0.010	0.009	0.009	0.003	0.005	0.006	0.003	0.016	0.016	0.011	0.015
IH	0.007	0.007	0.006	0.006	0.003	0.005	0.006	0.003	0.016	0.016	0.011	0.015

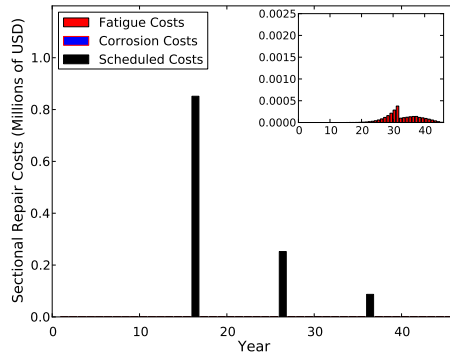
Table 6.3: Scantlings for vessels A, B, C, and D ( $h_w$  and  $b_f$ ). Units are all  $m$ .

Functional Location	$b_f$				$h_w$			
	A	B	C	D	A	B	C	D
BSBT	0.296	0.299	0.300	0.300	0.127	0.138	0.150	0.119
SBBT	0.296	0.299	0.300	0.300	0.127	0.138	0.150	0.119
SBIH	0.296	0.299	0.300	0.300	0.127	0.138	0.150	0.119
SAIH	0.296	0.299	0.300	0.300	0.127	0.138	0.150	0.119
DIBT	0.296	0.299	0.300	0.300	0.127	0.138	0.150	0.119
WTDK	0.353	0.348	0.351	0.379	0.199	0.161	0.194	0.126
IH	0.353	0.348	0.351	0.379	0.199	0.161	0.194	0.126

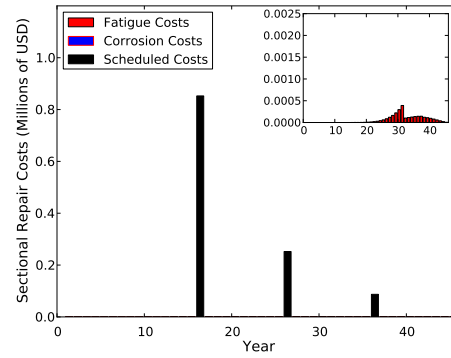
Tables 6.2 and 6.3 show similar types of trends as the hull form discussion above. The stiffener spacing is not shown; though for all designs it approached the maximum limit of 1.5 times the original for each functional location. Here one can see many similarities in the designs, highlighting the fact that across this design space there are certain trends that aid in the reduction of lifetime cost. This, once again, shows the strength of the LEGA to design within this type of subspace; where there are certain trends that permeate the entire space. However, one can also find the differences in structures that lead to the differences in production and maintenance cost. The differences are more prominent in the inner decks (IH), and the weather deck (WTDK), while the side shell plating is relatively similar between the four designs. The differences between the designs are also more prominent for the flange height and breadth ( $h_w$  and  $b_f$ ) than for the other scantlings. These scantlings even differ in the thicknesses between the four structures. This shows the algorithm's ability to reveal trends in how to alter a vessel's structure to reduce the overall lifetime cost and maintain a balance between different categories of cost that depend on the structure.

Finally, it is also important to examine the difference in yearly maintenance costs between the four vessels. This can reveal information to the designer as to how the algorithm is developing ships that are cheaper to maintain, and what the benefit is of minimizing maintenance over the ship's lifetime. The yearly maintenance costs for the four vessels can be seen in Figure 6.7.

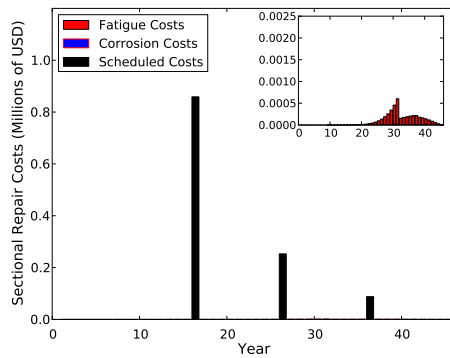
Figure 6.7 shows two scales for each vessel. The first is a large scale, to capture the magnitude of the scheduled maintenance costs incurred by each vessel. The second is a smaller scale, in order to capture the fatigue costs accumulating through each design's service life. The scheduled costs are very similar between each of the designs. This shows the benefit of the design trends that can be seen in each of the vessels through the different Pareto zones. Aspects such as the smaller bulbous bow, the wider stiffener spacings, and thicker plates can be seen in all four designs. This helps



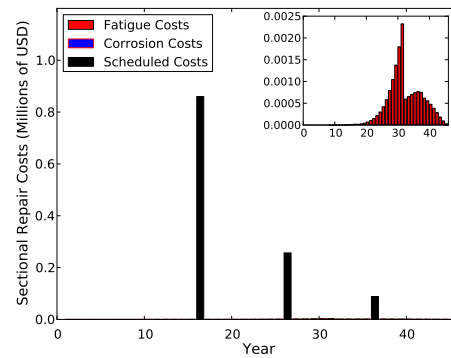
(a) Yearly maintenance for Vessel 'A'



(b) Yearly maintenance for Vessel 'B'



(c) Yearly maintenance for Vessel 'C'



(d) Yearly Maintenance for Vessel 'D'

Figure 6.7: Yearly maintenance costs for vessels *A*, *B*, *C*, and *D* (In millions of USD).

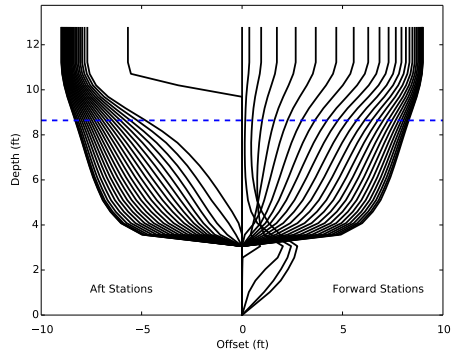
reduce the number of plates that need to be replaced due to corrosion, and also ensure that the repairs are always done during a scheduled maintenance cycle. These are the design features that the LEGA is able to find during the discipline analysis and pass back to the system-level optimizer, facilitating the development of these trade-spaces. The trends that lead to this type of yearly maintenance costs are important, since it is critical to a naval vessel to avoid the need to make emergency repairs outside of their schedule.

The differences in the accumulated fatigue damage, however, are also important. While smaller in magnitude than the scheduled costs, they are still important to understanding the differences in the designs. Note that the decrease in fatigue at the 30 year mark is due to the probabilistic service life extension beginning, during

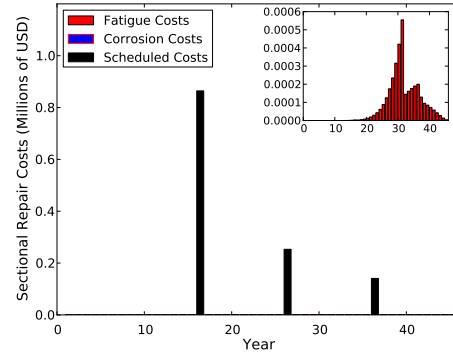
the thirty-first year of operation the costs begin to get scaled by the probability of operating in the given year. As can be seen, as the ship becomes increasingly cheap to produce, it becomes more susceptible to fatigue damage later in life. This will directly influence both the ship's ability to have a service life extension program executed as well as the cost to do so. Large amounts of fatigue damage can be costly for ship owners to repair, and have a big impact on the safety of the vessel's structure. This means that vessel,  $D$ , while being cheaper to produce will have a larger amount of fatigue damage when it approaches the end of its service life. This will lead to, at worst, a ship that cannot have its service life extended even if fleet requirements demand it and, even if it can have its life extended, the cost to do so may be a significant monetary burden. By utilizing this multi-disciplinary algorithm designers are able to understand these trade-offs and develop ship's whose structure and shape complement each other to reduce the cost to maintain and operate the vessel, allowing for the ship to be more robust to the fleet's future needs.

The benefit behind using a multi-objective tool to aid in solving the lifetime cost problem can be seen by examining designs  $R$  and  $M$  from Figure 6.2a. The previously discussed designs,  $A$ ,  $B$ ,  $C$ , and  $D$  are all taken from the 'knee' region of their respective Pareto zones, meaning that for their level of production cost they represent an excellent balance between resistance and maintenance cost. However, designs  $R$  and  $M$  are ones that may be over designed for either resistance or maintenance, and have sacrificed a large amount in other objectives for a small reduction in a single one. Designs such as this are easier to arrive on unknowingly in design spaces with Pareto-fronts such as the one shown here, which has steep sides meeting at a near-90 degree angle near the 'knee'. The bodyplans and maintenance for these two vessels can be seen in Figure 6.8.

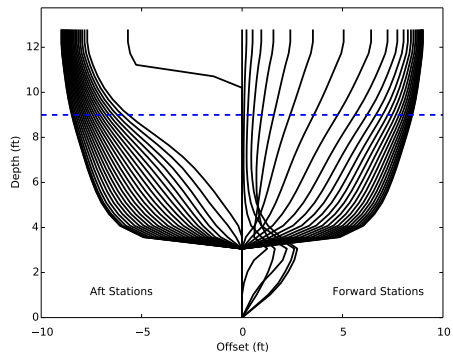
The difference between these two hullforms is much greater than the difference between  $A$ ,  $B$ ,  $C$ , and  $D$ . The higher curvature throughout design  $R$  increases the



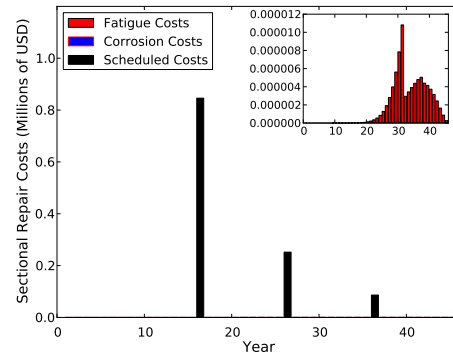
(a) Bodyplan for vessel  $R$ .



(b) Yearly maintenance for vessel  $R$ .



(c) Bodyplan for vessel  $M$ .



(d) Yearly maintenance for vessel  $M$ .

Figure 6.8: Design details for vessels  $R$  and  $M$

complexity significantly, making the vessel higher to produce. Similarly the structure of the vessel is much weaker, causing the weight to drop to decrease resistance, however, increasing the maintenance cost significantly. However, the vessel with low maintenance costs,  $M$ , is blocky, with larger structural components that cost more in raw steel to produce and reduce the hydrodynamic performance of the hull significantly. The difference in the two hulls can also be seen in the yearly maintenance costs. Vessel  $R$  has significantly increased fatigue costs (note the different scales in zoomed in areas of the Figures) at the end of its design life. This means that, though it will cost less to operate during its lifetime, it may have fatigue damage that limits its ability execute on a service life extension program. The danger of using sequential optimization to solve this type of problem is, if a design either of these parts of

the design space was originally decided on, it would be difficult to find a balanced one later on. This means that large sacrifices would have been unknowingly made in multiple categories of lifetime cost simply for small gains in the first one. By using a tool such as the one provided that allows the designer to map out the design space, decisions can be made that ensure a design that is balanced between these competing objectives and has a reduced overall lifetime cost.

## **6.2 Maintenance Scheduling**

As has been discussed previously the lifetime cost to maintain a vessel is affected by the logistics of how and when said maintenance is done. One of the advantages of the algorithm outlined in section 3.1 is that it allows for the direct input of a maintenance schedule. In the optimization shown in section 3.2 this schedule was considered a constant parameter in the design, which represents current practices in the naval field. However, by using this type of maintenance costing framework it is possible to allow the maintenance schedule itself to be a design variable within the optimization. This allows the designer to posit a novel problem that combines the logistics of a vessel with its engineering design. This also allows the designer to more effectively analyze the ability for a vessel to execute a service life extension plan and, more importantly, maintain it such that the cost for an extension is reduced if it must be taken.

### **6.2.1 Schedule Optimization**

As an example of this an optimization problem can be formatted using the costing algorithm described in section 3.1. Instead of optimizing the structural scantlings, however, the design vector can be the schedule to maintain the ship. In this example the structure is considered a constant. The design vector becomes the entries of the



set  $\{S\}$  as shown in equation 3.1 The following problem is then formulated:

$$\begin{aligned}
& \text{minimize: } C_T(S_1, S_2, \dots, S_n) \\
& \text{subject to: } S_1 < S_2 < \dots < S_n \\
& S_{i+1} - S_i > 2 \text{ for } i = 1, \dots, n - 1 \\
& 2 < S_i \leq L_E \forall i
\end{aligned} \tag{6.7}$$

In equation 6.7  $S_1$  through  $S_n$  represent the years in which maintenance will be performed, and  $n$  is fixed for the entirety of the optimization. In order to ensure a reasonable schedule is found constraints are placed on the optimizer such that the entries of  $\{S\}$  are of increasing value, and that every entry is at least greater than 2 years apart from any other.

The formulation shown in equation 6.7 was run on the nominal combatant structure from [Ashe et al. \(2009\)](#) for  $n = 3, 4, 5$  maintenance cycles. For this work the scheduled dry docking, emergency dry docking, and pier-side facility costs were assumed to be 500,000, 1,000,000, and 100,000 USD respectively. During this optimization the maintenance cost was calculated using the framework shown in Figure 3.3; this means that the global strength check was done using Smith's method to estimate ultimate strength. This led to the maintenance schedules shown in Figure 6.9 being determined.

Figure 6.9 shows that the algorithm does not favor fixed maintenance cycles to minimize maintenance cost, instead it seems to focus on packages of maintenance cycles at the beginning and end of the ship's service life. The optimization routine is finding years to perform maintenance in for which the cost of dry-docking the vessel is best spent. It also tends to place at least one maintenance cycle in the latter years of the vessel's life in order to ensure operational effectiveness through the probabilistic service life extension. The yearly costs associated with each of these maintenance

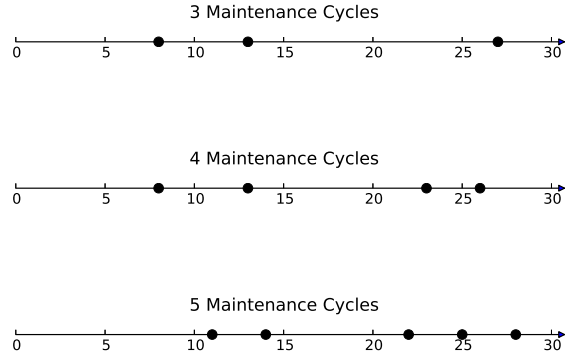


Figure 6.9: The maintenance cycles found for the problem formulation in equation 6.7 for  $n = 3, 4, 5$ .

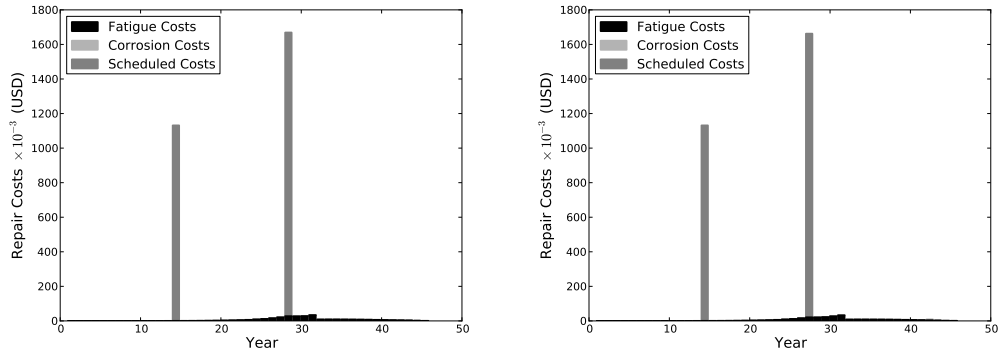
schedules, as well as the original fixed-interval schedule, can be seen in Figure 6.10.

Figure 6.10 shows one of the driving factors for why, in this optimization, three maintenance cycles is optimum. In Figures 6.10*b* and 6.10*c* even though scheduled maintenance is performed 4 and 5 times, panels are not replaced in every dry-docking. This figure also shows that the optimizer tends towards maintenance schedules for which repairs based on corrosion damage are bundled into fewer cycles. It can be seen in Figure 6.10*d* that the original maintenance schedule does not do this, and this leads to higher lifetime costs. The different aspects of total lifetime costs for each of these schedules can be seen in Table 6.4.

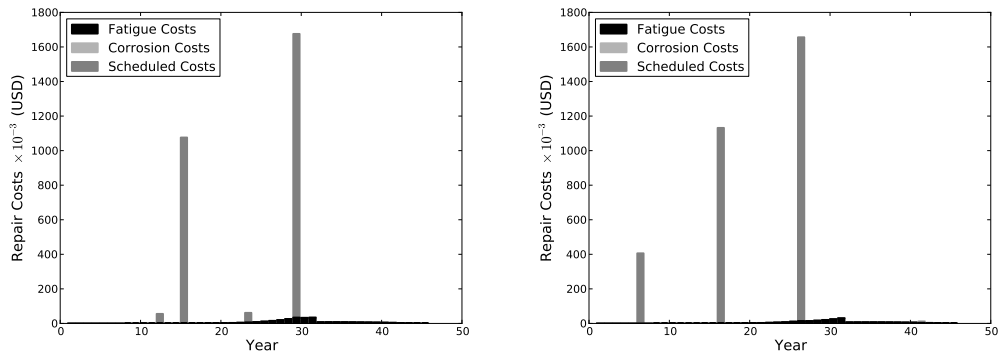
Table 6.4: Aspects of maintenance cost for different schedules ( $USD \times 10^3$ ).

$n$	$C_F$	$C_C$	$C_S$	$C_R$
Fixed (3)	233.1	13.2	3179.0	1583.7
3	263.8	4.35	2773.0	1529.6
4	249.9	7.85	2773.0	2052.0
5	276.5	1.97	2828.5	2514.3

The values in Table 6.4 help explain the schedules seen in Figure 6.9. It can be seen that the fixed interval schedule yields the lowest overall fatigue costs, this is because regular replacement of panels limits the maximum probability of a fatigue



(a) Yearly costs for 3 Cycle optimization. (b) Yearly costs for 4 cycle optimization.



(c) Yearly costs for 5 cycle optimization. (d) Yearly costs for fixed schedule.

Figure 6.10: Yearly costs for different values of  $n$  and the original schedule.

crack initiating. However, the corrosion and scheduled costs for the fixed interval schedule are significantly higher. The corrosion costs (which are only incurred for panel replacements *not* done during a maintenance cycle) are all incurred during the service life extension. Thus, the maintenance performed at the tail end of the design service life in Figures 6.10a, 6.10b, and 6.10c minimizes the number of panels that need to be replaced during the extension. It should be noted that this is why these costs are also small compared to the others - as all costs incurred during the service life extension are weighted by the distribution shown in Figure 3.2.

This result highlights the potential for lifetime cost savings by taking into account the possibility of service life extensions during the initial design phase. The scheduled costs for the three optimized schedules are also less than for the fixed-interval schedule.

This is because the optimizer is finding years to perform maintenance in such that individual panels within the structure are replaced as few times as possible over the course of the vessel’s life, whereas when using the fixed-interval strategy certain panels end up being replaced 2 or 3 times. The flat rates, obviously, increase with the number of cycles, however, if the costs are examined without accounting for the flat rates it can be seen that by using  $n = 4$  the costs purely due to maintenance are minimized.

### 6.2.2 Effects of Service Extension

The optimum maintenance schedule is undoubtedly affected by the nature of the assumed service life extension. In order to explore this sensitivity the optimization in equation 6.7 was done for two different cases. As a comparison for the results, the optimization results from Figure 6.9 will be considered ‘Ship A’. An optimization assuming no service life extension ( $L_D = 30$  and  $L_E = 0$ ) will be referred to as ship B and one assuming a 100% probability of extending the life by 15 years ( $L_D = 45$  and  $L_E = 0$ ) will be ship C. These optimizations were done for  $n = 3, 4, 5$  cycles as before. The schedules found using no extension can be seen in Figure 6.11.

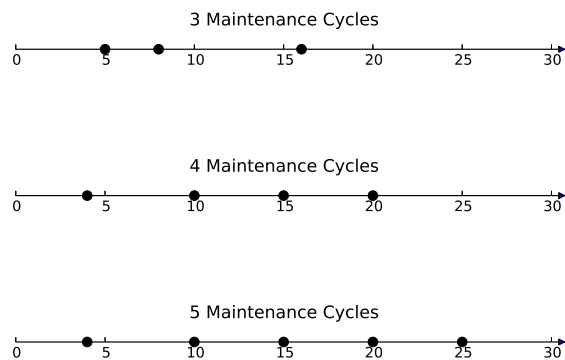


Figure 6.11: The maintenance cycles found using no possible service life extension (ship B).

Figure 6.11 shows that when the maintenance cycles are being optimized for a deterministic service life, it makes sense to utilize a fixed-interval maintenance schedule once more than 3 maintenance cycles are used. This is most likely due, in part, to the deterministic nature of the forecasting of corrosion damage used during the scheduled repairs. The opposite design approach to the one shown in Figure 6.11 is to consider the design life of the vessel to be deterministically 45 years. This is the most conservative approach, as it assumes there is a 100% probability of reaching the maximum extension time. If the optimization in equation 6.7 is performed for  $n = 3, 4, 5$  and  $L_D = 45$  the results in Figure 6.12 can be found.

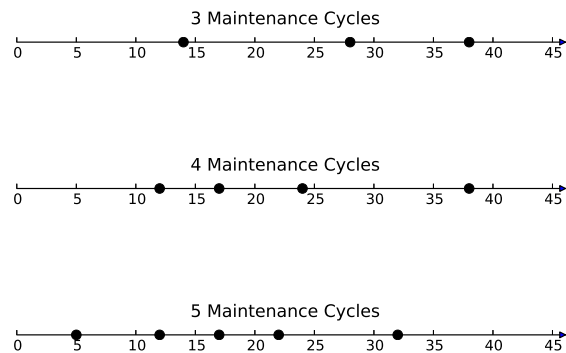


Figure 6.12: The maintenance cycles found using a 45 year service life (ship C).

The schedules in Figure 6.12 show that as the service life becomes longer fixed-intervals no longer represent the optimum distribution of maintenance cycles. This implies that even using a deterministic service life the best repair schedule for a vessel may not be intuitive depending on the planned length of operation, the type of vessel, and the number of expected maintenance cycles.

While the schedules seen in Figures 6.11 and 6.12 are optimum for the specific service lives of 30 and 45 years respectively, they are not robust for uncertain operational extensions. To see this Table 6.5 shows the effect of changing the service life

to (deterministically) 40 years for  $n = 3, 4, 5$ .

Table 6.5: Total maintenance cost for optimum maintenance schedules when using a deterministically 40 year service life. (*Millions of USD*).

$n$	Ship A	Ship B	Ship C
3	5.19	12.69	5.21
4	5.68	11.55	6.15
5	6.26	7.55	6.66

It can be seen in Table 6.5 that when the service life is altered the schedule found using the uncertain extension is able to accommodate the change with minimal extra cost to the ship owner. This is particularly useful since the exact nature of the operational life of the vessel is most likely unknown during the initial design phase for most naval vessels, or will change in subsequent years. It can also be seen that planning the maintenance cycles around a service life estimate that under-predicts the true time the vessel stays operational for has a significantly higher negative impact on the lifetime maintenance cost than over-estimating the duration.

Furthermore Table 6.6 shows the effect of utilizing a 30 year service life for each of the schedules found using the optimization algorithm.

Table 6.6: Total maintenance cost for optimum maintenance schedules when using a deterministically 30 year service life. (*Millions of USD*).

$n$	Ship A	Ship B	Ship C
3	3.25	3.24	3.95
4	3.74	3.71	4.34
5	4.25	4.20	4.54

From Table 6.6 it can be seen that, while using the scheduled optimized for a 30 year life is clearly best, the financial impact of utilizing the schedule found using the probabilistic service life extension is minimal. This highlights the robustness of using a framework such as this, along with an uncertainty model for the possibility of extending the operation of a naval ship, to develop maintenance schedules. By using this approach the lifetime cost will be minimal for large service life extensions,

however, will still be small if the original design life is realized.

### 6.3 Effect of Schedule on Trade-Spaces

To understand the effect of considering the schedule as a design variable on the trade-spaces, the problem shown in equations 6.4 through 6.6 is re-solved. In the new formulation of the problem, the schedule is a design variable within the structural discipline problem. The schedule is added as design variable using four binary coded variables:  $y_1$ ,  $y_2$ ,  $y_3$ , and  $y_4$ . These binary variables are each four bits of information long and can be used to calculate the following maintenance schedule:  $[y_1, y_1 + y_2, y_1 + y_2 + y_3, y_1 + y_2 + y_3 + y_4]$  The rest of the problem formulation remains the same as the above section. Solving this problem generates the three-dimensional Pareto-front seen in Figure 6.13.

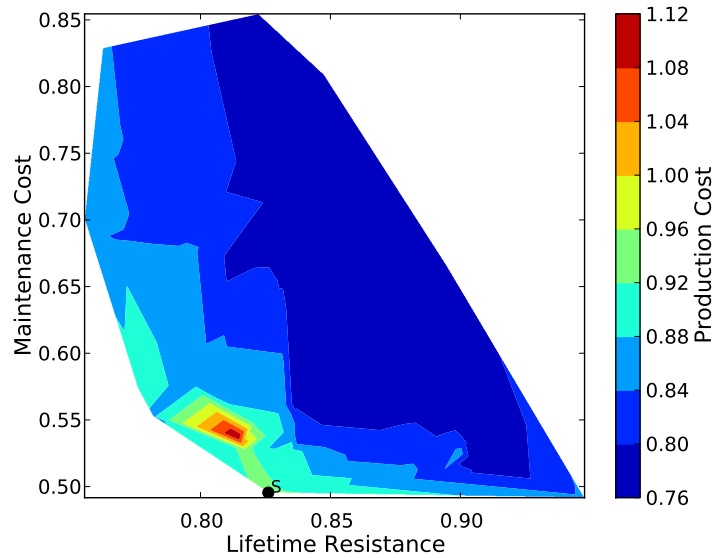


Figure 6.13: Contour plot for scheduled optimization formulation.

It is important to note that this is a harder test problem for the eMOCO as it is now larger and mixed discrete-continuous in nature. In turn, these results now show some signs of needing more time to fully converge. This is probably the reason for the

large peak production-cost region as well as the points that cost more in maintenance than those seen in Figure 6.2a. However, two important features of this front should be noted:

1. The nature of the Pareto zones are changing from the shape seen in the previous chapters.
2. There are points that cost less in maintenance than any found in the unscheduled problem formulation.

The first point is of significant import. Throughout this thesis the results that have been found are consistent in that the lifetime cost Pareto-fronts that have been developed, both two and three-dimensional, have displayed steep sides meeting at a  $90^\circ$  angle at a ‘knee’ region. The result shown here are different. The Pareto-zones seen in Figure 6.13 display a shallower curve with a broader ‘knee’ region than any of the previous results. This type of Pareto-front represents a more forgiving design space for the engineers working within it, as design changes that result in a small gain in one objective will only result in a small loss in others. This allows designers to make design changes without fear of drastically increasing lifetime cost due to one of these categories of cost. The increased flexibility given by allowing the schedule to be a design variable allows the designer more leeway to make decisions within the design space without large negative impacts to the lifetime cost of a naval ship.

The second point highlights the potential ability of using the maintenance schedule as a design variable to reduce the overall maintenance cost of naval vessels. In order to show this ability the bodyplan and structure for the vessel labeled  $S$  in Figure 6.13 are shown in Figures 6.14a and 6.14b.

The important factor to note here is that the vessel shown in Figure 6.14 is remarkably similar to the ones shown in Figure 6.3. The trends, design-wise, through this trade-space remain similar. However, the maintenance cost for this vessel is less



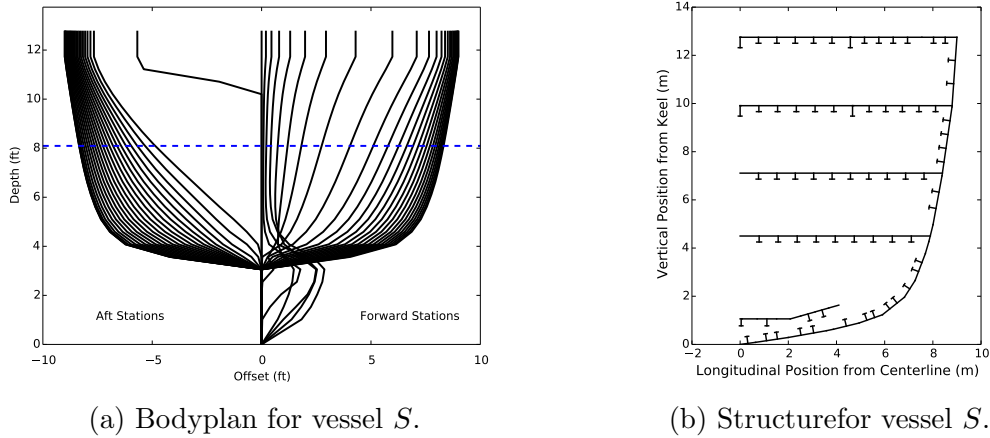


Figure 6.14: Structure and Bodyplan for vessel  $S$  from Figure 6.13.

than any found by solving the unscheduled problem, This is due to the inclusion of the maintenance schedule as a design variable. The schedule for this vessel is [12.0, 22.0, 26.0, 43.0]. This differs noticeably from the default schedule of [5, 15, 25, 35]. It favors maintenance towards the end of the vessel's life, instead of the beginning, which is in line with the results shown in section 6.2. These results show that by optimizing the schedule along with the structure, a vessel that has reduced costs throughout its life can be achieved.

The effect of using the optimized schedule can be seen in Figure 6.15, where the yearly maintenance costs for ship  $S$  are shown. This figure is important because it shows that the optimizer is developing schedules that drastically reduce the amount of maintenance needed to be done in the scheduled cycles. Specifically, a much smaller amount is needed during the maintenance performed during the probabilistic service life extension. This re-enforced what the results seen throughout this chapter show: that by reducing the structural maintenance costs during a service life extension program the overall lifetime costs can be reduced. By allowing the maintenance schedule to be a design variable the vessel has become much more robust to having service life extension programs executed with minimal costs to the owner.

While the work shown in the previous two sections is exploratory it shows that

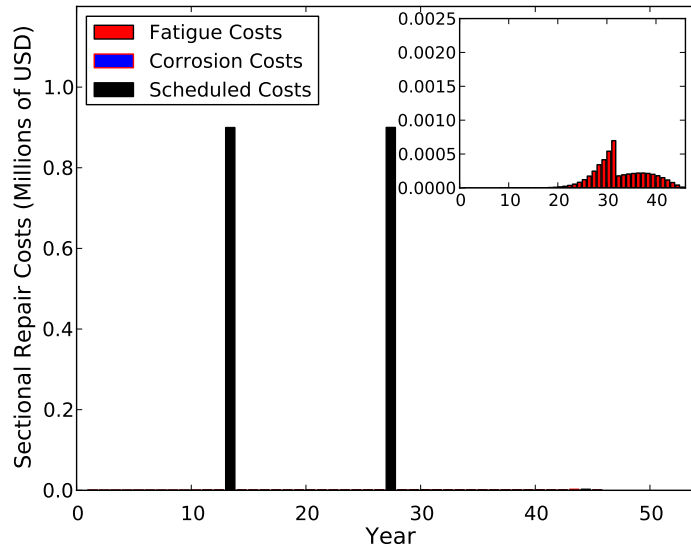


Figure 6.15: Yearly maintenance costs for vessel  $S$ .

by using the eMOCO framework developed here and considering logistics along with engineering design, savings in lifetime cost can be found. The results show that the eMOCO can effectively optimize this new, more difficult design space. The mixed discrete-continuous nature of the problem makes it considerably more difficult to solve, and the results show that the eMOCO framework and LEGA discipline optimizer are able to work within it. They also show that the schedule is important to the overall maintenance cost of the vessel, as well as to the nature of the trade-offs within this design space. They indicate that by allowing the optimizer to consider the maintenance schedule as design variable, not only can cost savings be found, by a designer can alter the trade-offs to allow for decisions to have less negative impact on different categories of lifetime cost.

## 6.4 Contributions

This chapter has shown that by using the eMOCO, and a combined formulation using the structural and hydrodynamic problems developed in chapters 3 and 4, three

dimensional Pareto-fronts can be developed. These novel trade-spaces, comparing production cost, maintenance cost, and lifetime resistance, reveal new information about the naval lifetime cost problem. They show that the shape of the trade-space found in previous chapters is retained when moving to three objective functions. This shape seems to be fundamental to the nature of this problem, and highlights the difficulty in solving it, as well as the benefit of using multi-objective optimization to do so. The shape of these fronts is consistently a ‘knee’ area formed by steep sides meeting at a near  $90^0$  angle to each other. This type of Pareto-front indicates a problem that, if solved sequentially using single-objective optimization, could result in unnecessary losses in lifetime cost. This is because a small gain in one objective may be made at large cost to the others if the design is outside of the ‘knee’ region. Revealing this, especially in regards to the three-dimensional front, shows the benefit of using the eMOCO framework to solve this problem.

The specific ships within the results are also important to this chapter. They show that there are design trends that permeate the ‘knee’ regions of the front regardless of which Pareto-zone is being examined. This is important because it shows that the LEGA designed in chapter 5 is well suited to solving this problem. However, the results also show that there are key differences in the ships in the ‘knees’ of different Pareto-zones that reveal trends in designs that lead to reduced costs in various lifetime cost categories. By understanding these trends a designer can learn to develop vessels that are well-balanced in each of the categories of cost, while still maintaining operational and safety levels. This comparison of ships from within the Pareto-front has shown unique information regarding specific design choices that can be made to reduce the lifetime cost of naval vessels.

The final two sections of this chapter show, via exploratory work, the potential of considering the maintenance schedule as a design variable. This is novel, as the schedule is usually considered a static parameter in optimization problems. To show

that optimizing the schedule could have a positive effect on the maintenance cost, a single-objective optimization was solved where the only design variable was the maintenance schedule. These results shows that, not only can money be saved by optimizing the schedule to the design, but the schedules found by the optimizer are different than the standard fixed-interval schedule that is traditionally used.

This result was extended by solving the three-dimensional problem with the maintenance schedule added as a design variable. The results for this mixed discrete-continuous problem show that, by allowing the schedule to be a design variable, the fundamental nature of the trade-offs can be altered. In these results the sides of the Pareto-zones are not quite as steep as the ones seen throughout the other chapters of this thesis. This novel result is significant in that the altering of the trade-offs allows a designer to have more leeway in their engineering decisions simply by altering logistics. The results also show that by planning on spending more maintenance during the vessel's life, significant savings can be found during the later years of its operation and, specifically, during any service life extension programs that may be executed. This shows that by utilizing the eMOCO framework and by considering the maintenance schedule as a design variable it is possible to build cheaper vessels that are more robust to changes in their operational life.

## CHAPTER 7

# Conclusions

### 7.1 Conclusions and Contributions

This work has presented contributions towards the understanding of trade-offs between different contributing categories of lifetime cost for naval vessels. As shown through the previous chapters these trade-offs are difficult to resolve and traditional optimizers struggle to develop them. Therefore, a unique enhanced multi-disciplinary design framework has been developed that is tailored to solving for the trade-offs between different categories of lifetime cost in the naval design space. This optimization framework has been shown to be able to effectively develop these difficult trade-spaces and give an engineer new insight into the nature of these trade-offs. By understanding these trade-offs an engineer can better work towards designing a vessel that has a minimized lifetime ownership cost and is robust to changes in mission or service life over the course of its operation.

In order to facilitate this a novel framework for estimating the lifetime maintenance cost for naval vessels has been presented. This framework uses physics-based calculations to estimate the yearly structural damage a ship's structure incurs. It also uniquely utilizes an assumed maintenance schedule to perform dry-dockings where this structural damage is repaired and costs are charged to the vessel. By using this method of dry-docking the vessel, the framework can account for scheduled mainte-

nance and unscheduled maintenance and the cost difference between the two. Another unique feature of the framework is its ability to incorporate a service life extension period probabilistically into the ship's lifetime. This allows it to estimate the maintenance cost of the vessel even if its design service life is extended.

By utilizing this framework within an optimization routine trade spaces between production cost and the cost to maintain a vessel were developed. The Pareto-fronts show the ability of this framework to aid a designer in developing ship structures that have minimal costs with respect to both production and maintenance in order to reduce their lifetime expenses. The framework has also shown success in developing structures that are robust to changes in the vessel's service life; these structures show only moderate increases if the original service life is realized whereas they are significantly less expensive if it is extended. This allows the shipowner to ensure that their lifetime costs will remain low despite uncertainty in operational life. This type of trade-off has not been examined in depth before, especially while accounting for service life uncertainty. The results show that the shape of the trade-space has a sharp 'knee' that a single-objective optimizer would struggle to identify. This highlights the importance of being able to visualize this trade-space by using a multi-objective optimization routine. By exploring this trade space it can be seen the importance in using multi-objective optimization to understand the choices designers face and how those choices will impact the lifetime cost of a new vessel.

Similarly, a novel transformation method was developed for use with hydrodynamic optimization problems. The search method, and corresponding constraints based on the parameterization of the ship's area curves have many advantages:

1. They allow for the designer to have a large amount of control over the size of design space that is searched via simple  $\epsilon$  values.
2. The transformation functions allow for the optimizer to search a large design space with minimal design variables. This makes it a more effective search

method than those that use direct control points on the surfaces hull as the size of the design vector is minimized. This is particularly useful when using population-based optimizers as they can become much less effective with large design vectors.

3. The parametrization of the area curves allows for constraints that directly control the shape of the hull without having to perform a shape analysis of an actual three dimensional model.

The method was demonstrated by producing trade spaces between producibility and lifetime resistance. The demonstration was done for two ship types: a nominal destroyer and a KCS SIMMAN container ship. The optimization exercise performed highlight the potential benefit to understanding this type of trade-space during the time when design decisions can still be made. It was also shown that the nature of these trade spaces, while possibly having similar trends, can have varying shapes and may not be entirely intuitive from the outset. The aspects of the design that are changed along this trade-space are also not necessarily evident and this methodology allows these aspects to be explored and better understood.

The difficulty in developing the trade-spaces for naval combatants led to the development of a novel multi-disciplinary optimization framework, the eMOCO, designed specifically to tackle the naval lifetime cost problem. Part of what makes this a difficult problem to solve is the differing nature of the design spaces involved. The hydrodynamic design space is defined by  $C_1$  continuous objectives and constraints that may be suited to the use of a gradient based optimizer to effectively solve it. However, the structural space has multiple features that make it suited for evolutionary optimization:

1. Possibility of discrete variables such as maintenance schedules and discrete structure choices.

2. The design space can have flat, multiple weak minima, that are difficult for gradient-based optimizers to navigate.

In order to allow the MDO framework to, not only overcome this, but take advantage of it two enhancements were made to the traditional multi objective collaborative optimization framework to create an enhanced one (eMOCO). These two enhancements represent unique and novel approaches to an MDO algorithm. The first is the addition of a goal programming mechanism at the discipline level that minimized objective functions that only use that discipline's design variables. This allows the discipline level optimizer to send design points to the system level optimizer that are locally optimized for each discipline's objective. This can help the system level optimizer move the Pareto front through the design space more effectively, especially in areas where the space may be flat or have weak local minima. Using the goal programming method also allows for the engineer using the eMOCO to use their engineering intuition to create a hierarchy for the objectives they are minimizing, instead of leaving it entirely in the hands of the optimizer.

The second enhancement focuses on increasing the computational effectiveness of problems that utilize population based optimizers at the discipline level. A significant issue when doing this is that current literature generates a small population around each point in the system level population using a design of experiments and then runs the discipline optimizer on each of these sub-populations, returning the best point to the system-level. This, however, becomes intractable quickly as this is a large number of population based optimization runs to execute. In order to overcome this a new single-objective genetic algorithm, called the locally-elitist genetic algorithm (LEGA) was developed that allows the discipline optimizer to solve its problem in a single execution. These two enhancements produce an optimization algorithm that is shown to perform better than a traditional MOCO on MDO test problems from literature and are capable of effectively solving the difficult naval lifetime cost problem.



Using the eMOCO trade-spaces were developed that compared three categories of lifetime cost: production, maintenance, and resistance. The creation of these trade-spaces is novel, and they have not been explored in current literature to date. These trade-spaces show that as the objective for one of the categories changes the trade-offs for between the other two change as well. This is a significant finding, it means that if a designer wanted to reduce lifetime cost, sequential minimization of the objectives may lead to designs that are actually far from optimal. In order to understand how design decisions related to one these objectives will affect the other two, it is vital to be able to produce this type of three-dimensional trade-space using a simultaneous multi-disciplinary optimization approach.

In order to further understand how this optimization framework could be used with the developed maintenance costing framework, the concept of using the scheduling logistics as a design variable was explored. By considering the maintenance schedule as a design variable instead of a static parameter the design can be adaptable throughout its service life. This can alleviate some of the problems designers face when developing a vessel with an uncertain lifetime. It also lets engineers overcome, to a small degree, the troublesome problem of being unable to alter the design of a vessel during the time when the most information is known. To show a proof of concept for this novel idea a single-objective optimization was done to minimize maintenance cost using only the schedule as a design variable. The results of this optimization showed that by simply optimizing the maintenance schedule for the structure under consideration the maintenance cost could be reduced. It also showed that the traditional evenly-spaced maintenance intervals were not optimal for naval design.

These results were extended by re-solving the three-dimensional naval lifetime cost problem while including the maintenance schedule as a design variable. This addition altered the nature of the problem; making it mixed discrete-continuous. The eMOCO and LEGA were able to successfully optimize within this new, and more difficult,

design space. The results showed that by doing so the fundamental nature of these trade-spaces, as found throughout the rest of this thesis, may be possible to alter. Changing this trade-space would offer the ship designer more flexibility with respect to their choices and allow them to alter the design without fear of drastically increasing the lifetime cost. It also showed, once again, that the optimal maintenance schedule may not be the traditional fixed-interval cycles. Instead, by spending more money on maintenance cycles later in life, it may be possible to reduce the maintenance costs during the end years of a vessel's life and, especially, during any service life extension programs. Including schedule in the optimization problem shows that it may be possible to alter the shape of the resulting Pareto front. Preliminary results indicate that with the ability to vary the maintenance schedule the knee region may become less distinct.

## 7.2 Recommendations for Future Work

The work presented in this thesis has opened up many new questions into the nature of trade-offs in lifetime cost. The value of the eMOCO is that the specific analyses used within it can be easily changed to better understand how the analysis method changes the nature of the results. It would be valuable to attempt the use of higher fidelity resistance calculation algorithms, given that thin-ship theory does have some significant drawbacks. However, this could result in the problem becoming computationally difficult to solve. This could possibly be countered by developing response surfaces for the discipline level in order to allow for higher fidelity calculations to be used. Additions such as this could aid in more effectively analyzing the hydrodynamic performance of the vessel to ensure the accuracy of the optimization and better understand its sensitivities.

The unique nature of the maintenance cost algorithm also warrants further inves-

tigation. The addition of the facility costs can be extended with data from specific shipyards, maintenance facilities, or dry-docking records. The probabilistic service life extension could also be augmented with a more realistic distribution. It is likely that the actual distribution governing the probability of an extension to the service life being implemented does not follow a beta distribution. If data could be collected to better understand this probability the ability for the framework to minimize the maintenance cost of a ship would be increased. Though this data is difficult to acquire, accurate information on the auxiliary costs to perform ship maintenance could be invaluable in determining the best approach to reducing the lifetime cost of naval vessels.

Apart from increasing the fidelity of the logistical analysis through better data, the results can be improved by further exploration of using the maintenance schedule as a design variable. It was shown in preliminary results that this can greatly reduce the overall lifetime cost and that the optimal schedule is not necessarily the intuitive one. It is also clear that it alters the nature of the trade-spaces when the schedule is considered as a design variable. However, the implications of this were not fully explored. In chapter 1 a general lifetime cost design problem was presented. Of the design disciplines given in that problem logistics was explored the least throughout this thesis. A better understanding of the interactions between the engineering design and logistics of a naval vessel could aid greatly in the reduction of lifetime costs.

One aspect that was not explored in this work is the effect of the schedule on the resistance portion of the vessel. It is likely that during a scheduled dry-docking the hull would be cleaned, reducing the resistance the vessel experiences. This would change the expected value of the lifetime resistance metric throughout each year of operation and would most likely change the nature of the trade-offs. The logistics of a naval vessel are also dictated by fleet logistics, and this would be interesting to explore. Including things such as operational availability and fleet deployment

logistics into the lifetime cost problem could help naval designers develop vessels, and even fleets, with reduced cost over their operation lifetime.

## BIBLIOGRAPHY

- Anderson, L. T., Gerhard, L. K., and Sievenpiper, L. B. (2013). Operational Ship Utilization Modeling of the DDG-51 Class. In *ASNE Day Proceedings*.
- Ashe, G., Cheng, F., Kaeding, P., Kaneko, H., Dow, R., and Broekhuijsen, J. (2009). Committee V.5 Naval Ship Design. In *17th International Ship and Offshore Structures Congress*, volume 2. Seoul National University.
- Aute, V. and Azarm, S. (2006). A Genetic Algorithms Based Approach for Multidisciplinary Multiobjective Collaborative Optimization. American Institute of Aeronautics and Astronautics.
- Ayyub, B. M., Assakkaf, I. A., and Kihl, D. P. (2002). Reliability-Based Design Guidelines for Fatigue Ship Structures. *Naval Engineers Journal*, 114(2):113–138.
- Bankes, F. and Spicknall, M. (1991). Importance of Considering Life-Cycle Maintenance and Modernization Costs in the Design of Navy Ships. *Journal of Ship Production*, 7(4):227–233.
- Benedetti, L., Boucasse, B., Broglia, R., Fabbri, L., Gala, F. L., and Lugni, C. (2007). PMM Model Test With DDG51 Including Uncertainty Assessment. Technical Report 14, INSEAN.
- Bernitsas, M. M. (1981).  $K_T$ ,  $K_Q$ , and Efficiency Curves for the Wageningen B-Series Propellers. Technical Report 237, Department of Naval Architecture and marine Engineering, University of Michigan, Ann Arbor.
- Bole, M. (2007). Cost Assessment at Concept Stage Design Using Parametrically Generated Production Product Models. In *International Conference on Computer Applications in Shipbuilding*, volume 3, pages 13–26, Portsmouth, UK.
- Brenner, M. and Sener, B. (2011). Design for Energy Efficiency: Simulation-Driven Design and Hydrodynamic Optimization for Greener Ships and EEDI Compliance. In *1st International Symposium on Naval Architecture and Maritime*, Istanbul, Turkey.
- Brizzolara, S., Curtin, T., Bovio, M., and Vernengo, G. (2011). Concept Design and Hydrodynamic Optimization of an Innovative SWATH USV by CFD Methods. *Ocean Dynamics*, 62(2):227–237.

- Bunch, H. (1993). Catalogue of Ship Producibility Improvement Concepts. Technical Report 324, University of Michigan, Dept. of Naval Architecture and Marine Engineering.
- Caprace, J.-D., Fernandez, F. A., Losseau, N., and Rigo, P. (2009). A Fuzzy Metric for Assessing the Producibility of Straightening in Early Design. In *The 14th International Conference on Computer Applications in Shipbuilding*, pages 211–218. The Royal Institution of Naval Architects.
- Caprace, J.-D. and Rigo, P. (2012). A Real-Time Assessment of the Ship Design Complexity. *Computer Aided Design*, 44:203–208.
- Chung, H.-Y., Manuel, L., and Frank, K. H. (2006). Optimal Inspection Scheduling of Steel Bridges Using Nondestructive Testing Techniques. *Journal of Bridge Engineering*, 11(3):305–319.
- Collette, M. (2011). Hull Structures as a System: Supporting Lifecycle Analysis. *Naval Engineers Journal*, 123(3):45–55.
- Collette, M. and Incecik, A. (2006). An Approach for Reliability-Based Fatigue Design of Welded Joints on Aluminum High-Speed Vessels. *Journal of ship research*, 50(1):85–98.
- Collette, Y. and Siarry, P. (2005). Three New Metrics to Measure the Convergence of Metaheuristics Towards the Pareto Frontier and the Aesthetic of a Set of Solutions in Biobjective Optimization. *Computers and Operations Research*, 32:773–792.
- Deb, K. (2008). *Multi-Objective Optimization Using Evolutionary Algorithms*. John Wiley & Sons, Chichester; New York.
- Deb, K., Pratap, A., Agarwal, S., and Meyarivan, T. (2002). A Fast and Elitist Multiobjective Genetic Algorithm: NSGA-II. *Evolutionary Computation, IEEE Transactions on*, 6(2):182–197.
- Depince, P., Rabeau, S., and Bennis, F. (2005). Collaborative Optimization Strategy for Multi-Objective Design. In *Proceedings of Computers and Information in Engineering Conference*, pages 197–205.
- Fafandjel, N., Zamarin, A., and Hadjina, M. (2010). Shipyard Production Cost Structure Optimisation Model Related to Product Type. *International Journal of Production Research*, 48(5):1479–1491.
- Geremia, P., Maki, K. J., Lavini, G., and Genuzio, H. (2012). Hull Design Method Combining and Innovative Flow Solver With Efficient Multivariate Analysis and Optimization Strategies. In *11th International Conference on Computer and IT Applications in the Maritime Industries*, pages 103–111.
- Gill, P., Murray, W., and Saunders, M. (2005). SNOPT: An SQP Algorithm for Large-Scale Constrained Optimization. *SIAM Review*, 147(1):99–131.

- Goff, C. I., McNamara, C. L., Bradley, J. M., Trost, C. S., Dalton, W. J., and Jabaley Jr., M. E. (2011). Maximizing Platform Value: Increasing VIRGINIA Class Deployments. *Naval Engineers Journal*, 123(3):119–139.
- Gratsos, G. A., Psaraftis, H. N., and Zachariadis, P. (2009). Life Cycle Cost of Maintaining the Effectiveness of a Ships Structure and Environmental Impact of Ship Design Parameters: An Update. In *RINA Conference on the Design and Operation of Bulk Carriers*.
- Grigson, C. (1999). A Planar Friction Line for use in Performance Prediction. In *Transactions of the RINA*.
- Gunawan, S., Azarm, S., Wu, J., and Boyars, A. (2003). Quality-Assisted Multi-Objective Multidisciplinary Genetic Algorithms. *AIAA Journal*, 41(9):1752–1762.
- Han, S., Lee, Y.-S., and Choi, Y. B. (2012). Hydrodynamic Hull Form Optimization Using Parametric Models. *Journal of Marine Science and Technology*, 17(1):1–17.
- Han, X., Bui, H., Mandal, S., Pattipati, K. R., and Kleinman, D. L. (2013). Optimization-Based Decision Support Software for a Team-In-The-Loop Experiment: Asset Package Selection and Planning. *IEEE Transactions on Systems, Man, and Cybernetics: Systems*, 43(2):237–251.
- Hannapel, S. E. (2012). *Development of Multidisciplinary Design Optimization Algorithms for Ship Design Under Uncertainty*. PhD thesis, The University of Michigan.
- Harries, S., Valdenazzi, F., Abt, C., and Viviani, U. (2001). Investigation on optimization strategies for the hydrodynamic design of fast ferries. In *6th International Conference on Fast Sea Transportation, Southampton*.
- Hart, C. G. and Vlahopoulos, N. (2009). An Integrated Multidisciplinary Particle Swarm Optimization Approach to Conceptual Ship Design. *Structural and Multidisciplinary Optimization*, 41(3):481–494.
- He, J., Hannapel, S., Singer, D., and Vlahopoulos, N. (2011). Multidisciplinary Design Optimisation of a Ship Hull Using Metamodels. *Ship Technology Research*, 58(3):156–166.
- Hwang, J. T., Lee, D. Y., Cutler, J. W., and Martins, J. R. (2013). Large-Scale MDO of a Small Satellite using a Novel Framework for the Solution of Coupled Systems and their Derivatives. In *Proceedings of the 54th AIAA/ASME/ASCE/AHS/ASC Structures, Structural Dynamics, and Materials Conference*.
- Inozu, B., Nicolai, M. J., Whitcomb, C. A., MacClaren, B., Radovic, I., and Bourg, D. (2006). New Horizons for Shipbuilding Process Improvement. *Journal of Ship Production*, 22(2):87–98.

- Jambulingam, N. and Jardine, A. K. S. (1986). Life Cycle Costing Considerations in Reliability Centered Maintenance: An Application to Maritime Equipment. *Reliability engineering*, 15(4):307–317.
- Jayabalan, V. and Chaudhuri, D. (1992). Optimal Maintenance and Replacement Policy for a Deteriorating System with Increased Mean Downtime. *Naval Research Logistics*, 29:67–78.
- Joshi, S. and Gupta, R. (1986). Scheduling of Routine Maintenance Using Production Schedules and Equipment Failure History. *Computers & industrial engineering*, 10(1):11–20.
- Junca, M. and Sanchez-Silva, M. (2013). Optimal Maintenance Policy for Permanently Monitored Infrastructure Subjected to Extreme Events. *Probabilistic Engineering Mechanics*, 33:1–8.
- Kim, H., Hyunyul, K., and Chi, Y. (2012). Hydrodynamic Optimization of Ship Hull Form Using Finite Element Method and Variable Fidelity Models. In *The proceedings of the twenty-second (2012) International Offshore and Polar Engineering Conference*, pages 888–896, Rhodes, Greece. International Society of Offshore and Polar Engineers.
- Kim, S. and Frangopol, D. M. (2010). Cost-Based Optimum Scheduling of Inspection and Monitoring for Fatigue-Sensitive Structures Under Uncertainty. *Journal of Structural Engineering*, 137(11):1319–1331.
- Kim, S. and Frangopol, D. M. (2011a). Inspection and Monitoring Planning for RC Structures Based on Minimization of Expected Damage Detection Delay. *Probabilistic Engineering Mechanics*, 26(2):308–320.
- Kim, S. and Frangopol, D. M. (2011b). Optimum Inspection Planning for Minimizing Fatigue Damage Detection Delay of Ship Hull Structures. *International Journal of Fatigue*, 33(3):448–459.
- Kim, S. and Frangopol, D. M. (2011c). Probabilistic Bicriterion Optimum Inspection/Monitoring Planning: Applications to Naval Ships and Bridges Under Fatigue. *Structure and Infrastructure Engineering*, pages 1–16.
- Kim, S., Frangopol, D. M., and Soliman, M. (2013). Generalized Probabilistic Framework for Optimum Inspection and Maintenance Planning. *Journal of Structural Engineering*, 139(3):435–447.
- Kramer, M., Motley, M., and Young, Y. (2010). Probabilistic-Based Design of Waterjet Propulsors for Surface Effect Ships. In *29th American Towing Tank Conference*.
- Krol, W. P. (1991). Midship Section Design Using a Bilevel Production Cost Optimization Scheme. *Journal of Ship Production*, 7(1):29–36.



- Kuhn, J., Chevalier, K., Schlageter, E., Scragg, C., and Wyatt, D. (2007). Use of Linear Programming and Basis Functions for Hull-Form Optimization. In *9th International Conference on Numerical Ship Hydrodynamics*.
- Kuo, Y. and Chang, Z.-A. (2007). Integrated Production Scheduling and Preventive Maintenance Planning for a Single Machine Under a Cumulative Damage Failure Process. *Naval Research Logistics*, 54(6):602–614.
- Kwon, K. and Frangopol, D. M. (2012). Fatigue Life Assessment and Lifetime Management of Aluminum Ships Using Life-Cycle Optimization. *Journal of Ship Research*, 56(2):91–105.
- Kwon, K., Frangopol, D. M., and Kim, S. (2013). Fatigue Performance Assessment and Service Life Prediction of High-Speed Structures Based on Probabilistic Lifetime Sea Loads. *Structure and Infrastructure Engineering*, 9(2):102–115.
- Lamb, T. (1994). Shell Plate Definition Guide for Ship Designers. Technical Report NSRP0421, National Shipbuilding Research Program.
- Lambe, A. B. and Martins, J. R. (2012). Extensions to the Design Structure Matrix for the Description of Multidisciplinary Design, Analysis, and Optimization Processes. *Structural and Multidisciplinary Optimization*, 46(2):273–284.
- Lee, C.-Y. and Chen, Z.-L. (2000). Scheduling Jobs and Maintenance Activities on Parallel Machines. *Naval Research Logistics*, 47(2):145–165.
- Lee, J., Lee, S., and Van, S. (1998). Wind Tunnel Tests on a Double Deck Shaped Ship Model. In *3rd Annual Conference on Hydrodynamics*, Seoul, Korea.
- Lewis, K., Lucas, T., and Mistree, F. (1994). A Decision-Based Approach for Developing Ranged Top-Level Aircraft Specifications - A Conceptual Exposition. American Institute of Aeronautics and Astronautics.
- Li, D.-Q. (2005). Cost-Benefit Assessment of Inspection and Repair Planning for Ship Structures Considering Corrosion Model Uncertainty. *China Ocean Engineering*, 19(3).
- Li, F., Li, G., Sun, G., Luo, Z., and Zhang, Z. (2010). Multi-Disciplinary Optimization for Multi-Objective Uncertainty Design of Thin Walled Beams. *Computers Materials and Continua*, 19(1):37–56.
- Li, J. and Parson, M. G. (1996). The Use of Fuzzy Logic in Shipping and Shipbuilding Market Modeling, Analysis, and Forecasting. *Journal of Ship Production*.
- Lin, Z.-L. and Huang, Y.-S. (2010). Nonperiodic Preventive Maintenance for Repairable Systems. *Naval Research Logistics (NRL)*, 57(7):615–625.
- Long, T., Liu, L., Zhou, S., Wang, J., and Meng, L. (2008). Multi-Objective Multidisciplinary Optimization of Long-Endurance UAV Wing Using Surrogate Model in ModelCenter. American Institute of Aeronautics and Astronautics.

- Mahmood, S. and De-bo, H. (2011). Hull Form Optimization of Trimaran Using Genetic Algorithm. In *Computational Science and Engineering (CSE), 2011 IEEE 14th International Conference on*, pages 150–154.
- Maki, K., Doctors, L., Scher, R., Wilson, W., and Troesch, A. (2008). Conceptual Design and Hydrodynamic Analysis of a High-Speed Sealift Adjustable-Length Trimaran. In *Transactions of SNAME*.
- MAN (2009). *Marine Engine Product Catalog*. MAN B&W.
- Manen et. al, J. (1988). *Principles of Naval Architecture, Chapter 6: Propulsion*, volume 2. Society of Naval Architects and Marine Engineers, New York.
- Martins, J. and Lambe, A. B. (2012). Multidisciplinary design optimization: Survey of architectures. *AIAA Journal*.
- Martins, J. R. R. A., Sturdza, P., and Alonso, J. J. (2003). The Complex-Step Derivative Approximation. *ACM Transactions on Mathematical Software*, 29(3):245–262.
- McAllister, C., Simpson, T., Hacker, K., Lewis, K., and Messac, A. (2004). Integrating Linear Physical Programming Within Collaborative Optimization for Multiobjective Multidisciplinary Design Optimization. *Structural and Multidisciplinary Optimization*, 29(3):178–189.
- Mermiris, G., Das, P., Moatsos, I., and Winkle, I. (2005). Towards a Method for the Optimisation of Midship Section in Terms of Production Cost in Preliminary Ship Design. In *Proceedings of the International Conference on Offshore Mechanics and Arctic Engineering*, volume 1B, pages 981–990.
- Motley, M. and Young, Y. (2011). Performance-Based Design and Analysis of Flexible Composite Structures. *Journal of Fluids and Structures*, 27(8):1310–1325.
- Narli, E. and Sariz, K. (1998). Fairing of High Speed Displacement Hull Forms by B-spline Approximation and Fitting. *Naval engineers journal*, 110(2):3547.
- Nelson, M., Temple, D., Hwang, J., Young, Y., Martines, J., and Collette, M. (2013). Simultaneous Optimization of Propeller-Hull Systems to Minimize Lifetime Fuel Consumption. *Applied Ocean Research*, 43:46–52.
- O’Rourke, R. (2005). Navy Ship Acquisition: Options for Lower-Cost Ship Designs – Issues for Congress. Technical Report RL32914.
- Paik, J. K., Kim, S. K., and Lee, S. K. (1998). Probabilistic Corrosion Rate Estimation Model for Longitudinal Strength Members of Bulk Carriers. *Ocean Engineering*, 25(10):837–860.
- Paik, J. K., Lee, J. M., and Ko, M. J. (2004). Ultimate Shear Strength of Plate Elements with Pit Corrosion Wastage. *Thin-Walled Structures*, 42(8):1161–1176.

- Paik, J. K., Lee, J. M., Park, Y. I., Hwang, J. S., and Kim, C. W. (2003a). Time-Variant Ultimate Longitudinal Strength of Corroded Bulk Carriers. *Marine Structures*, 16(8):567–600.
- Paik, J. K., Lee, M., Hwang, J. S., and Park, Y. I. (2003b). A Time-Dependent Corrosion Wastage Model for the Structures of Single- and Double Hull Tankers FSOs and FPSOs. *Marine Technology*, 40(3):201–217.
- Parsons, M. G., Nam, J.-H., and Singer, D. J. (1998). A Scalar Metric for Assessing the Producability of a Hull Form in Early Design. In *Great Lakes/Great Rivers Section of The Society Of Naval Architects And Marine Enginners*.
- Percival, S., Hendrix, D., and Noblesse, F. (2001). Hydrodynamic Optimization of Ship Hull Forms. *Applied Ocean Research*, 23:337–355.
- Perez, R. E., Jansen, P. W., and Martins, J. R. R. A. (2012). pyOpt: A Python-Based Object-Oriented Framework for Nonlinear Constrained Optimization. *Structures and Multidisciplinary Optimization*, 45(1):101–118.
- Rahman, M. K. and Caldwell, J. B. (1995). Ship Structures: Improvement by Rational Design Optimisation. *International Shipbuilding Progress*, 42(429).
- Rigo, P. (2001). Least-Cost Structural Optimization Oriented Preliminary Design. *Journal of Ship Production*, 17(4):202–215.
- Rigterink, D., Collette, M., and Singer, D. J. (2013). A Method for Comparing Panel Complexity to Traditional Material and Production Cost Estimating Techniques. *Ocean Engineering*, 70:61–71.
- Ruiyi, S., Liangjin, G., and Zijie, F. (2011). Multi-Objective Collaborative Optimization Based on Evolutionary Algorithms. *Journal of Mechanical Design*, 133:104502.
- Sankararaman, S., Ling, Y., and Mahadevan, S. (2010). Statistical Inference of Equivalent Initial Flaw Size With Complicated Structural Geometry and Multi-Axial Variable Amplitude Loading. *International Journal of Fatigue*, 32(10):1689–1700.
- Sariz, E. (2006). An Optimization Approach for Fairing of Ship Hull Forms. *Ocean Engineering*, 33(16):2105–2118.
- Seto, N. (2010). Multi-disciplinary Design Optimization of Supersonic Transport Wing Using Surrogate Model. In *27th International Congress of the Aeronautical Sciences, Nice, France, ICAS-Paper*.
- Smith, C. (1977). Influence of Local Compressive Failure on Ultimate Longitudinal Strength of a Ship’s Hull. In *Proceedings of the International Symposium on Practical Design in Shipbuilding*, pages 73–79.
- Soliman, M., Frangopol, D. M., and Kim, S. (2013). Probabilistic Optimum Inspection Planning of Steel Bridges With Multiple Fatigue Sensitive Details. *Engineering Structures*, 49:996–1006.

- Souza, G. and Ayyub, B. (2000). Probabilistic Fatigue Life Prediction for Ship Structures Using Fracture Mechanics. *Naval Engineers Journal*, 112(4):375–397.
- Stambaugh, K. and Barry, C. (2014). Naval Ship Structure Service Life Considerations. *Naval Engineers Journal*, 126(3):103–117.
- Tamiz, M., Jones, D., and Romero, C. (1998). Goal Programming for Decision Making: An overview of the current stat-of-the-art. *European Journal of Operations Research*, 111:569–581.
- Tappeta, R. V. and Renaud, J. E. (1997). Multipleobjective Collaborative Optimization. *Journal of Mechanical Design*, 119:403–411.
- Tasdemir, A. and Nohut, S. (2012). Fatigue analysis of ship structures with hinged deck design by finite element method. A case study: Fatigue analysis of the primary supporting members of 4900 PCTC. *Marine Structures*, 25(1):1–12.
- Tedford, N. P. and Martins, J. R. R. A. (2009). Benchmarking multidisciplinary design optimization algorithms. *Optimization and Engineering*, 11(1):159–183.
- Temple, D. and Collette, M. (2013). Optimization of Structural Design to Minimize Lifetime Maintenance Cost of a Naval Vessel. In *Analysis and Design of Marine Structures - Proceedings of the 4th International Conference on Marine Structures*, pages 525 – 532, Espoo, Finland.
- Temple, D. and Collette, M. (2015a). Minimizing lifetime structural costs: Optimizing for production and maintenance under service life uncertainty. *Marine Structures*, 40:60–72.
- Temple, D. and Collette, M. (2015b). Understanding the Trade-offs Between Producibility and Resistance for Differing Vessels and Missions. *Journal of Ship Design and Production*, 31(2):1–12.
- Temple, D. W. and Collette, M. (2012). Multi-Objective Hull Form Optimization to Compare Build Cost and Lifetime Fuel Consumption. In *The 11th International Marine Design Conference*, pages 391 – 403.
- Tuck, E. O. (1989). The Wave Resistance Formula of J.H. Michell (1898) and its Significance to Recent Research in Ship Hydrodynamics. *The Journal of the Australian Mathematical Society*, 30.
- Tuck, E. O. and Lazauskas, L. (2008). Drag on a Ship and Michells Integral. In *22nd Int. Congress of Theoretical and Applied Mechanics, Adelaide, South Australia*.
- Turan, O., Olcer, A., Lazakis, I., Rigo, P., and Caprace, J. (2009). Maintenance/Repair and Production-Oriented Life Cycle Cost/Earning Model for Ship Structural Optimisation During Conceptual Design Phase. *Ships and Offshore Structures*, 4(2):107–125.

- Wang, P., Takagi, T., Takeno, T., and Miki, H. (2013). Early fatigue damage detecting sensors A review and prospects. *Sensors and Actuators A: Physical*, 198:46–60.
- Windhorst, R., Galloway, E., Lau, E., Saunders, D., and Gage, P. (2006). Aerospace Vehicle Trajectory Design and Optimization Within a Multi-Disciplinary Environment. *Journal of Aerospace Computing, Information, and Communication*, 3(9):471485.
- Wirsching, P. H. (1984). Fatigue Reliability for Offshore Structures. *Journal of Structural Engineering*, 110(10):23402356.
- Yang, J.-M. and Hwang, C.-N. (2002). Optimization of Corrugated Bulkhead Forms by Genetic Algorithms. *Journal of Marine Science and Technology*, 10(2):146–153.
- Zadeh, L. (1965). Fuzzy Sets. *Information and Control*, 8(3):338–353.
- Zalek, S., Beck, R., and Parsons, M. (2008). Nonlinear Hullform Transformation for Use with Design Optimization. In *Proceedings of the 2008 Grand Challenges in Modeling and Simulation Conference*, volume 40 of *Simulation series*, pages 227–238, Edinburgh, Scotland.